LA-UR-17-22589
Approved for public release; distribution is unlimited.

Title: COMPARISON OF 252CF TIME CORRELATED INDUCED FISSSION WITH AmLi INDUCED FISSION ON FRESH MTR RESEARCH REACTOR FUEL

Author(s): Joshi, Jay Prakash

Intended for: Report

Issued: 2017-03-30

COMPARISON OF ^{252}CF TIME CORRELATED INDUCED FISSSION WITH AmLi INDUCED FISSION ON FRESH MTR RESEARCH REACTOR FUEL

by

Jay Prakash Joshi

B.S. Radiation Physics

The University of Texas at Austin

A THESIS

Presented to the Faculty of the Graduate School of the

MISSOURI UNIVERSITY OF SCIENCE AND TECHNOLOGY

In Partial Fulfillment of the Requirements for the Degree

MASTER OF SCIENCE IN NUCLEAR ENGINEERING

2017

Approved by

Dr. Sohaib Usman, Advisor

Dr. Alexis C. Trahan, LANL Mentor

Dr. Ayodeji Babatunde Alajo

Dr. Hyoung Koo Lee, Department Chair

ABSTRACT:

The effective application of international safeguards to research reactors requires verification of spent fuel as well as fresh fuel. To accomplish this goal various nondestructive and destructive assay techniques have been developed in the US and around the world. The Advanced Experimental Fuel Counter (AEFC) is a nondestructive assay (NDA) system developed at Los Alamos National Laboratory (LANL) combining both neutron and gamma measurement capabilities. Since spent fuel assemblies are stored in water, the system was designed to be watertight to facilitate underwater measurements by inspectors. The AEFC is comprised of six ^{3}He detectors as well as a shielded and collimated ion chamber. The ^{3}He detectors are used for active and passive neutron coincidence counting while the ion chamber is used for gross gamma counting. Active coincidence measurement data is used to measure residual fissile mass, whereas the passive coincidence measurement data along with passive gamma measurement can provide information about burnup, cooling time, and initial enrichment. In the past, most of the active interrogation systems along with the AEFC used an AmLi neutron interrogation source. Owing to the difficulty in obtaining an AmLi source, a ^{252}Cf spontaneous fission (SF) source was used during a 2014 field trail in Uzbekistan as an alternative. In this study, experiments were performed to calibrate the AEFC instrument and compare use of the ^{252}Cf spontaneous fission source and the AmLi (α,n) neutron emission source. The ^{252}Cf source spontaneously emits bursts of time-correlated prompt fission neutrons that thermalize in the water and induce fission in the fuel assembly. The induced fission (IF) neutrons are also time correlated resulting in more correlated neutron detections inside the ^{3}He detector, which helps reduce the statistical errors in doubles when using the ^{252}Cf interrogation source instead of the AmLi source. In this work, two MTR fuel assemblies varying both in size and number of fuel plates were measured using ^{252}Cf and AmLi active interrogation sources. This paper analyzes time correlated induced fission (TCIF) from fresh MTR fuel assemblies due to ^{252}Cf and AmLi active interrogation sources.

KEYWORDS

Neutron coincidence; time correlated induced fission; active interrogation; Cf^{252}; AmLi

ACKNOWLEDGEMENTS

I would like to thank my advisor at MS&T, Dr. Sohaib Usman, and my mentor at LANL, Dr. Alexis Trahan, for the continuous supervision and advice throughout my Masters Research. I would like to thank Dr. Ayodeji B. Alajo for his insightful talks and inspirations. I would like to thank MS&T Nuclear Engineering department chair, Dr. Hyoung koo Lee, for providing a prestigious NRC fellowship during the first three semesters of my graduate school and for his time and support.

I would like to thank my other mentors at LANL, Dr. Howard Menlove, Dr. Martin Swinhoe, Carlos Real, Johnna Marlow, Margaret Root for their time and support and for always believing in me. I'd especially like to thank Dr. Menlove and Dr. Swinhoe for answering my questions. I would like to express my gratitude to Dr. John Hendricks for continuously helping me on my research work, and helping me with my works whenever I got stuck

For my wife, Eshna, I appreciate everything you have done for me. There were times during my undergraduate degree as well as graduate degree when I was down and discouraged, your love and warmth always got me on track. Your love provided a safe home for me. We laughed, got sad, and planned our lives together. Thank you for everything.

Last but not the least, I would like to acknowledge the support from the Nuclear Noncompliance Verification (NNV) program of the U.S. National Nuclear Security Administration (NNSA) Office of Nonproliferation and International Security (NIS) for supporting my MS thesis project.

TABLE OF CONTENT

LIST OF FIGURES

LIST OF TABLES

NOMENCLATURE

AEFC	Advanced Experimental Fuel Counter
^{252}Cf	Californium-252 source
AmLi	Americium-Lithium source
SF	Spontaneous Fission
IF	Induced Fission
IAEA	International Atomic Energy Agency
NPT	Non-Proliferation Treaty
LANL	Los Alamos National Laboratory
HV	High Voltage
NPT	Nuclear Nonproliferation Treaty
NDA	Non-Destructive Assay
DA	Destructive Assay
^{235}U	Uranium-235 fuel
^{239}Pu	Plutonium-239 fuel
TCIF	Time Correlated Induced Fission
^{3}He	Helium-3 detectors
R	Real gate/count rate
A	Accidental gate/count rate
(α,n)	Alpha-neutron reaction

HDPE	High Density Polyethylene
HEU	Highly Enriched Uranium
LEU	Low Enriched Uranium
ADC	Analog to Digital Converter

1. INTRODUCTION

1.1. BACKGROUND

The Advanced Experimental Fuel Counter (AEFC) was originally designed to verify research reactor spent fuel. Initially, verification was focused on obtaining ^{235}U residual mass, burnup, and plutonium content. Plutonium was a part of the verification because it is produced in the fuel as it is being burned and could be used to make a weapon. The reason why residual ^{235}U mass is key is because during the first few decades in the early days of the research reactors, the fuel used was mostly highly enriched uranium (HEU) with approximately 93%, 60%, or 36% ^{235}U enrichment. From the safeguards point of view ^{235}U can be separated from the HEU and can be used directly to make weapon. In the recent decades, efforts are being made to convert HEU fuel to low enriched uranium (LEU). Uranium fuel is called LEU when ^{235}U enrichment in it is less than 20% by weight. With LEU fuel, plutonium content becomes important from the safeguard's perspective as plutonium content increase vastly in the spent fuel as the fuel is changed from HEU to LEU due to the increase of ^{238}U content. If a country does not possess a reprocessing facility then plutonium content in spent fuel does not become critical, but in countries with reprocessing facilities, spent fuel verification becomes very important. Investigation of MTR fuel is crucial from the safeguards point of view as MTRs were installed in the countries that were not supposed to make nuclear weapons.

This research focuses on the underwater verification of fresh MTR fuel using ^{252}Cf and AmLi active interrogation sources. ^{252}Cf source is used as an active interrogation source because of the difficulties in obtaining an AmLi source. It was found in the previous AEFC field trails that measurements with ^{252}Cf active sources resulted in doubles rates with lower uncertainty compared to when AmLi was used. It was seen that the time correlated neutrons in the background from ^{252}Cf did not hurt in the coincidence counting; rather, they reduced uncertainties.

The novel aspect of this research work is the underwater interrogation of highly enriched fresh MTR fuel assemblies. The AEFC is the neutron coincidence system with underwater capabilities, which is shielded from the fission product gamma rays when measuring spent fuel. The work focuses on the calibration of the AEFC with ^{252}Cf active source and fresh MTR fuel.

1.2. HISTORY OF NUCLEAR PROLIFERATION

In 1939, Albert Einstein wrote a letter to the then President of the US, President Franklin D. Roosevelt, in which he showed his concerns that Germany might be close to having a fission based nuclear bomb, and stated how important it was for the USA to start its own program as soon as possible. [1] This urgency ultimately led to the production of first successful fission bomb in 1945, which was tested in the north of Alamogordo, New Mexico, USA, now known as a Trinity Site. Later, two bombs were dropped in the Japanese cities Hiroshima and Nagasaki. [2] The whole world witnessed the devastation that nuclear weapons did to the two Japanese cities. The World War II ended, however the fear of the nuclear weapon rose. Over the past 71 years many countries aspired to produce their own nuclear weapon, some were successful while some were not. Almost all those countries justified their aspiration with the need for national security and to enhance their international status. [3]

While the two bombs used in Japan took more than 200,000 lives, they were able to stop the war. [4] Further, it gave the impression that nuclear weapons were the reason for World War III not to arise. Countries and people around the world saw that the wars that broke after WWII were either between the countries with no nuclear weapons or between two countries in which only one had nuclear weapons. This appears to have driven the less powerful countries to pursue towards having a nuclear weapon. The aspiration of more and more countries to have a nuclear weapon became a threat to the global security. [3]

1.2.1. THE NONPROLIFERATION TREATY (NPT)

By 1952, three countries, USA, UK, and Russia, had already produced nuclear weapons. The world was already beginning to witness a proliferation of nuclear weapons. The US President Dwight D Eisenhower gave a speech in New York to the UN General assembly on "Atom for Peace" in 1953 as he understood the danger of excessive unmonitored nuclear material. In his speech he proposed formation of the IAEA, which got an international focus. The creation of IAEA created nuclear safeguards as well as expanded peaceful use of atoms. [5]

The Nonproliferation Treaty (NPT) was drafted in 1965 in the Geneva disarmament conference, which banned further acquisition and transfer of nuclear weapons. This was direct effect of the US President John F. Kennedy, as he described the "Greatest global threat of the future to be as many as 25 states owning nuclear weapons." The treaty entered into effect in 1970

with 43 member countries including the Soviet Union, the US, and the UK. The missions of the NPT were non-proliferation, peaceful use of atom, and disarmament. The treaty clearly stated that it would help states build a research and commercial power plant capabilities for the peaceful use. [5]

North Korea ratified the NPT in 1985, which is almost two decades after they received their first research reactor from the Soviet. North Korea continued its nuclear weapons program while they were NPT member state. The North Korea incident clearly indicated the flaws in the treaty. It showed if a country signs NPT, IAEA would help train and build nuclear technology and infrastructure for that country, but IAEA did not have authority to investigate undeclared facilities and at the same time a country could withdraw from NPT any time. NPT was not sufficient for the non-proliferation mission of IAEA. There was a need of additional protocol, a strong infrastructure for the timely detection of diversion of the significant quantities of special nuclear material from peaceful nuclear activities to the manufacture of nuclear weapons, and the ability to verify the operator declared fuel parameters such as initial enrichment, burnup, cooling time, and the fissile mass content of the spent fuel. [5]

With an increase in the number of nuclear facilities around the world, faster, efficient, and effective ways to investigate spent as well as fresh fuel is important. Nondestructive assay (NDA) techniques have been very useful for the IAEA safeguards for treaty monitoring and verifying nuclear activities. The most important work of IAEA safeguard is to make sure nuclear material is not diverted for weapons purpose. The AEFC is one of the nondestructive assay (NDA) systems designed to account and verify nuclear material in a research reactor and make sure that nuclear material is not diverted for weapons purposes.

1.3. NDA TECHNIQUE

NDA is an important tool for nuclear material safeguards to verify the nuclear material inventory. The NDA technology was started more than 50 years ago in mid 1960s during the time when the NPT was written. Over the past 50 years, there have been significant improvements in NDA techniques and instrumentation. Many of the improvements are in detection capabilities such as highly efficient detectors, and electronic processing such as better preamplifiers, amplifiers, analog to digital converters, and data analysis. There have been developments of better computer software for the analysis of the data generated in the

measurements. Better computing power has helped in the advancement of NDA techniques by allowing large data collection and complex Monte Carlo simulations and calculations. [10]

NDA can be used in all steps of nuclear fuel cycles such as mining/milling, fabrication plant, enrichment plant, reactor operation as well as in the backend of a fuel cycle. The technique is used to identify any undeclared material and operation, and verify operator declared fuel parameters such as initial enrichment, burnup, cooling time, residual fissile mass, or any diverted assembly from a reactor core or a spent fuel pool. The NDA systems can collect and store data from different detectors simultaneously, and at the same time analyze data immediately after the measurement completion. [10]

Unlike destructive analysis (DA), in which the fuel sample is physically destroyed for the sample fuel characterization, the AEFC is one of the NDA techniques that uses neutrons and gamma ray signals from the fuel sample. DA techniques are more accurate than NDA because they use techniques like mass spectroscopy in which material is characterized relative to reference standards.

Spent fuel is heterogeneously irradiated, which results in there being more burnup at the middle of the fuel assembly compared to the ends in axial direction. This scenario makes DA techniques difficult and time consuming because there would be a need to account for the errors in sampling. In DA techniques, the whole sample is broken and grinded to make it homogenous, whereas in fact the fuel is heterogeneously burned in a reactor. The change in neutron and gamma signals are discrete axially, therefore fuel would have to be broken into many pieces axially and grinded separately to get accurate results in the DA. This whole process is complex and comes with contamination risks as fuel sample should be physically broken. NDA techniques such as the AEFC are faster, easier, less hazardous, and can be repeated as many times as required. The IAEA inspectors have been using NDA techniques to verify and characterize spent fuel for decades due to these attractive options offered by the NDA techniques. [2]

1.4. ADVANCED EXPERIMENTAL FUEL COUNTER (AEFC)

The AEFC is a NDA system developed at the LANL combining both neutron and gamma measurement capabilities. Since spent fuel assemblies are stored in water, the system was designed to be watertight to facilitate underwater measurements by inspectors. The AEFC is comprised of six ^{3}He detectors as well as a shielded and collimated ion chamber. The ^{3}He

detectors are used for active and passive neutron coincidence counting while the ion chamber is used for gross gamma counting. Active coincidence measurement data is used to measure residual fissile mass (i.e., $^{235}U + ^{239}Pu$), whereas the passive coincidence measurement data along with passive gamma measurement can provide information about burnup, cooling time, and initial enrichment. [6]

The SF source ^{252}Cf was successfully used as an active interrogation source in lieu of AmLi in the 2014 field trail in Uzbekistan by Menlove et al. [1]. Before that, ^{252}Cf was thought to be unfavorable as an active interrogation source because it would produce a burst of time correlated neutrons during each fission event. While AmLi produces random neutrons in time with no active source background coincidences, ^{252}Cf gives a complex coincidence background. [7]

Table 1-1: Measurement Signals, Spent Fuel Attributes, and AEFC Operating Parameters [6]

Measurements	**Fuel Attribute**
Passive Interrogation Signals	
Singles rate (^{3}He detector)	SF + (α,n)
Doubles rate (^{3}He detector)	SF + IF
Ion chamber	Relative Burnup (^{137}Cs) + profile
Active Interrogation Signals	
Singles rate	IF
Doubles rate	IF

Table 1-1 shows active and passive signals that can be acquired from the spent fuel measurements using the AEFC detection system. The table shows that in passive mode total singles rate is the sum of SF and (α,n) reaction, while the total doubles rate come from just SF. Ionization chamber provides the information about the relative burnup and a burnup profile by measuring gross gamma counts after cooling time corrections. In the active interrogation mode, total singles and total doubles rates come from only IF events.

2. THEORY AND BACKGROUND

2.1. NEUTRON DETECTION MECHANISIM

Neutrons are neutral, and do not interact with electrons in an atom unlike gamma rays or alpha particles. Neutrons interact with the nucleus, which results in a release of one or more charged particles. The charged particles are then detected and processed by the detection systems. Scattering and nuclear reactions are two basic neutron interactions. Scattering interaction is effective only with the light nucleus such as hydrogen and helium, in which neutron transfers enough energy to create a recoil nucleus. Recoil nucleus ionizes surrounding material. The ionization results in a release of particles such gamma rays, alpha, beta, or x-rays that are ultimately detected. In case of nuclear reaction, the products such as gamma rays, proton, alpha, or the fission fragments are detected. In both cases, the electrical signal produced by the charged particles or gamma rays are detected. [9]

2.2. ^{3}He PROPORTIONAL NEUTRON DETECTORS

When a neutron reacts with ^{3}He nuclides, energetic charged particles are released into gas inside the detector. The charged particles ionize surrounding gas molecules, which causes avalanche process that leads to detection. The energy released from a nuclear reaction is deposited in the detector. When ^{3}He reacts with the neutron, the reaction gives off a tritium, a proton, with 765 KeV energy shared between two nuclides. The reaction that occur inside the detectors containing ^{3}He is given in equation 1 below: [8][9]

$$3_{He} + n \rightarrow 3_{H} + 1_{H} + 765\ KeV \qquad 1$$

^{3}He detectors are used widely in verifying and accounting nuclear material by the IAEA inspectors. The detectors are used to perform coincidence counting to verify a fissile mass in a fresh and spent fuel as well as monitor fuels in all phases in a nuclear fuel cycle. To possess capabilities to discriminate pulses created by the gamma interactions, ^{3}He detectors are operated in proportional region rather than operating in Geiger region. The neutron absorption cross section of ^{3}He follows $1/v$ relationship in a thermal region up to approximately 200 KeV, where v is a neutron velocity. ^{3}He is very sensitive to the thermal neutrons as it has high neutron absorption cross section of 5330 barns. [9] Since ^{3}He has high thermal neutron cross section, the

detectors are put inside the neutron moderator such as water or high density polyethylene during entire measurements process. [8][9]

^{3}He detectors use ^{3}He(n,p)^{3}H nuclear reaction to detect moderated neutrons. Released charged particles, a proton ($^{1}H_{1}$) and a triton ($^{3}H_{1}$) give off electrons that are attracted by the anode wire high voltage. The electrons accelerate towards anode and create a detection cloud via charge multiplication. A charge sensitive amplifier detects a charge induced by a detection cloud nearby to the cathodes by means of capacitive coupling. Figure 2-1 below shows visual representation of a pulse height spectrum of typical ^{3}He detector. [8][9]

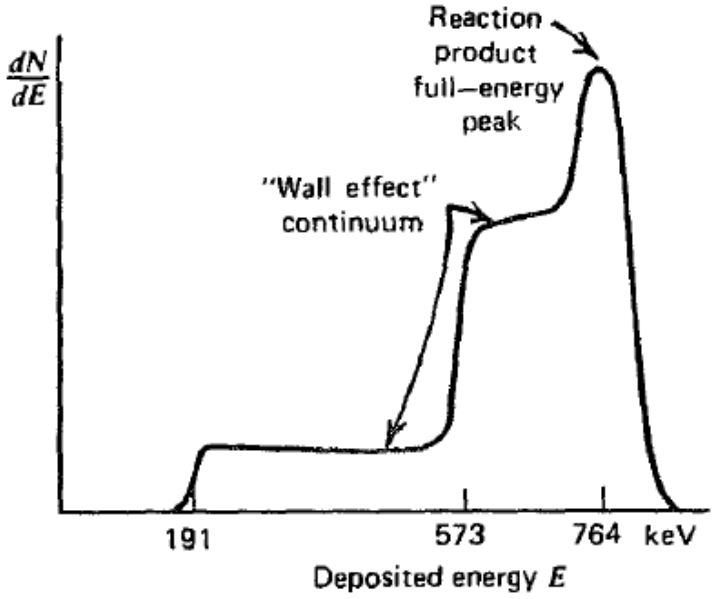

Figure 2.2-1: Pulse height spectrum from a typical size 3He detector [9]

The Q-value of the nuclear reaction is approximately 765 KeV and the energy is carried by the daughter products in the form of kinetic energy. Since the emission of daughter products follow conservation of momentum, the daughter products travel in opposite direction. Possibility of energy deposition depends on only one daughter register, both daughters escape, or both daughter register kinetic energy in the detector, however the output pulse is proportional to 765 KeV. [8][9]

The main peak at 765 KeV in figure 2-1 is a kinetic energy liberated in a ^{3}He and thermal neutron nuclear reaction. By the law of conservation of momentum, less energy is carried by heavier ^{3}H daughter compared to the lighter ^{1}H. Approximately 191 KeV and 574 KeV of kinetic

energy are split between ^{3}H and ^{1}H daughter nuclides respectively. If a reaction occurs close to the detector wall, one of the two daughter nuclides might get absorbed in the wall while trying to escape from the detector and other might get absorbed in the detector gas. Because of this wall effect peaks at 197 KeV and 574 Kev along with long plateau is seen in a pulse height spectrum of 3He detector. [8][9]

Table 2-1 below provides the specifications of ^{3}He detectors and preamplifiers and their operating parameters such as pressure inside the detector tubes, operating voltage range, gate length, pre-delay, and detector die away time used in the AEFC system.

Table 2-1: Detector and Amplifier Specifications in the AEFC [6]

Parameter	**Values**
Number of detector tubes (RS-P4-0810-119)	6
Diameter of ^{3}He detector	25.4 mm
Active length of ^{3}He detector	254 mm
Pressure inside the detector tube	4 Atmosphere
Operating Voltage	1640-1680 V
PDP-10A preamplifiers	6
Die-away time	85 μs
Gate	128 μs
Pre-delay	4.5 μs

2.3. NEUTRON COINCIDENCE COUNTING

The AEFC consists of six ^{3}He detectors that use coincidence counting to characterize research reactor fuel. For example, a SF event in ^{252}Cf releases in average 3.76 neutrons, and these neutrons then cause IF in a fuel assembly. On average 2.44 neutrons are released from ^{235}U IF event. If only one out of an average 3.76 neutrons from ^{252}Cf source is captured inside a fuel assembly and causes IF, an average of approximately 5.2 neutrons will be released in the whole

process that are time correlated. Although coincidence detection depends on the efficiency of detection system, there is an increase in effective average neutrons per fission (ν). [7][12]

If two neutrons are detected by any of the six ^{3}He detectors within the specified time window 128μsec, they are defined as coincidences. There is a chance that the coincidences measured are accidentals from background and active source, but these accidentals can be separated from the real coincidences from fuel. The process of separation is explained by the Rossi-Alpha distribution, which is explained in section 2.5 below. The probability of detecting uncorrelated neutrons increases with the increase in active interrogation source strength; however, these uncorrelated neutrons can be separated statistically. [7][10]

Shift register is used to acquire neutron coincidence data in a measurement. Shift register opens a pre-delay and gate for each neutron detected in any of six ^{3}He detectors, and gives a recovery time to the detectors to perform coincidence counting. The shift register opens a pre-delay of 4.5 μs each time a trigger occurs in order to eliminate the dead time effect. After a pre-delay, it opens R+A and A gates of 128 μs separated by a long delay. A long delay is several die away times of a neutron that triggers a pre-delay, which is long enough to allow preamplifier to recover from the trigger pulse. Due to the long delay (~ 1000μs), coincident neutrons detected in accidental gate (A) are true accidentals because after the long delay all neutrons from the precursor triggering Sf or IF events are already gone. The neutrons counted after a long delay are just accidentals and they are constant throughout the A gate. The visual representation of R+A and A gates can be seen in figure 2 in section 2.5. The real coincidence is then given by the equation 2 below: [7][10]

$$R = (R+A) - A \qquad 2$$

2.3.1. UNCERTAINTIES IN COINCIDENCE COUNTING DUE TO COUNTING STATISTICS IN SHIFT REGISTER

The coincidence counting statistics is complex due to the presence of real and accidental pulse trains. The shift register has to discriminate between the real and accidental count rates as well as provide uncertainties of measurements related to these count rates. In general in a shift register uncertainty in real count rate is given by the equation 3. [22]

$$\frac{\sigma R}{R} = \frac{\sqrt{((R+A)+A)}}{R} = \frac{\sqrt{(R+2A)}}{R} \qquad 3$$

In the case of JSR-15 shift register used in this research work, accidental gate A triggers on clock frequency of approximately 50MHz therefore accidentals rates are counted a lot more than the R+A gate. This makes contribution of A rates in the measurement uncertainty negligible. Then the uncertainty in R measurements depends only on R+A uncertainties. The JSR-15 shift register uncertainty in real count rate is given by the equation 4. [22]

$$\frac{\sigma R}{R} = \frac{\sqrt{((R+A))}}{R} = \frac{\sqrt{(R+A)}}{R} \qquad 4$$

The measurement uncertainty for random neutrons is different process than when the correlated neutrons. Random neutrons follow Poisson distribution therefore when the number of counts is n neutrons the relative error is given by the equation 5. [22]

$$\frac{\sigma_n}{n} = \frac{Var(n)}{n} = \frac{1}{\sqrt{n}} \qquad 5$$

While correlated neutrons such as from SF do not follow Poisson distribution, the numbers of SF events follow Poisson distribution. If a total number of neutrons emitted in SF is T, $\bar{\nu}$ is an average SF multiplicity, and the number of SF events is S, then, [22]

$$T = \bar{\nu}S \qquad 6$$

The relative error for measuring n correlated SF neutrons with the absolute detector efficiency ε this given by,

$$\frac{Var(n)}{n} = 1 + \varepsilon\frac{\overline{\nu^2} - \bar{\nu}}{\bar{\nu}} \qquad 7$$

In the equation 7, the variance approaches Poisson distribution when $\bar{\nu}$ approaches 1 or ε approaches 0. Therefore, the measurement uncertainty of SF in coincidence counting depends on multiplicity and absolute detector efficiency. [22]

2.4. DIE-AWAY TIME

When neutrons are emitted from a source, two events are possible, (1) they can travel for ever until they decay or (2) interact with matter until it gets absorbed. Neutrons may scatter multiple times and ultimately get absorbed or decay away. Every neutron detection system designed has a die away time, which is an average neutron lifetime in a detector system after which neutron emitted from a fission event are no longer available i.e. either they are decayed

away or are captured in some material in the system. Neutrons are removed from a system by getting captured in a detector tube, absorption in a surrounding material, and leakage from a system. The die away time in a system is represented by an exponential decay of the form: [10]

$$N(t) = N(0)e^{-t/\tau} \qquad 8$$

In equation 8, N(t) is a neutron population at time t and τ is a die away time, a mean lifetime in the system. Different systems have different size, shape, material composition, and efficiency. The AEFC system has a gate width of 128μsec, which is greater than the die away time of the AEFC system. Typically, most systems have die away time ranging 30 to 100 μsec.

The die away time of a detection system can be determined by the experimental measurements. It is done by measuring the same sample with the same settings and procedures except two different gate G_1 and G_2 where G_1 is half of G_2. Two coincidence rates R_1 and R_2 will be obtained corresponding to gate G_1 and G_2. The die away time is given by the equation 9 below. [7]

$$\tau = -\frac{G_1}{\ln(R_2/R_1 - 1)} \qquad 9$$

2.5. ROSSI-ALPHA DISTRIBUTIONS

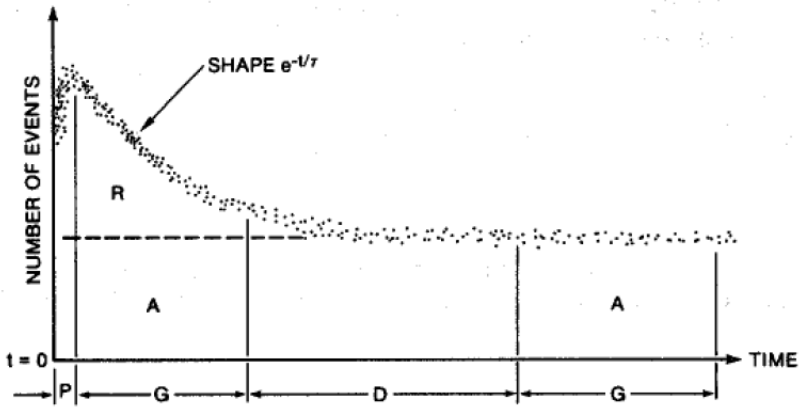

Figure 2-2: Rossi-Alpha distribution [10]

To explain coincidence counting, the Rossi-Alpha distribution should be well understood. Rossi-Alpha distribution is a probability distribution of the time interval between neutron pulses detected during the measurement process. Figure 2-2 demonstrates the Rossi-alpha distribution, where P is a pre-delay, G is a gate length, and D is a long delay gate. Neutrons produced in

induced fission event in the same fission chain in a fuel assembly are time correlated instead of random. The purpose of R-A distribution in the AEFC is to experimentally determine a probability distribution of detecting time correlated neutrons released from the same fission event. First neutron detected inside any of six ^{3}He detectors acts as a trigger and opens a time window. All neutrons detected within that specified time window are time correlated coincidences to the initial triggering neutron. Subsequently, each neutron after the first triggering, neutron triggers its own window of equal time length and thus a distribution is produced. If a random source (AmLi) is measured, a flat distribution will be obtained, but if a source that emits time correlated neutron (^{252}Cf) is measured, a distribution obtained will look like an exponential function. The distribution in figure 2-2 is described by the equation 10 below.

$$S(t) = A + Re^{-t/\tau} \qquad 10$$

Where A is accidental coincidences, R is real coincidence, and τ is the die away time. [7][10]

The accidental rate is proportional to the square of totals rate and is given by the equation 11.

$$A = GT^2 \qquad 11$$

In equation 11, G is a gate length and T is a totals rate. The totals rate consists of both accidental rates as well as real rates. [10]

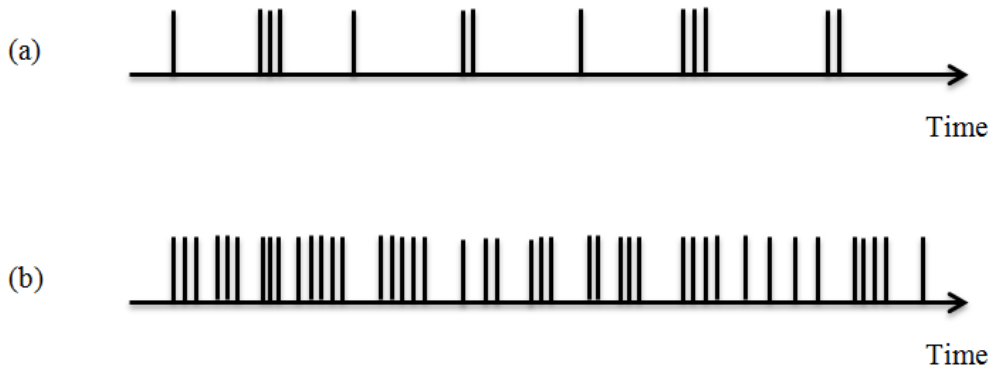

Figure 2-3: Neutron pulse train in a time axis. (a) Ideal pulse train (b) Actual pulse train [7][10]

Figure 2-3 represents a train of electronic pulses. The pulse train (a) represents an ideal pulse train that contains easily distinguishable correlated and uncorrelated pulse train events, however pulse train (b) is the real pulse trail that is obtained during the measurements. The case (b) is complex as correlated and uncorrelated events cannot be separated easily.

2.6. DETETOR DEADTIME MODELS

In a radiation detection system, a radiation is detected and converted to an electronic pulse. When a detector detects a pulse, it requires a small-time interval before it starts detecting again. This small-time interval needed to record two events as two different events is called detector dead time. Detector itself or the associated electronics such as preamplifiers, amplifiers, or ADC can be a source of the dead time. Any events in a detector during this dead time are lost. The dead time effect is higher when count rate is high, but when count rate is very small the dead time can be reduced to almost zero. Therefore, in high count rate scenario there can be a substantial loss of counts. There are models of paralyzing and non-paralyzing dead-time that can be used to determine the overall loss of counts in a detection system. [21]

In a gas detector, such as ^{3}He, dead time is due to a gas drift time i.e. intrinsic dead time. In electronics system, the dead time occur at two different phases:

- Shaping time required for amplifier
- Analog to digital conversion during data acquisition

All three stages, where dead times occur in a detection system are accounted for in the two dead time models. [21]

Figure 2-4 shows the regions where dead time can occur as discussed above. The detector detects a radiation and produces a small pulse which only last for a small fraction of second. The pulse is moved to the preamplifier where a long tail is added to the original pulse so that the information carried by the original pulse is not lost in the process. The output of the preamplifier which is a long tailed pulse is amplified and shaped by the amplifier. Finally, the analog output pulse from amplifier is converted to the digital logic pulse and counted in a counter or MCA. [21]

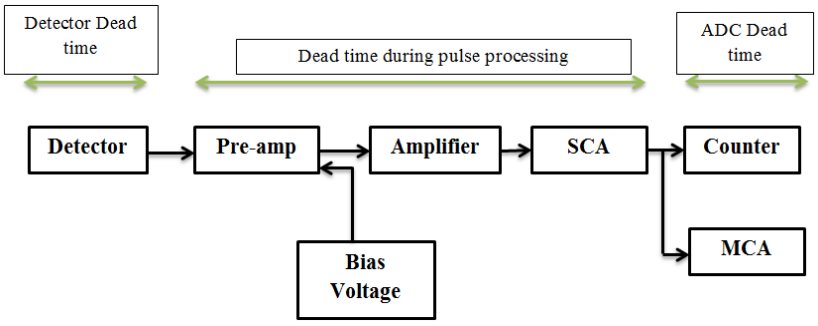

Figure 2-4: Typical block diagram of radiation detection system showing regions of possible source of dead time [21]

2.6.1. NON-PARALYZING DEADTIME

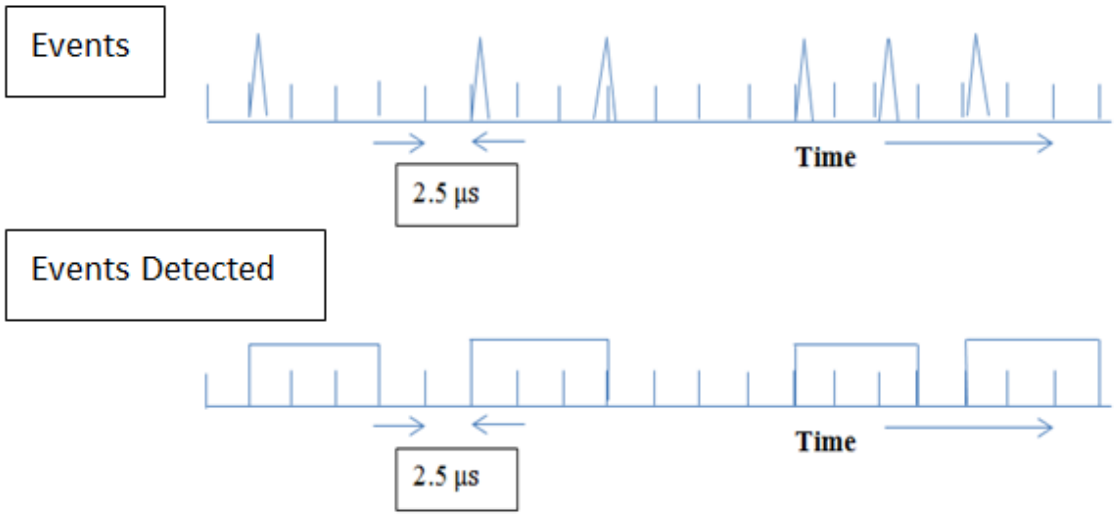

Figure 2-5: Non-Paralyzing dead time model describing events counted in a detection system for the dead time of 7.5 µs [9]

In the AECF, the dead time is non-paralyzing. Figure 2-5 is an example of how non-paralyzing dead time model works. The system represented by figure 2-5 has a dead time of 7.5µs, so the system is dead for a fixed time of 7.5 µs and then it starts registering events again. Mathematically, observed count rate (m) in non-paralyzing model is given by the equation 13.

$$\frac{m}{n} = 1 - m\tau \qquad 12$$

$$m = \frac{n}{1+n\tau} \qquad 13$$

Where n is an average true count rate and τ is a dead time of a detection system. The term $1 - m\tau$ represents the fraction of time when the system registered counts. [21]

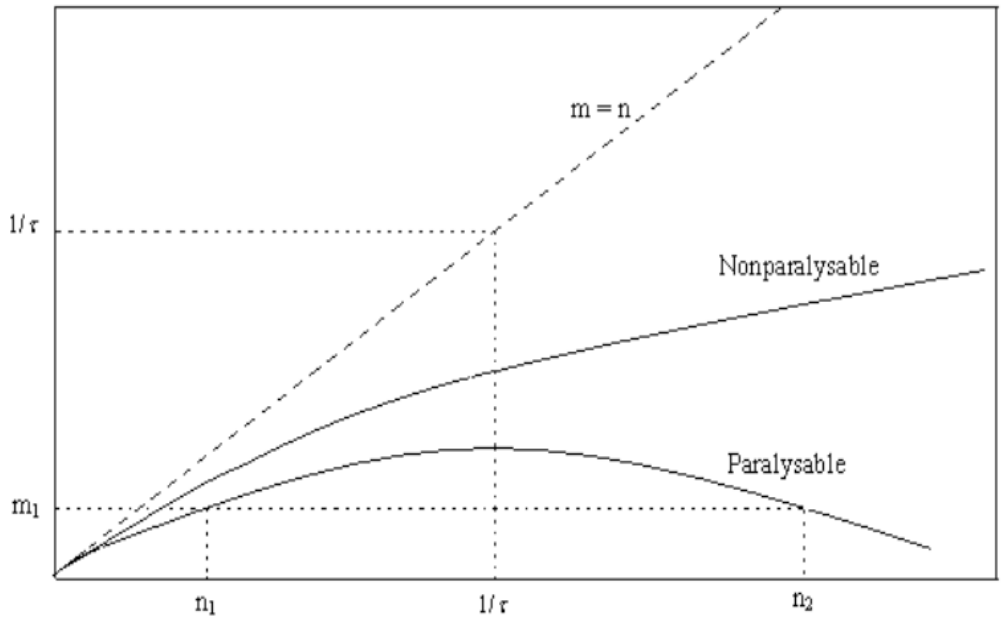

Figure 2-6: Comparison of paralyzing and non-paralyzing dead time for different count rates [21]

Figure 2-6 shows the behavior of paralyzing and non-paralyzing dead time models for different count rates. Initially, when true count rate is very small i.e. approximately zero both paralyzing and non-paralyzing models give same results, which is m=n. When true count rate starts increasing, non-paralyzing model results in more observed count rated than paralyzing model. At true count rate equals to $1/\tau$, paralyzing model gives its maximum observed count rate and starts decreasing. As true count rate passes $1/\tau$, observed count rate in non-paralyzing model increase however with the smaller rate compared to the count rate before the $1/\tau$. When the count rate is extremely high, paralyzing model do not record any events because a detection system will never get time to recover. [21]

2.7. NEUTRON MULTIPLICITY AND MULTIPLICITY COUNTING

Multiple neutrons and gamma rays are emitted in each fission reaction. Neutrons that are emitted within 4×10^{-14} seconds are prompt neutrons, while delayed neutrons are emitted roughly within tenth of a second of scission and these delayed neutron population is very small compared to the prompt neutron population. Neutron Multiplicity (ν) is defined as the average emission of neutrons during the fission event of some nuclide. Average number of neutrons emitted per fission event varies depending upon the isotope and it is distributed from 0 to 8 neutrons per fission. This neutron distribution is a multiplicity distribution that contains the sum

of 0, 1, 2, 3, 4, 5, 6, 7, 8, or more neutrons within the coincidence gate width. The multiplicity distribution of ^{252}Cf is shown in the figure 2.7 below. [14]

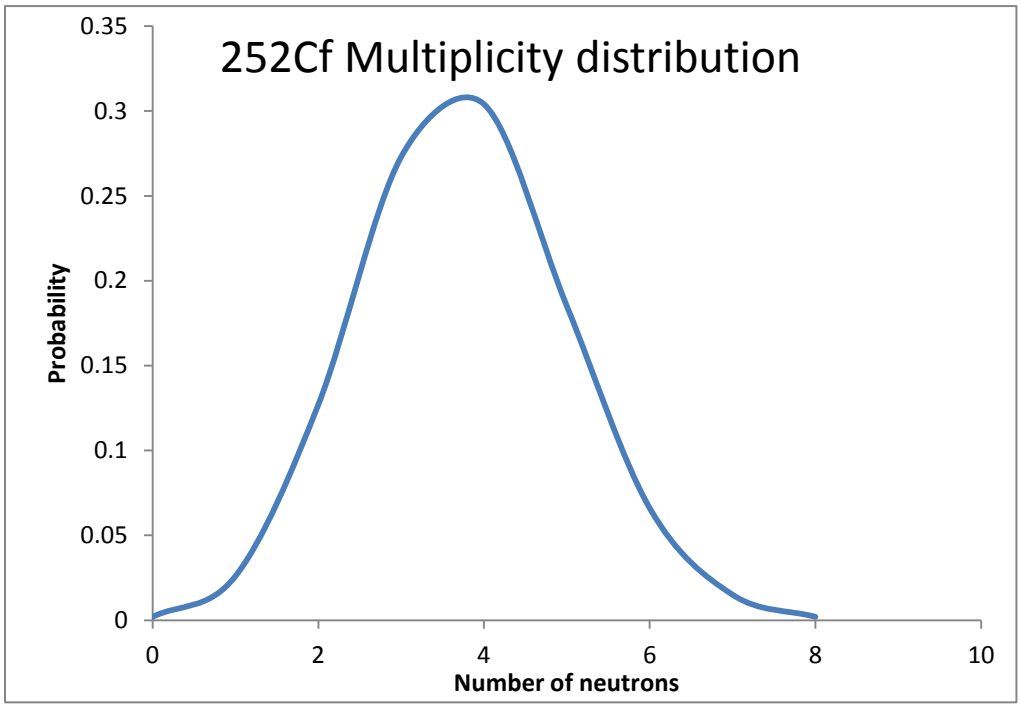

Figure 2-7: Multiplicity distribution of 252Cf [14]

Multiplicity is based on the factorial moments, where first moment yields singles, second moment yields doubles, and third moment yields triples, and so on. While coincidence counting deals with singles and doubles, multiplicity counting allows analyzing higher order moments such as triples, quads, and etc. Multiplicity counting is just an extension of coincidence counting to the collection of higher multiples of neutrons. Singles, doubles, and triples follow the following three equations 14, 15, and 16 given below. [7][10][12]

$$\text{Singles (S)} = F\varepsilon M\nu_1(1+\alpha) \qquad 14$$

$$\text{Doubles (D)} = \frac{F\varepsilon^2 f_d M^2}{2}\left[\nu_2 + (M-1)\frac{\nu_1\nu_2}{\nu_1-1}(1+\alpha)\right] \qquad 15$$

$$\text{Triples (T)} = \frac{F\varepsilon^3 f_t M^3}{6}\left[\nu_3 + (M-1)\frac{3\nu_2\nu_2+\nu_1\nu_3(1+\alpha)}{\nu_1-1} + 3\frac{(M-1)^2}{(\nu_1-1)^2}\nu_1(1+\alpha)\nu_2{}^2\right] \qquad 16$$

2.8. SELF SHIELDING

The material composition of MTR fuel is uranium Aluminum Alloy. The Uranium atoms in UAl are mostly ^{235}U and ^{238}U isotopes. ^{235}U and ^{238}U have high thermal neutron absorption cross section, which gives rise to the self-shielding inside the fuel assembly. The neutron flux in the fuel assembly gets reduced because of this self-shielding effect. When thermal neutrons pass through the fuel, some get absorbed inside the fuel and some get scattered before the rest escape from the fuel. ^{235}U has a high fission cross section along with the high absorption cross section in thermal region, therefore when it absorbs neutron it will either transmute to other nuclide or fission and produce some more neutrons, but ^{238}U has a very small fission cross section, so when it absorbs neutron mostly the neutrons are lost.

The research reactor fuel assemblies might contain different ^{235}U enrichment ranging from 10% to 93%. For the fuels that are enriched 10%, self-shielding is mostly by ^{238}U while some by ^{235}U. For the fuels that are enriched 93%, the self-shielding is just opposite i.e. mostly due to ^{235}U. Multiplication is significantly higher in a fuel with 93% enriched fuel compared to the 10% enriched because of the difference in ^{235}U mass. [7][13]

2.9. ^{252}CF SF SOURCE

SF occurs due to a quantum tunneling mechanism effect rather than by interacting with other neutrons like in IF. The nucleus gets to the scission point from its ground state by tunneling through the fission barrier. In this process, a heavy nucleus splits into two or more smaller fragments without any external impact, which is due to an opposition between the attractive nuclear forces and coulombic repulsive force. Nuclear force holds nucleons in the nuclei, whereas coulomb repulsion drives the protons apart. In case of lighter nuclei, repulsive Coulomb force is easily overwhelmed by a nuclear force, however in case of heavier nuclei, repulsive Coulomb force dictates over nuclear force, which is why SF occurs in heaver nuclei. [14]

In the AEFC, a SF source, ^{252}Cf, is used as an active interrogation source. ^{252}Cf is an actinide which emits in average of 2.34×10^{12} n/s per gram and decays with an effective half-life of 2.57 years. Since ^{238}U must undergo 14 transmutations to produce a ^{252}Cf isotope, very small amount is produced in a fuel. For example, about 0.025 grams of ^{252}Cf is produced by the Oak Ridge National lab every year from feedstock at Savannah River Site. Though the production is a small quantity, a very small amount of ^{252}Cf is enough to make a source. [18]

$$^{252}_{98}\mathrm{Cf} \rightarrow {}^{94}_{38}\mathrm{Sr} + {}^{154}_{60}\mathrm{Nd} + 3.76\mathrm{n} \qquad 17$$

Average number of spontaneous neutrons from ^{252}Cf is 3.76 neutrons and the average energy of the fission neutron spectrum is 2.3 MeV. The advantages of ^{252}Cf sources such as intense neutron concentration, long half-life of 2.57 years, higher average neutron yield of 3.76 neutrons per fission, substantial neutron output of 2.34×10^{12} n/s, and its availability makes it a very good candidate of being used as an active neutron source. [7][9]

2.10. AmLi, (α,n) NEUTRONS SOURCE

The AmLi (α,n) random source is used as active interrogation source in the AEFC. ^{241}Am in AmLi is a transuranic element or actinide, which is produced during a transmutation of ^{238}U isotope in a nuclear fuel. Over the time there is a buildup of Plutonium-241 in a burned fuel. ^{241}Pu decays with a half-life of 14.4 years to produce ^{241}Am whose half-life is approximately 432.7 years. ^{241}Am then decays to neptunium-237 by emitting an alpha particle with an average energy of 5.46 MeV. ^{237}Np is stable as it decays very slowly with a half-life of 2 million years. When ^{241}Am can be combined with lighter elements such as lithium (Li) or beryllium (Be) to produce neutrons. [15]

$$^{241}_{95}\mathrm{Am} \rightarrow {}^{237}_{93}\mathrm{Np} + {}^{4}_{2}\alpha + \gamma(59.54\ \mathrm{KeV}) \qquad 18$$

$$^{4}_{2}\alpha + {}^{7}_{3}\mathrm{Li} \rightarrow {}^{1}_{0}\mathrm{n} + {}^{10}_{5}\mathrm{B} + \mathrm{Q(value)} \qquad 19\ [15]$$

It is difficult to obtain AmLi in the US because it contains lithium which is highly flammable. In case there is fire due to lithium, it can cause serious contamination of radioactive ^{241}Am.

2.11. TCIF EFFECT IN THE AEFC WITH ^{252}CF

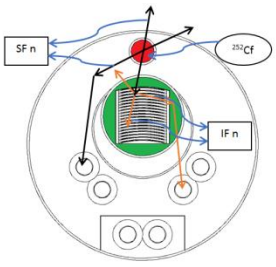

(a)

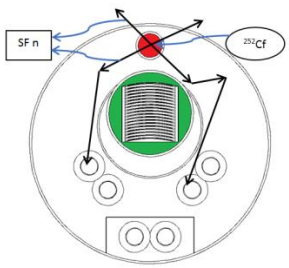

(b)

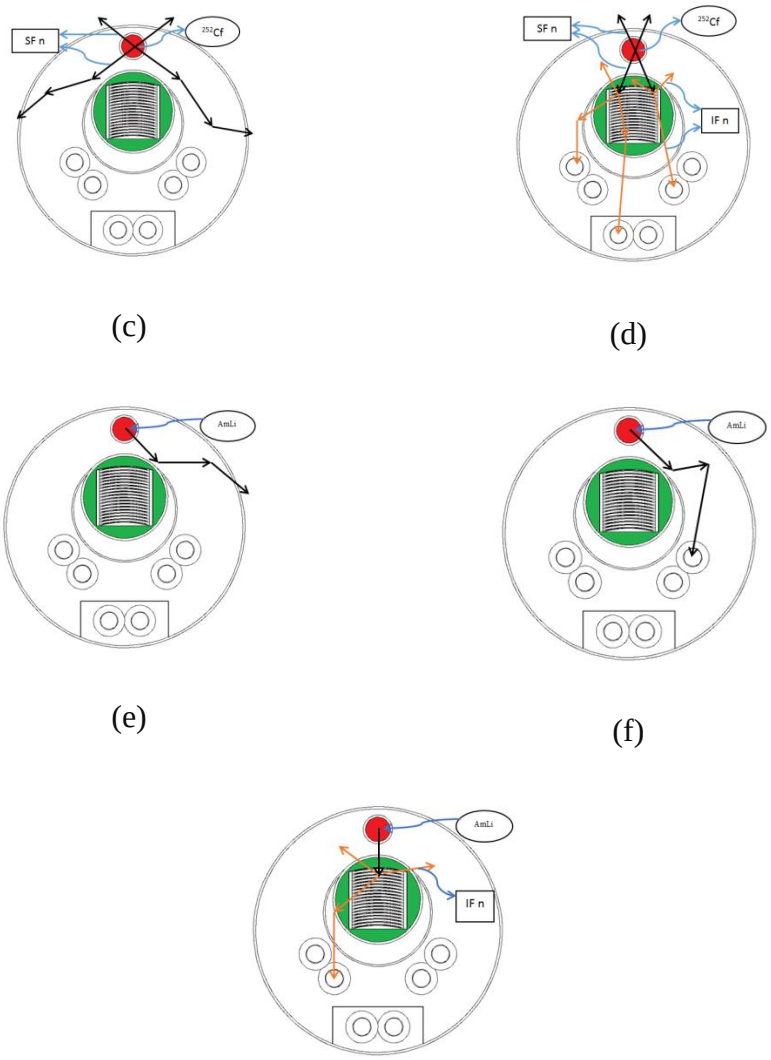

Figure 2-8: Possible neutron detection scenarios in the AEFC with ^{252}Cf and AmLi active sources.

In the figure 2-8, part a shows SF neutrons both being detected and inducing fission in the fuel, causing a boost in coincidences due to the TCIF effect. Part b shows none of the 4 neutrons from SF getting absorbed in a fuel. In this case the doubles rate is due to the neutrons from SF. Part c shows all neutrons from SF event escape the system, hence no counts registered. Part d shows another coincidence boost due to the TCIF effect in ^{252}Cf. Part e shows an (α,n) neutron escaping the system resulting in no detections. Part f shows a neutron from AmLi

undergoing multiple scattering events before being detected. Part g shows a neutron detected from an IF event caused by an AmLi source neutron.

TCIF term was brought up by Dr. Howard Menlove at the LANL. [18] The TCIF effect is related to the neutrons emitted in IF event from the fuel assembly to the neutrons produced in a precursor fission event in an active interrogation source. When ^{252}Cf is used as an active interrogation source, the trigger event to start coincidence gate can be caused either due to the IF neutron from the fuel or SF neutron from the active source. The multiplicity (ν) in ^{252}Cf is 3.76 and multiplicity in IF is 2.44, therefore the combined multiplicity is much higher when ^{252}Cf is used compared to the combined multiplicity with AmLi (α,n) source. When an effective multiplicity increases, the coincidence rates such as doubles increase as well. [18]

Also, the TCIF measurements in the AEFC depend on the coupling probabilities between the active source, fuel assembly, and the six ^{3}He detectors. Coupling between active source and fuel sample resulting in IF (P_1), at least one neutron from IF is detected in any of the six ^{3}He detectors (P_2), and finally the active source background getting detected in any of the six 3He detectors (P_3) are the three coupling probabilities that makes up the combined probability in the AEFC. P_1 is a function of effective fission cross section, distance between active source and the fuel, and HDPE moderator, P_2 depends on the detector efficiency to detect neutrons induced from the fuel, and P_3 depends on the detector efficiency to detect neutrons from the active source. These coupling probabilities P1, P2, and P3 are very low in the AEFC. The combined probability determines the extent of coincidence rate boost due to the TCIF effect. Even though the coupling probabilities between the three regions are very low, in average, the measurements result with ^{252}Cf is expected to show significant increase in the doubles rate compared the doubles rate when AmLi source is used. [18] Table 3 and 4 show the efficiencies and coupling probabilities of the AEFC. The values were calculated by using MCNP results.

The experimental measurements show the efficiency of active source background for ^{252}Cf and AmLi to be 0.94% and 0.59%. With the fuel assembly included in the AEFC, efficiency of net IF with AmLi changes to 1.19%, while 0.987% for ^{252}Cf. The reason behind lower efficiency for AmLi active background might be due to the over moderation of low energy AmLi neutrons causing less numbers of neutron reach detectors. Higher efficiency for AmLi IF might be due the under moderation for the neutrons to reach fuel assembly. Even though AmLi produced 1.21 times higher number of IF events in the fuel than ^{252}Cf, ^{252}Cf provided higher

number of doubles count rates. This proves that the boost in the doubles count rate is due to boost in combined multiplicity of IF+SF due to the TCIF effect described by the figures 2-8(a) and 2-8(b). [7][12][18]

2.12. UNCERTAINTY PROPAGATION

In radiation measurements, the total uncertainty in the measurement should account for uncertainties in both the source and background. In the AEFC coincidence measurements, background uncertainty comes from active source neutrons and room background neutrons. [9][7]

In case of the AEFC measurements, net singles and doubles are calculated as,

$$S_{net} = S_{active} - S_{background} \quad (20)$$

$$D_{net} = D_{active} - D_{background} \quad (21)$$

Active background rates are combination of the room background and the background from the source with no fuel present:

$$S_{background} = S_{room} + S_{active\ source} \quad (22)$$

$$D_{background} = D_{room} + D_{active\ source} \quad (23)$$

The uncertainty in the active background singles and doubles count rates are given by:

$$\sigma^2_{S_{active\ background}} = \sigma^2_{S_{active\ source}} + \sigma^2_{S_{room\ background}} \quad (24)$$

$$\sigma^2_{D_{active\ background}} = \sigma^2_{D_{active\ source}} + \sigma^2_{D_{room\ background}} \quad (25)$$

The uncertainty in the net active singles and doubles count rates are given by:

$$\sigma^2_{S_{net}} = \sigma^2_{S_{active\ fuel}} + \sigma^2_{S_{background}} \quad (26)$$

$$\sigma^2_{D_{net}} = \sigma^2_{D_{active\ fuel}} + \sigma^2_{D_{background}} \quad (27)$$

3. MECHANICAL DESIGN, DATA ACQUISITION, MEASUREMENT PROCUDERES

3.1. MECHANICAL DESIGN

The AEFC system is an underwater measurement system, therefore it is watertight. It consists of 6 ^{3}He neutron detectors, a gross gamma-ray counter (ion chamber), high-density polyethylene (HDPE) moderator, and lead shielding inside the cylindrical stainless steel casing. It has a 117-mm diameter throughput-hole for fuel assemblies. A funnel placed on top of the

throughput-hole helps guide assemblies to the desired measurement position. Interrogation source hole lies on the one side of the throughput hole, whereas the neutron and gamma detectors are placed on the opposite side behind the crescent shaped lead shielding. Six boron-lined ^{3}He detector tubes at 4 atm of gas pressure are each surrounded by a 10-mm-thick lead sleeve and HDPE moderator. The ion chamber is positioned on top of the HDPE behind the lead shielding with a collimator hole. The wiring of AEFC such as from detectors, preamplifiers, and HVPS passes through the waterproof Tygon tube. The interrogation source is confined inside a HDPE holder and connected to a Teleflex cable. Interrogation source is moved into and out of the AEFC through a PVC guide tube that runs from the AEFC to the top of the spent fuel pool. [6]

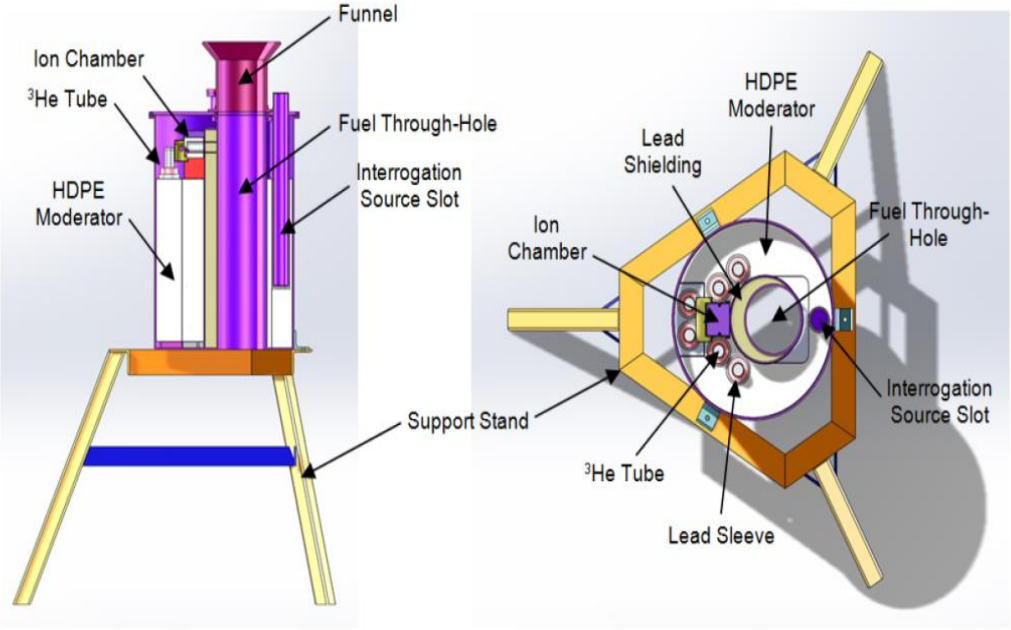

Figure 3-1: Mechanical design of the AEFC. [6]

Figure 3.-1 provides a visual representation of the AEFC system. Picture on the right is a top view of the system in which location of six ^{3}He detector, an ion chamber, crescent shaped lead shielding, lead sleeve, fuel through hole, and interrogation source slot can be seen. The picture on the left shows side view of the system. This view shows the axial dimensions and location of the material. The figure 3-2 below is top view of the AEFC when MTR fuel assembly is inserted inside the fuel through hole.

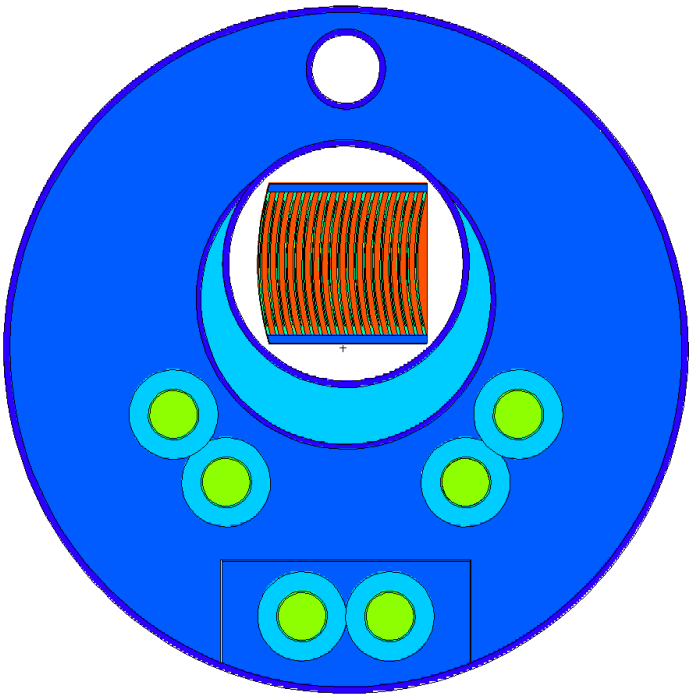

Figure 3-2: Picture of fresh MTR assembly inside the AEFC generated from MCNP plotter

3.2. DATA ACQUISITION

AEFC was placed inside a water tank that had a water level of approximately 117 cm from the base of the water tank. High voltage (HV), pre-delay, and gate were set to 1680V, 4.5µsec, and 128µsec. Neutron data was collected in a JSR shift register. The shift register data was then collected in a laptop and analyzed in "Rates Only" mode using IAEA Neutron Coincidence Counting (INCC) software to obtain the singles and doubles count rates. Although there is a gross gamma counter inside the AEFC system, gamma measurements were not performed. [6]

3.3. EXPERIMENTAL MEASUREMENT MEDHODOLOGY

Since a complete fuel assembly scan was desired, the measurements were started by putting the 108 cm long MTR fresh fuel assembly (L-108) completely inside the fuel throughput hole such that the bottom of assembly touched the bottom base of water tank. ^{252}Cf, an active interrogation source, was placed inside the source slot. Since the L-108 fuel assembly was too long, a full assembly scan was not performed. As the top of the He-3 detector was at 80.34 cm from the base of the tank, only 80.34 cm of the fuel assembly could be scanned. With 25.34 cm length of ^{3}He detectors, center of theses detectors lies 67.67 cm above the base of the water tank.

The starting point of scan in case of fuel assembly L-108 was at approximately 16.60 cm in a fuel active region. This implies that only approximately 44 cm of active fuel length out of 60 cm and 24 cm of bottom empty region could be scanned.

The fuel assembly has small holes approximately 3 cm below the top in an inactive region, which is often used to handle the fuel assembly by using either positioning jig or a string. In this experiment, a string was tied to the assembly using these holes. Since the movement of assembly was vertical, a hook of crane was placed some distance above the assembly. The hook of a crane was tied on both sides of a tank by using ratchet belt so that the hook would remain fixed during the entire experiment. A pulley was designed by moving the string from the top of hook to the clamp attached on the side of the water tank top. A string was pulled to its maximum stretch while the assembly was still touching the base of the tank. A measuring stick was used to mark 3 cm apart 23 steps. 23 separate 1 minute measurements were recorded with the 3 cm increment each time from the base of the tank. The active region of a fuel assembly was pulled out of the AEFC and with this setup 5-minute background Count Rate of ^{252}Cf and AmLi active interrogation sources were recorded separately. One of the objectives of this experiment was to perform three-point scan of a fuel assembly, but the length of L-108, 108 cm, made it impossible to measure the top third of the assembly at the center point of the active region of the detectors. Therefore, only middle and bottom scans were performed for this type of assembly.

The assembly was raised 13.64 cm above the base by using the same marking method. By raising the assembly by 13.64 cm the center of assembly aligned with the center of ^{3}He detector. In this center position, 10 min measurements were recorded separately with ^{252}Cf and AmLi sources. The assembly was rotated by 90 degrees and a measurement was recorded with the ^{252}Cf source. With the same orientation, the assembly was pulled 18 cm axially above the middle point and measurements was repeated and recorded for 10 minutes each.

Next, the 108.26 cm long L-108 MTR fuel assembly was replaced by the 90.48 cm long O-187R MTR fuel assembly. The bottom of this type of MTR assembly has approximately 18 cm less inactive region, therefore with this type of fuel it was possible to make a 3-point scan in the AEFC. The middle point of the active region was at 31.32 cm above the base, while the top and bottom were 18 cm up and down axially from the middle point.

The same process was used to mark the string as was used in the case of assembly L-108. 10 minute measurements of top, middle and bottom of active fuel assembly were recorded with

^{252}Cf source, while the middle scan with AmLi was performed overnight, approximately 13.322 hours. With ^{252}Cf source and fuel assembly rotated by 90 degrees, 10 minute measurements of middle part were recorded. To see the effects in TCIF with closer source-sample coupling, the ^{252}Cf source was placed in a fuel throughput hole aligned at the center of fuel assembly and ^{3}He detectors. With this setup, 10 minute measurements of middle part of the fuel assembly were taken. Finally, the fuel assembly was pulled out of detector region and with the ^{252}Cf source still inside fuel throughput hole, and active background measurements were recorded.

A separate measurement campaign was performed in which an aluminum fuel plate holder was fabricated to carryout measurements with varying ^{235}U mass. In this measurement campaign, a different ^{252}Cf source (A7869) with strength of 1.71E+05 n/s was used. Fuel plate configurations are shown in figure 3-3.

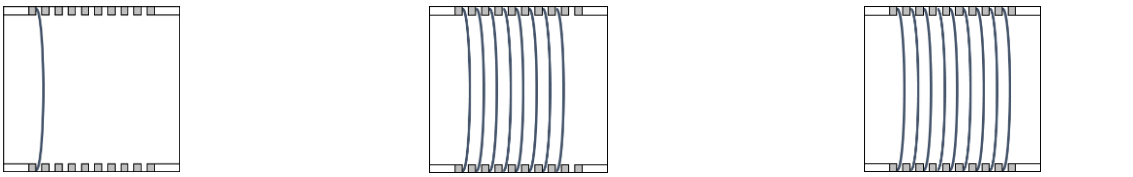

(a) 1 plate configuration (b) 8 plates configuration (c) 9 plates configuration

Figure 3-3: Varying Fuel plates in a fuel holder

Once again the experimental measurement started with the 20-minute measurement of new ^{252}Cf source to obtain a new ^{252}Cf background. The fuel plate holder was lowered into the water tank inside the AEFC fuel through hole. Three-point scan of the various numbers of fuel plates in a plate holder was performed. For middle measurement, axial center of fuel plates in the holder were all aligned with the axial center of ^{3}He detectors. For top and bottom measurements, the fuel plates were shifted 18cm up and down respectively axially. Singles and doubles of 20 minute measurements were recorded.

3.4. MCNP SIMULATION METHODOLOGY

The MCNP set was replicated as the experimental setup described in section 3.3.

3.4.1. FULL ASSEMBLY MCNP SETUP

As in the section of the experimental setup, all simulations were carried out using a "full MTR assembly" as shown in Figure 3-4a. The schematic showing the "full assembly" setup with the AEFC detector system is shown in Figure 3-5. The axial setup shown in Figure 3-5(b) is referred to as the "midpoint" configuration, in which the base of the fuel assembly is 13.67 cm from the inner base of the tank. In this "midpoint" configuration, the midpoints of ^{3}He detectors in AEFC aligned with the midpoint of the fuel assembly. The following scans were performed for the full assembly setup:

a. The Californium source was placed inside the source hole, and a measurement was performed using the "midpoint" configuration as shown in Figure 3-5(b).

b. The Californium source was placed inside the source hole, and a measurement at 18 cm above the "midpoint" configuration was performed.

c. The Californium source was placed inside the source hole, and fuel was lowered 13.67 cm from the "midpoint" configuration. Subsequently, 23 measurements with a 3 cm increase with each subsequent measurement took place.

d. The Californium source was placed inside the source hole, and a measurement was performed using the "midpoint" configuration as shown in Figure 3-5. The fuel assembly, however, was rotated 90 degrees in a counter-clockwise motion prior to the measurement occurring.

e. The Californium source placed inside the fuel hole at the same height as the source hole, and a measurement was performed using "midpoint" configuration as shown in Figure 3-5.

f. The AmLi source was placed inside the source hole, and a measurement was performed using the "midpoint" configuration as shown in Figure 3-5(b).

g. Finally, with the full assembly at mid-point configuration, simulations were performed with different ^{235}U enrichments.

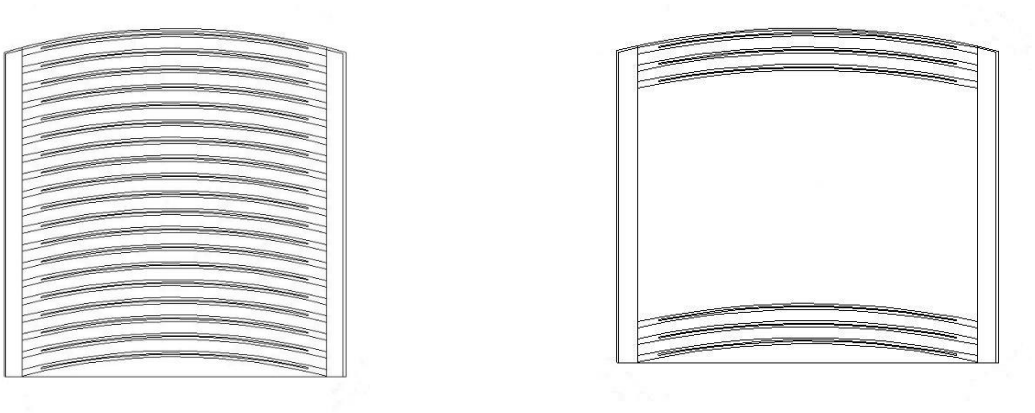

(a) MTR Full Assembly (b) MTR Partial Assembly

Figure 3-4: Radial depiction of the "full" and "partial" MTR assemblies generated from MCNP plotter.

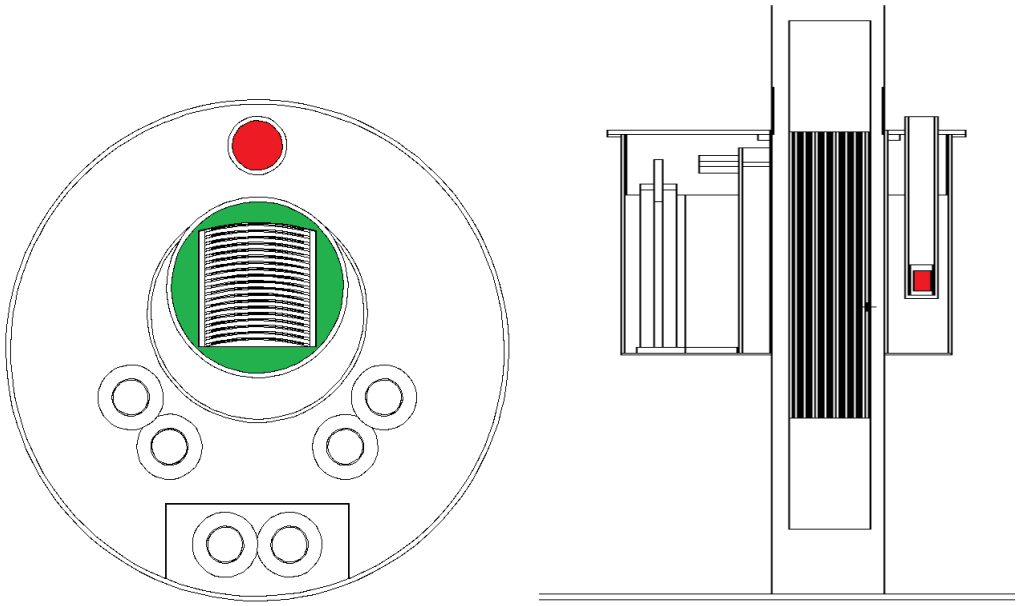

(a) Radial view (b) Axial view

Figure 3-5: The combined MTR Fuel assembly and AEFC experimental setup obtained from MCNP plotter. In the radial view, the source hole is colored red, and the fuel hole is colored green. The axial configuration shows the position of MTR assembly in the "midpoint" configuration.

3.4.2. PARTIAL ASSEMBLY MCNP SETUP

In the section of the experimental setup, all simulations were carried out using a "partial MTR assembly" as shown in Figure 3-4b. The following scans were performed for the full assembly setup:

a. The Californium source was placed inside the source hole, and a measurement was performed using the "midpoint" configuration as shown in Figure 3.5(b).

b. The Californium source was placed inside the source hole, and measurement at 18 cm above the "midpoint" configuration was performed.

c. The Californium source was placed inside the source hole, and a measurement at 18 cm below the "midpoint" configuration was performed.

d. The Californium source was placed the inside source hole, and a measurement was performed using the "midpoint" configuration as shown in Figure 3-5(b). The fuel assembly, however, was rotated 90 degrees in a counter-clockwise motion prior to the scan occurring.

e. The AmLi source was placed inside the source hole, and measurement was performed using the "midpoint" configuration as shown in Figure 3-5(b).

4. FRESH MTR FUEL, MATERIAL USED, AND SOME KEY DIMENSIONS

4.1. FUEL ASSEMBLY L-108

- Fuel assembly total length of 108.27 cm
- Active length of 60 cm in the middle of the assembly
- 24.13 cm of empty region in the both sides of the assembly

4.2. FUEL ASSEMBLY O-187R

- Total length of 90.48 cm
- Active length of 60 cm
- 24.13 cm of empty region in the top of the assembly
- 6.35 cm of empty region in the bottom of the assembly

4.3. MATERIALS USED

The following materials were used to complete AEFC fresh MTR fuel experiments at LANL:

- Clean AEFC system
- Water tank in high bay
- Crane in high bay for moving AEFC system
- ^{252}Cf (A7866)- 45670 n/s
- ^{252}Cf (A7869)- 170,695 n/s
- AmLi (N-165) – 37940 n/s
- JSR-15 shift register
- Laptop with INCC
- L-108 and O-187R, MTR type fresh fuel assemblies

4.4. KEY DIMENSIONS

a) Height of the AEFC is 112.1 cm from top of the funnel to the inside base of the water tank
b) Water depth of 117 cm
c) Center of He-3 detector to the base of the water tank is 67.67cm
d) Position of interrogation source at 67.67 cm from the base
e) Diameter of fuel through hole is 11.7 cm
f) Length of ^{3}He detector is approximately 25.34 cm

(a) AEFC System used in the Experiments [23]

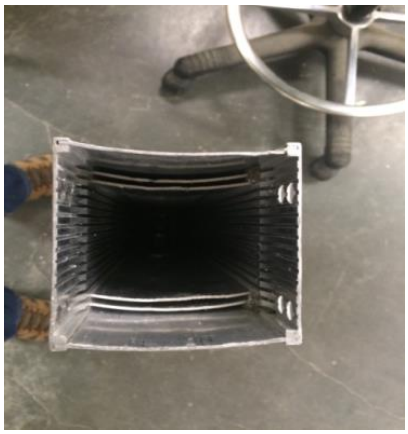

(b) MTR Half Assembly O-187R

(c) AEFC System inside the water with MTR Fuel Assembly from previous experiment [24]

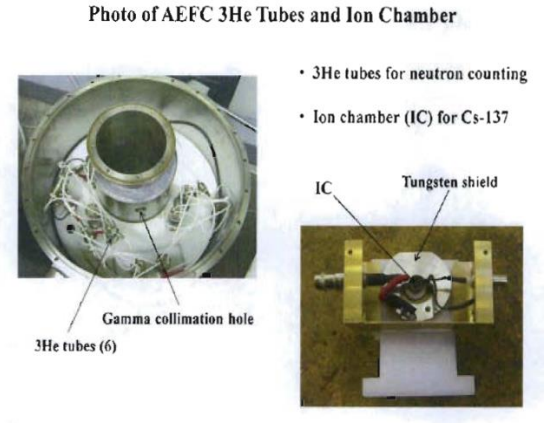

(d) AEFC internal components [24]

Figure 4-1: Pictures of the AEFC and its internal components and the fresh MTR fuel Assembly used in the experiments

5. EXPERIMENTAL RESULTS AND ANALYSIS

Since the source strengths of AmLi (N-165) and ^{252}Cf were approximately 37,940 n/s and 45,670 n/s at the time of experiments on 9/21/2016, the source strength of ^{252}Cf is 1.204 times higher than the AmLi source. All AmLi measurement count rates are normalized to the ^{252}Cf count rates by multiplying AmLi count rates by 1.204. The source strength of second ^{252}Cf (A7869) source was approximately 170,695 n/s, which is 3.7376 times the strength of first ^{252}Cf (A7866) source. The measurement results with A7869 source are normalized to the A7866 source strength by dividing A7869 results by 3.7376.

The results and analysis section starts with the benchmarking of full and partial assemblies. Then, the AEFC calibration is presented. The calibration section will contain singles and doubles count rates versus mass of ^{235}U. Then, a section will show the comparison of singles and doubles count rates due to ^{252}Cf and AmLi sources with a justification of the boost in doubles rate due to TCIF effect when ^{252}Cf source is used.

5.1. FULL ASSEMBLY (L-108) BENCHMARK

The L-108 MTR fresh fuel assembly was measured in 3 cm increments along the active length axially. The singles and doubles from the experiment are compared with singles and doubles from the MCNP simulation in Figure 15.

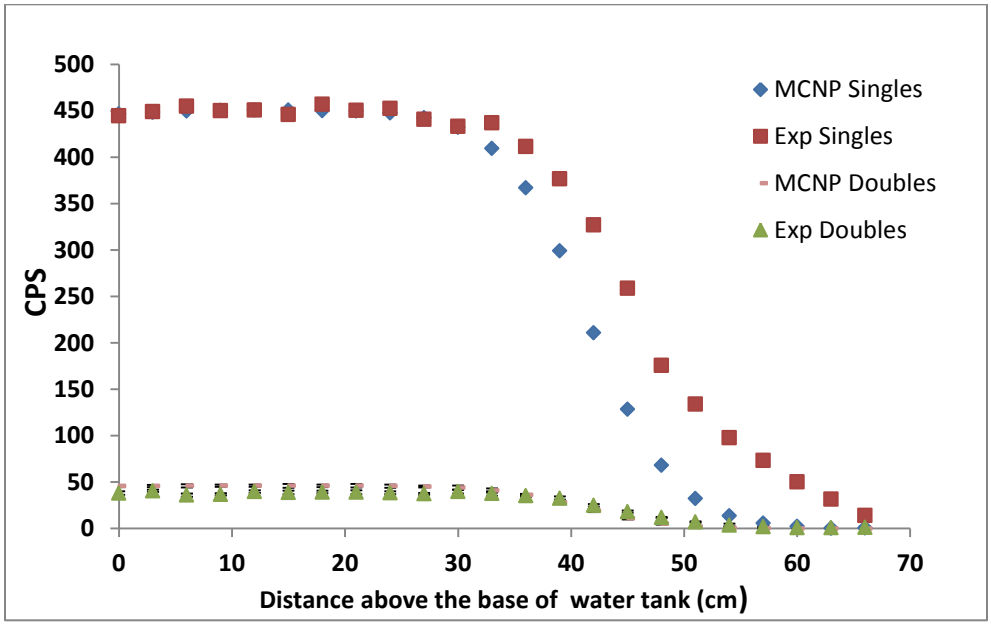

Figure 5-1: L-108 scan with ^{252}Cf SF source

When the fuel assembly L-108 is 0 cm above the base of a water tank, the center of the ^{3}He detector and interrogation source is aligned at 16cm below active fuel region from the top. Therefore, only 44 cm of active region can be scanned. Figure 5-1 shows singles and doubles count rate drop after the assembly was raised 36 cm above the base, and at approximately 44 cm above the base count rates are halved from the peak rates. ^{3}He detectors in the AEFC do not have collimators, which mean a larger region of the fuel is measured than just what is aligned with the active center of the detectors. The interrogation source is isotropic and the fuel assembly is inserted inside the AEFC in an axial direction inside the fuel through hole as shown in figure 3-5(b). Therefore, neutrons in the middle point measurement will not only come from exact middle point of an active fuel region but also from some length up and down axially. The singles and doubles profiles are flat from 0 cm to 33 cm in this region because there is enough active fuel region on either side in axial direction of the point of measurement. After reaching 36 cm

increment, both singles and doubles started decreasing, while at 44 cm increment the count rates are dropped to half of the maximum. From this point forward, each time the assembly was drawn 3 cm up, 3 cm of active length was replaced by 3 cm of inactive aluminum and water. At 44 cm above the base, there was active fuel region only on the top half from center of ^{3}He detector and inactive region (aluminum or water) on the bottom half, which is the reason for the half of maximum count rate at this point. Figure 5-1 also contains MCNP results. MCNP singles and doubles rates agree with the experimental singles and doubles rates within 10 percent and 20 percent respectively up to the 30-cm increment measurement point. After 30cm of measurements, MCNP and experimental singles and doubles start diverging. The reasons for this divergence could be many, such as no room background in MCNP results which has a larger effect in this region due to the decreased count rate overall, human errors while marking the string and pulling the fuel assembly into position, and overstretch of the string resulting in a different region of the fuel measured in the experiment than what was modeled in MCNP. The results are diverging at the end of fuel assembly, where there is very small amount of fuel meat in the line of sight of the source.

The MCNP results closely matched the experimental results for the two-point scan of the full assembly. The mid and bottom point measurements are 13.67 cm and 31.67 cm above the bottom of the active region of the fuel; the MCNP singles and doubles count rates agree with the experimental singles and doubles count rate within 3% for singles and 17% for doubles at these points. The figure 5-2 and 5-3 show the experimental and MNCP comparison of singles rates and doubles rates of 2-point scan of the full assembly L-108.

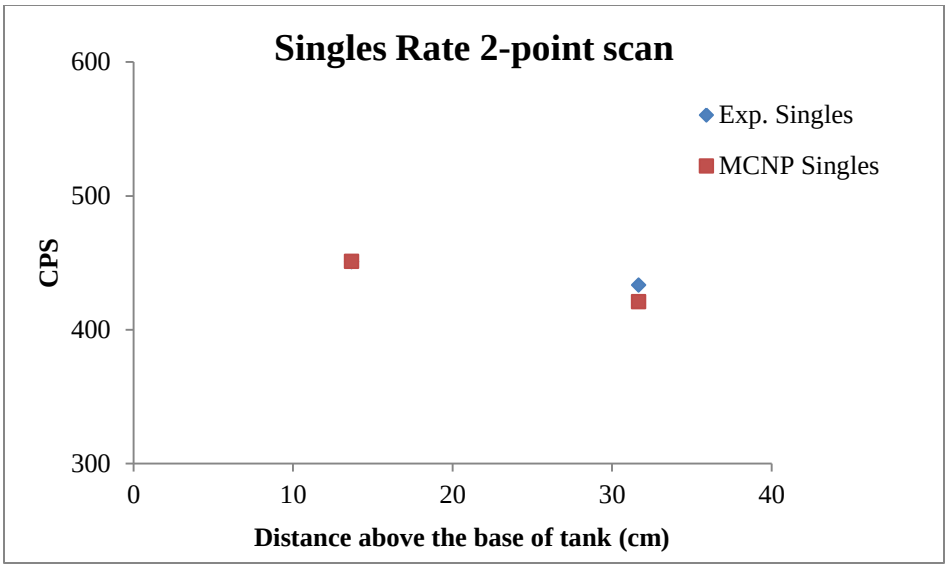

Figure 5-2: Singles results comparison of two-point scan of full assembly (L-108)

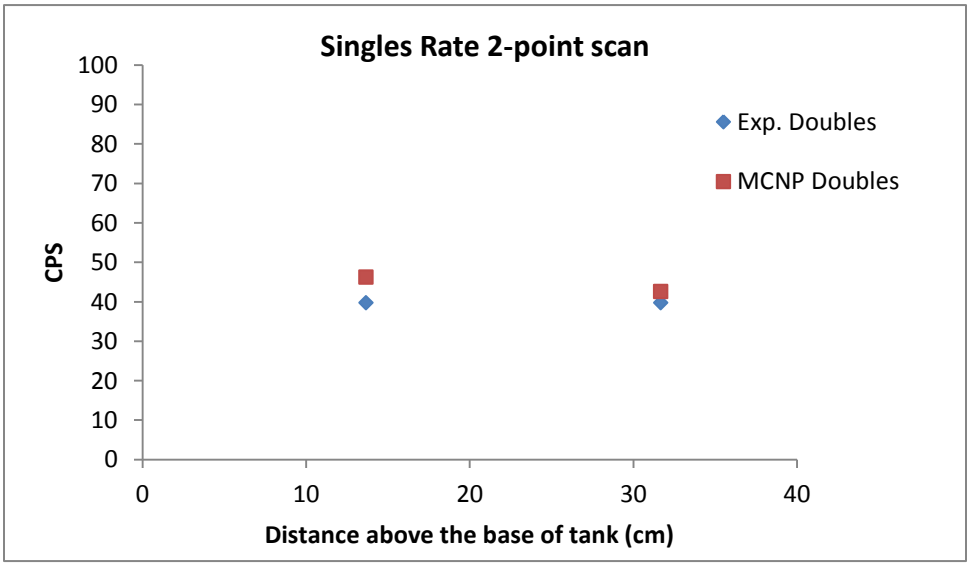

Figure 5-3: Doubles results comparison of two-point scan of full assembly (L-108)

Figure 5-4 and 5-5 are enlarged version of figure 5-1 to show the singles count rates with the error bars. Figure 5-4 shows singles rates up to 39 cm increment and figure 5-5 shows beyond 39 cm. Figure 5-6 is zoomed to display doubles count rates of figure 5-1 along with the error bars. It looks like experimental measurements might have shifted 3 cm to the right due to

the errors in handling fuel assembly. Experimental and MCNP results agree better when experimental results are adjusted 3 cm to the left as shown in figure 5-7.

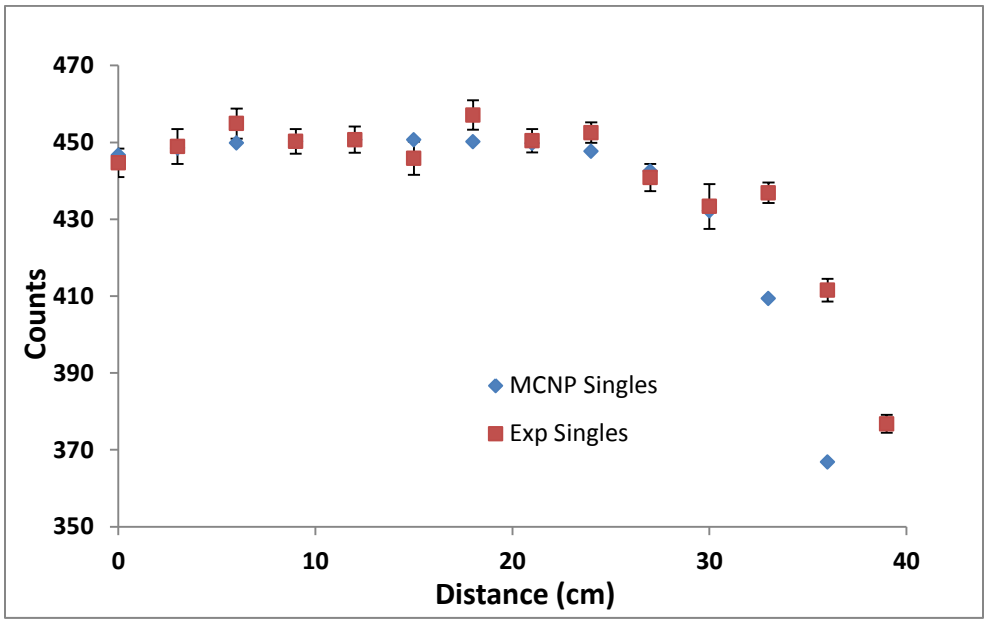

Figure 5-4: Magnified version of figure 5-1 showing singles rates up to 39 cm increment

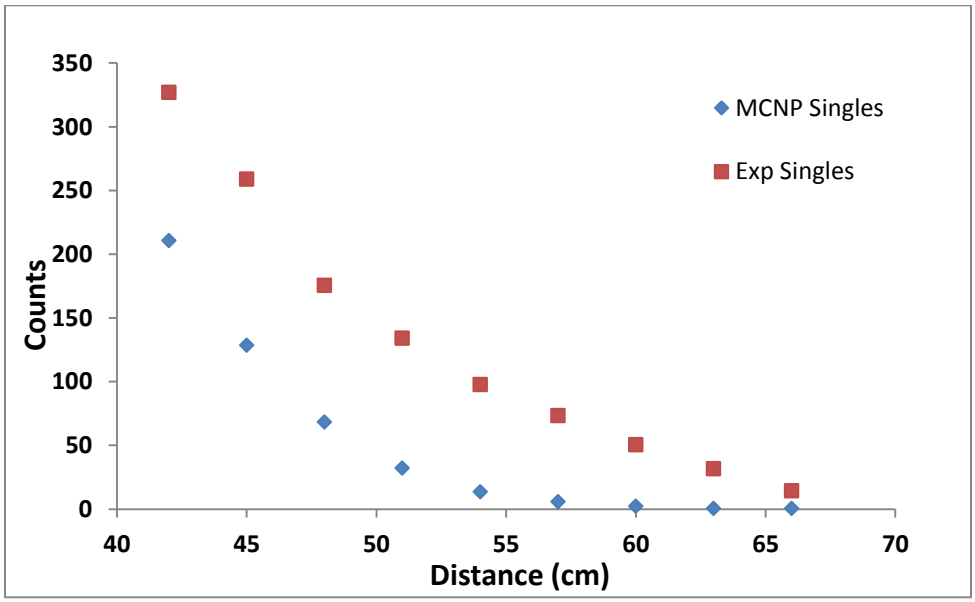

Figure 5-5: Magnified version of figure 5-1 showing singles rates beyond 39 cm increment

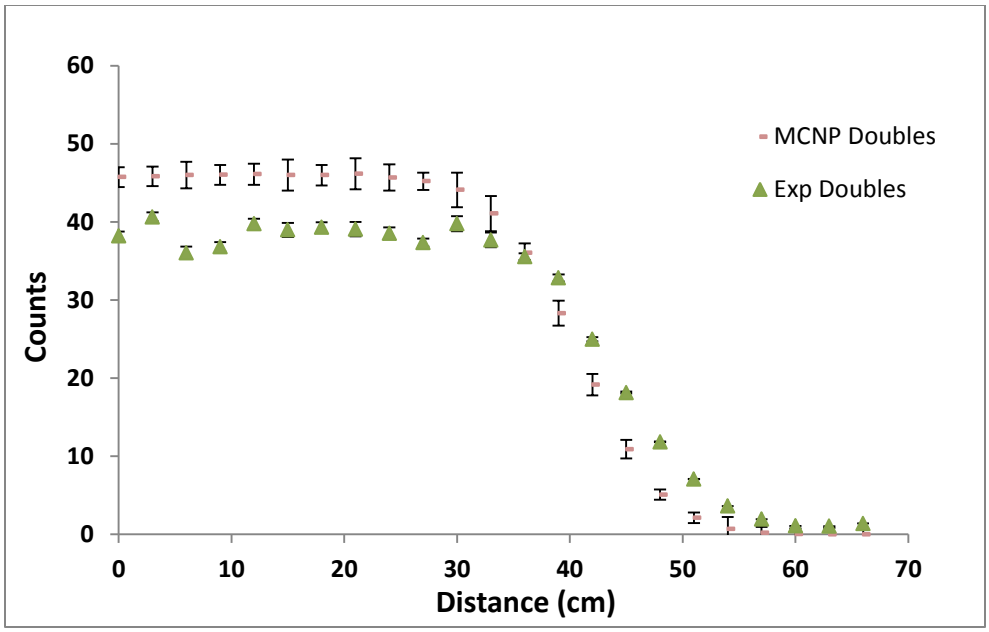

Figure 5-6: Magnified version of figure 5-1 showing doubles rates

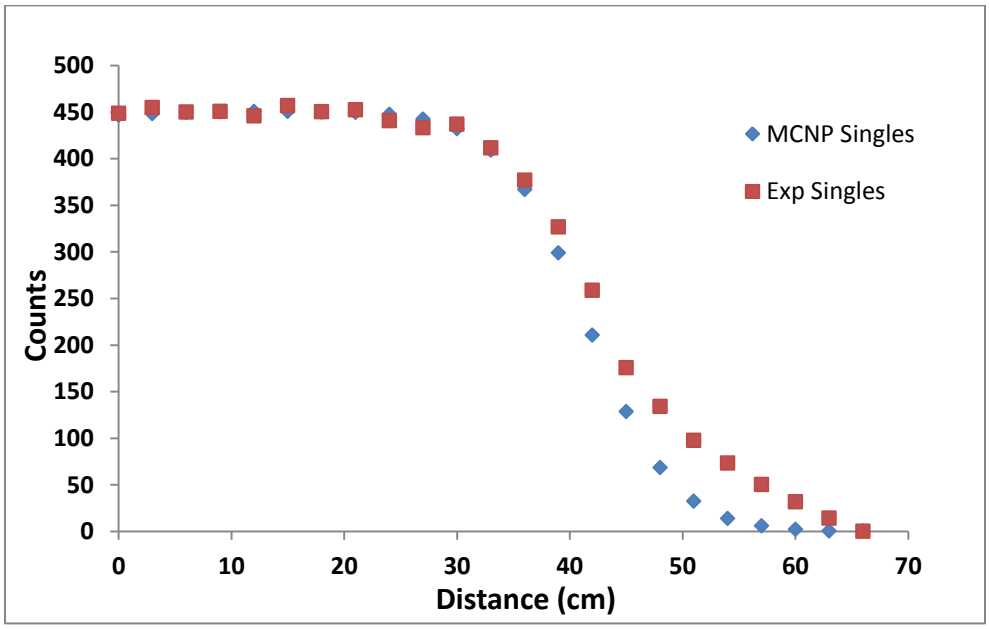

Figure 5-7: MCNP results compared to the Experimental results shifted by 3 cm to the left

5.2. PARTIAL ASSEMBLY (O-187R) 3- POINT SCAN

A three-point scan was also taken of the partial assembly, O-187, with only six fuel plates. The net singles and doubles count rates, or count rates with active background subtracted, are given in Figures 5-8 and 5-9. In these figures the experimental net count rates are also compared with the MCNP net count rates.

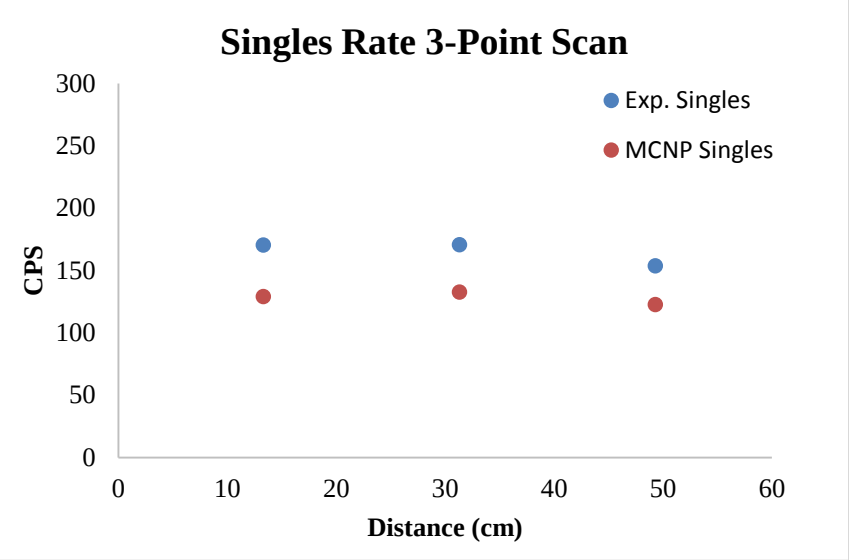

Figure 5-8: Comparison of MCNP and Experimental 3-point scan singles count rates of partial assembly

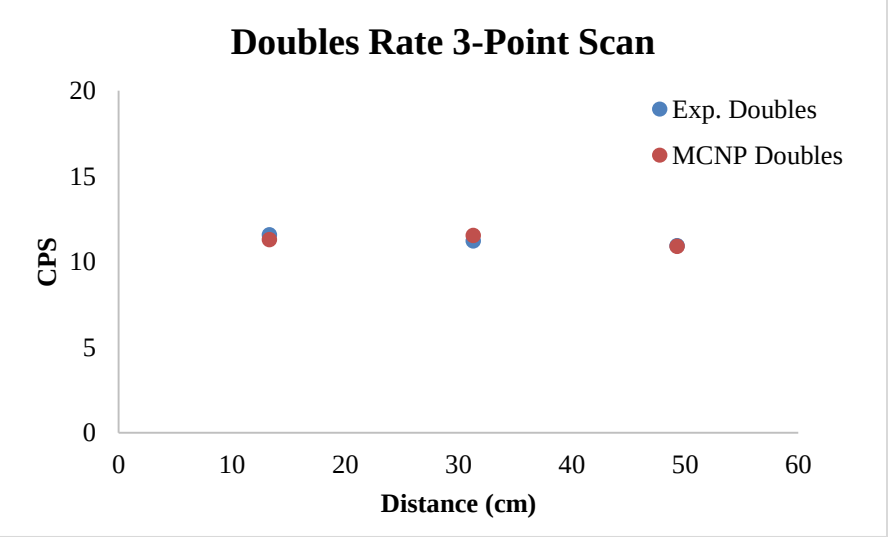

Figure 5-9: Comparison of MCNP and Experimental 3-point scan doubles count rates of partial assembly

Figure 5-8 and 5-9 show benchmarking of partial assembly in which MCNP singles are within 20-25% agreement while doubles are within 3% agreement with experimental results.

5.3. AEFC CALIBRATION

Figures 5-10 and 5-11 show comparisons of MCNP and experimental net singles and doubles count rates versus residual fissile mass (^{235}U) in the fabricated fuel plate holder varying from 0 plates to 9 plates, full L-108 assembly varying fuel plates from 4 to 19, and full L-108 assembly varying enrichment from 19 to 93.5 percent. Measurements are taken with the midpoint of the assemblies aligned with the midpoint of the active region of the ^{3}He detectors axially. The experimental points below 150 g of uranium are from the fabricated fuel plate holder and the point above 200 g of uranium is from the L-108 assembly. In all cases, the active background is subtracted.

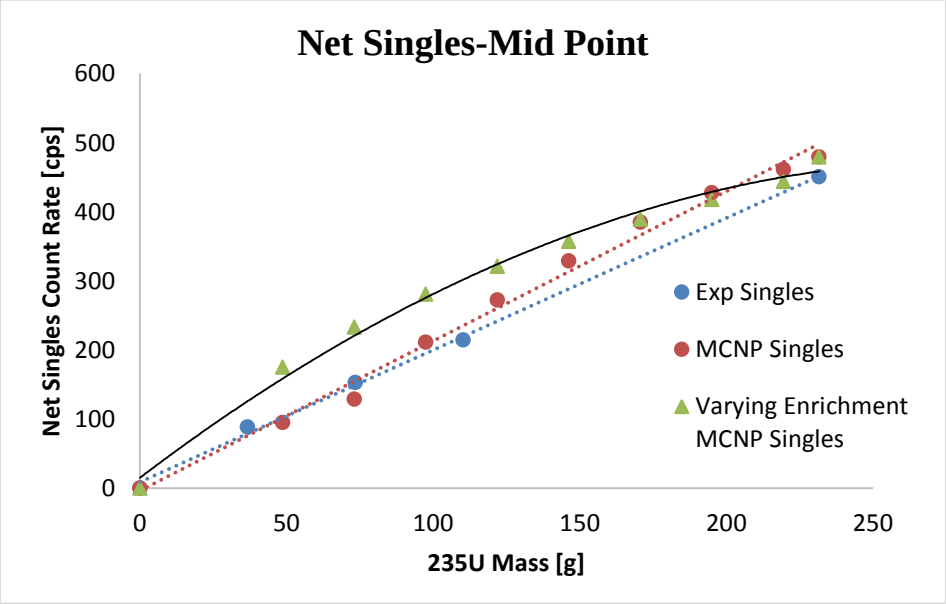

Figure 5-10: Calibration of singles count rates versus residual fissile mass of ^{235}U

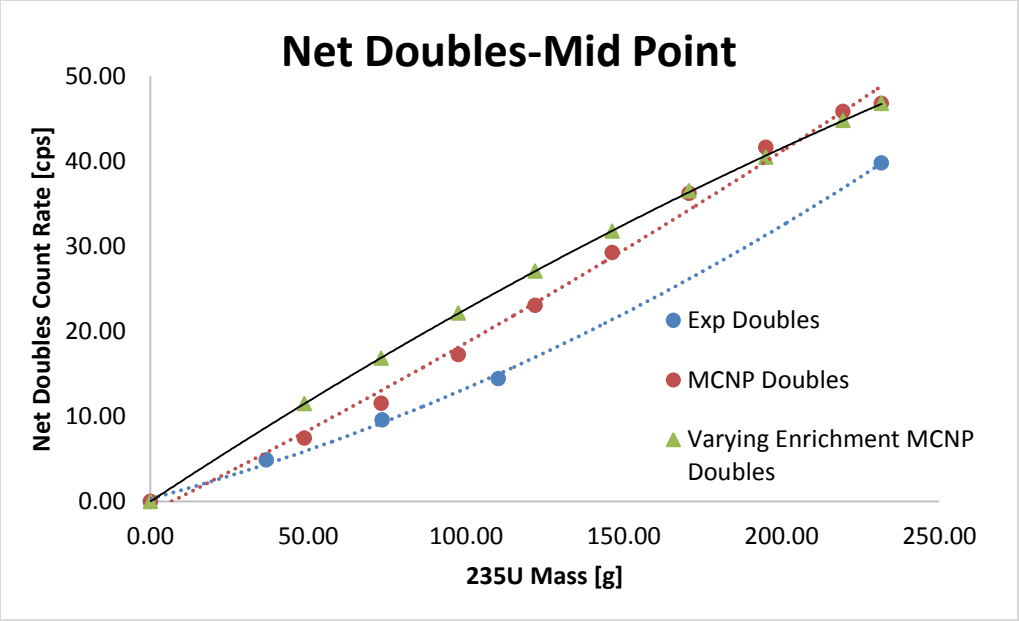

Figure 5-11: Calibration of doubles count rates versus residual fissile mass of ^{235}U

To verify residual fissile mass using an active interrogation source is one of the primary objectives of this research. The figure shows count rates change in two different scenarios, (1) change in count rates vs residual fissile mass when two fuel plates are removed in each steps. In this scenario, initial ^{235}U remains the same while residual fissile mass changes due to the removal of fuel plates. This will cause over moderation of either neutrons from the active source or neutrons from the IF depending on which side of the assembly the fuel plates are removed. Also, in this case ^{238}U content remains the same, around 7%, which has negligible effect. The second scenario (2) is change in count rates vs residual fissile mass when enrichment is changed. This case is more realistic to the IAEA non-proliferation safeguards for the verification process. In this scenario, the number of fuel plates remains the same but residual fissile mass changes. Each time the enrichment decreases, ^{238}U content increases. When ^{235}U mass decreases, there is less IF resulting in lower count rates. In figures 5-10 and 5-11, count rates with varying ^{235}U and ^{238}U content are higher compared to the constant enrichment; this is because when fuel plates are removed, IF neutrons cannot thermalize and propagate fission chains as easily as when the fuel plates all remain in place and close together. In the case of constant enrichment, singles are following a linear trend and doubles are following a convex 2nd degree polynomial, while in the case of varying enrichment the singles and doubles are following concave 2nd degree polynomial.

While the physical MCNP models for constant and varying enrichments contained the same ^{235}U mass, enrichments were different. This means the varying enrichment fuel has lower ^{235}U density compared to the constant enrichment until the ^{235}U reaches to the mass of 231 grams. At lower ^{235}U density in the fuel, varying enrichment case shows less self-shielding due to ^{235}U thermal neutron absorption not resulting in fission when compared to the higher enrichments. The self-shielding is mostly due to the ^{235}U in HEU fuels, while in LEU self-shielding is mostly by the ^{238}U. Thermal neutron absorption cross section of ^{235}U is approximately 35 times the thermal neutron absorption cross section of ^{238}U. Therefore, if the enrichment changes, self-shielding effect also change significantly. This might also be one of the reasons for higher singles and doubles count rates by varying enrichment case than constant enrichment before reaching to 93% enrichment. At 93% enrichment both cases have the same count rates because the two setups (varying fuel plate number and varying enrichment) are exactly the same for a full assembly.

Additional fuel assembly configurations were considered in simulation space as they could not be constructed in the lab with the experimental resources available. A three-point scan of a set of simulated assemblies with varying numbers of fuel plates from 4 to 19 was conducted in MCNP and compared to the average of the three points. Results are given in Figures 5-12 to 5-15.

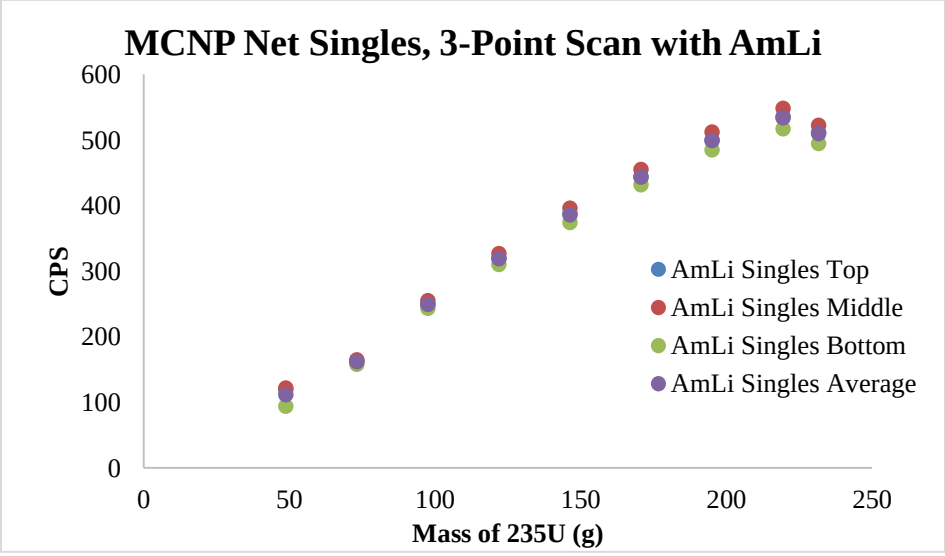

Figure 5-12: MCNP 3-point scan singles count rates versus mass of ^{235}U with AmLi source

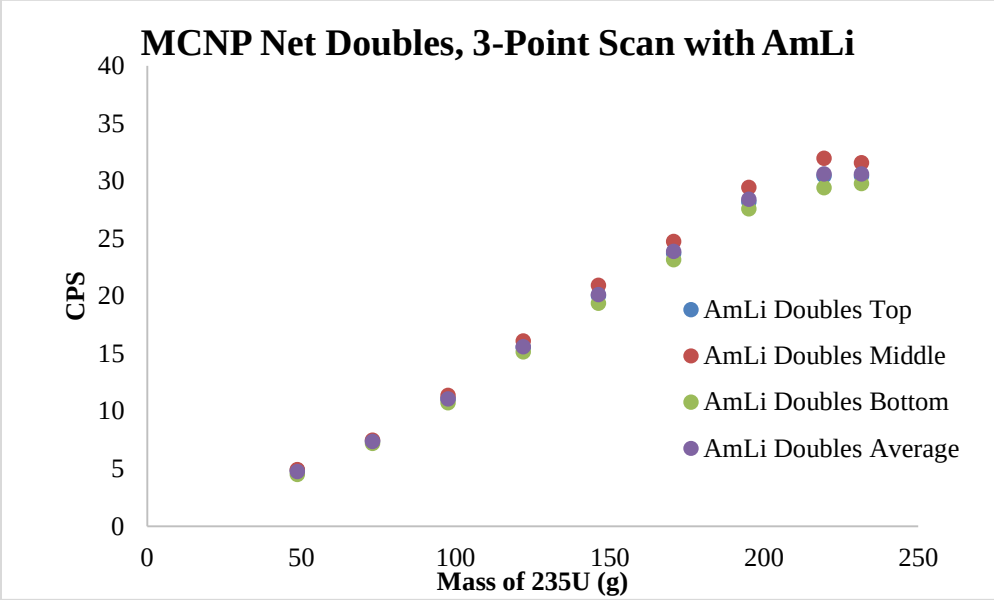

Figure 5-13: MCNP 3-point scan doubles count rates versus mass of ^{235}U with AmLi source

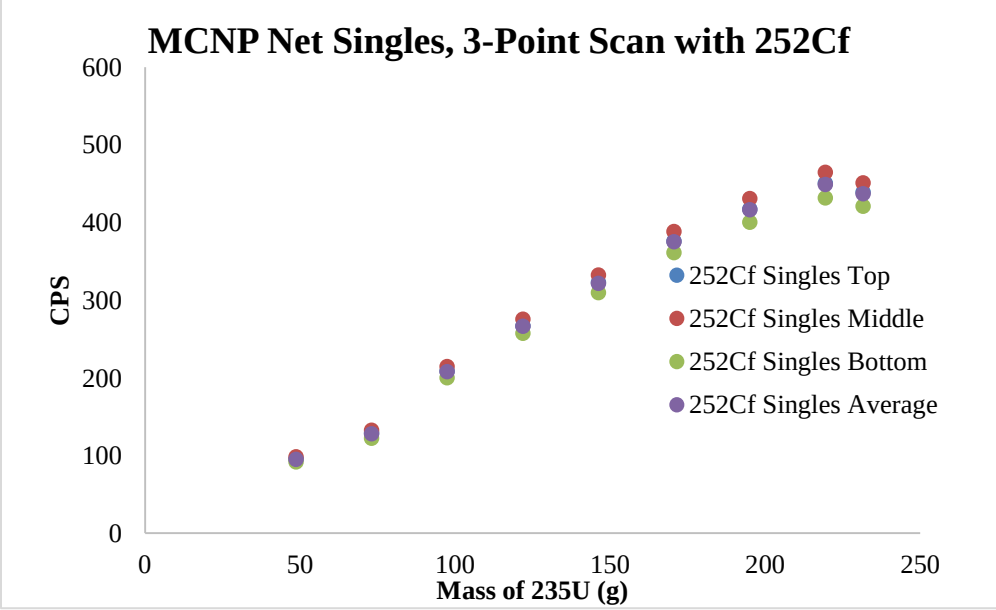

Figure 5-14: MCNP 3-point scan singles count rates versus mass of ^{235}U with ^{252}Cf source

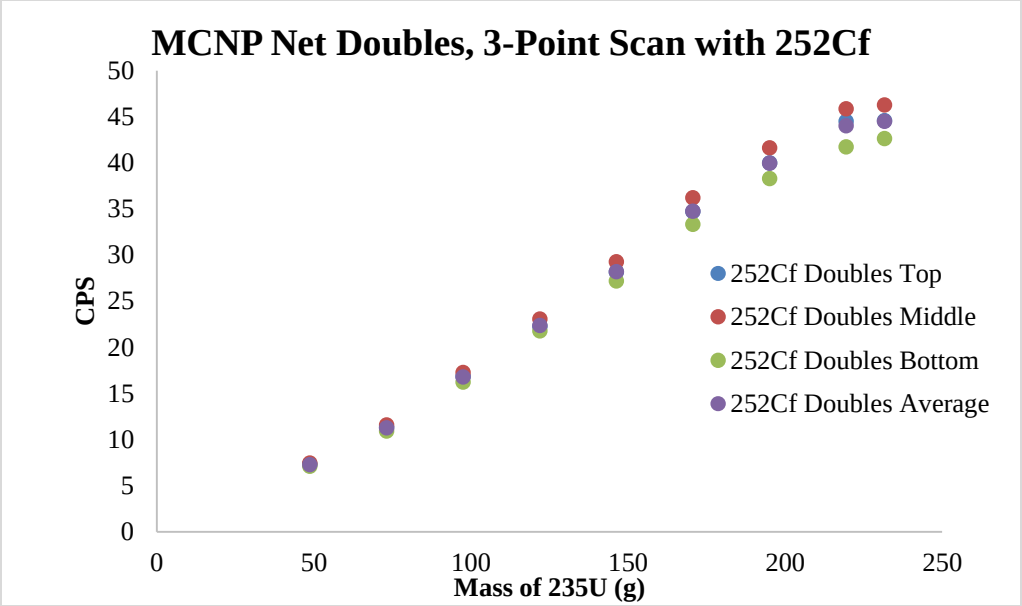

Figure 5-15: MCNP 3-point scan doubles count rates versus mass of ^{235}U with ^{252}Cf source

Figures 5-12- 5-15 show the comparison of singles and doubles count rates of three-point scan with the average of scan in simulation space. Since the fuel under investigation was fresh fuel, it had homogenously distributed ^{235}U content. Thus, top, middle, and bottom measurements count rates are very close to each other. If instead the fuel under investigation was burned/used fuel, we could have seen higher count rate in top and bottom while relatively very low count rate in the middle due to the higher residual fissile mass remaining at the ends compared to the middle. MCNP results show that for the same fissile residual mass, normalized singles count rates with AmLi are approximately 20 percent higher than with ^{252}Cf, while normalized doubles count rates are around 30 percent lower. In the table 5-1, experimental results of full assembly show that the singles are higher and doubles are lower by approximately 22 percent and 14 percent respectively with AmLi compared to the results with ^{252}Cf. In the case of partial assembly (O-187R), the singles count rate is approximately 14 percent higher with AmLi while doubles count rate is around 13 percent higher with ^{252}Cf.

Table 5-1: Comparison of singles and doubles with ^{252}Cf and AmLi in full assembly (L-108) and partial assembly (O-187R)

Full Assembly (L-108)			
AmLi		^{252}Cf	
S	D	S	D

544.08±1.39	32.78±0.38	442.98±1.84	38.20±0.68
Partial Assembly (O-187R)			
AmLi	252Cf	AmLi	252Cf
S	D	S	D
198.24±0.81	9.90±0.16	170.54±1.68	11.21±0.47

5.4. ^{252}Cf RATES COMPARISON

One of the objectives of this research was to investigate the effects of change in geometry of fuel assembly to the singles and doubles count rates. Mid-point configuration measurements were performed with the 90 degrees rotated assembly along with the original configuration described in section 5.1 and 5.2. Table 5-2 shows count rate comparisons between a mid-point measurement with ^{252}Cf and the mid-point measurement with fuel assembly rotated by 90 degrees.

Table 5-2: Comparison of count rates when geometry of fuel assembly is changed

	Singles	Doubles
Exp Original Configuration	450.71±3.41	39.78±1.34
MCNP Original Configuration	451.00±0.16	46.25±1.26
Exp 90 deg rotated Configuration	427.35±1.95	38.38±0.69
MCNP 90 deg rotated Configuration	375.35±0.16	40.31±1.28

In the measurements, singles rate decreased by 5.18 percent, while doubles rate decreased by 3.52 percent when the fuel assembly was rotated by 90 degrees. Figure 3-2 in section 3.1 provides a visual representation of 90 degrees rotated MTR fuel assembly set up. In the MCNP simulation results, singles rate decreased by 16.77 percent and doubles rates decreased by 13.43 percent when assembly was rotated by 90 degrees. For original configuration, singles rates agree within 1 percent and doubles rate agree within 17 percent, while for 90 degree rotated configuration singles rate agree within 13 percent and doubles rate agree within 6 percent. Although MCNP singles rate and doubles rate agreement with in 20 percent with the experimental measurement is good, the discrepancies in the benchmarking of singles and doubles might be due to the handling of fuel assembly while rotating. In MCNP, once geometry was created it remained fixed however in the experiment the fuel assembly was suspended in water

supported by a thin string. The assembly might have moved by some angle to cause the difference.

5.5. TCIF JUSTIFICATION

When source strengths of active sources AmLi and ^{252}Cf are normalized, IF rates provide interesting results. Table 5-3 shows the comparison of singles and doubles IF rates (i.e. count rates with active background subtracted) with AmLi and ^{252}Cf active interrogation sources.

Table 5-3: Comparison of experimental count rates per source strength with Amli and ^{252}Cf sources

	AmLi, N-165	^{252}Cf, A7-866
Singles IF/Source	1.19E-02	9.70E-03
Doubles IF/Source	7.18E-04	8.36E-04

The singles IF rate per source neutron with AmLi is 1.228 times the singles IF rate due to ^{252}Cf, because the lower energy of neutrons emitted from AmLi source have more chances to get absorbed into the fuel element. The doubles IF rate per source neutron with ^{252}Cf is 1.176 times the doubles IF rate due to AmLi, because the ^{252}Cf source produces time correlated neutrons. If the TCIF effect of ^{252}Cf source could be eliminated, AmLi source would have resulted in higher singles and doubles count rates because of the low energy of neutrons from AmLi compared to the ^{252}Cf. For example, if each neutron emitted from ^{252}Cf SF could be treated independently and separated in time to replicate the AmLi random neutron emission, the AmLi source would have a higher doubles count rate along with the higher singles count rate. With the TCIF effect, an actual boost in doubles count rate due to the ^{252}Cf source should be more than more than 1.176 times. Table 5-4 provides doubles IF rate to singles IF rate ratio for AmLi and ^{252}Cf.

Table 5-4: Experimental doubles IF to singles IF ratio for AmLi and ^{252}Cf sources

Source	Doubles IF/Singles IF
AmLi, N-165	6.03E-02
^{252}Cf, A7-866	8.62E-02

Net doubles to net singles ratio with ^{252}Cf is 1.431 times higher than the net doubles to net singles ratio with AmLi source. With AmLi source, on average, 16.595 singles are needed for each doubles count, but with ^{252}Cf only 11.596 singles are needed for each doubles count. The same effect can be considered in MCNP as shown in Tables 5-5 and 5-6.

Table 5-5: Comparison of MCNP count rates per source strength with Amli and ^{252}Cf sources

	AmLi, N-165	^{252}Cf, A7-866
Singles IF/Source	1.14E-02	9.88E-03
Doubles IF/Source	6.91E-04	1.01E-03

Table 5-6: MCNP Doubles IF to singles IF ratio for AmLi and ^{252}Cf sources

Source	Doubles IF/Singles IF
AmLi, N-165	6.02E-02
^{252}Cf, A7-866	1.01E-01

MCNP simulation results in table 5-5 and 5-6 show similar results to the experimental results shown in Tables 4 and 5. Here, net doubles to net singles ratio with ^{252}Cf is 1.7 time higher than with AmLi source.

6. CONCLUSION AND FUTURE WORK

The objectives of this research were to benchmark MCNP simulations using experimental results, to generate count rates versus residual fissile mass calibration curves with ^{252}Cf active source, to investigate the effects of change in fuel assembly geometry and source location to the count rates, and finally show the boost in doubles count rates (coincidence rates) when ^{252}Cf is used in lieu of AmLi active source. Section 5.1, 5.2, and 5.3 of results and analysis section show the benchmarking of experimental results. In section 5.1, MCNP simulation results show the benchmarking of singles and doubles count rates of full assembly within 10% and 20% respectively. Section 5.2 shows the benchmarking of singles and doubles count rates of partial assembly within 25% and 3% respectively. Section 5.3 shows calibration curves of count rates versus residual fissile mass with ^{252}Cf active source, where singles rate and doubles rate agree

within 10% and 20% respectively. Section 5.4 shows significant change in the count rates due to the change in the fuel assembly geometry. Experimental and MCNP simulation results show significant increase in singles count rate when the fuel assembly was rotated by 90 degrees. But, only MCNP simulation results show increase in doubles count rate. Section 5.5 shows higher IF singles and lower IF doubles per source with AmLi compared to ^{252}Cf. IF doubles to IF singles ratio is 1.431 times higher when ^{252}Cf is used compared to the AmLi source. This results from the boost in doubles count rate when ^{252}Cf is used. The reason behind this is that the time correlated SF neutrons emitted by ^{252}Cf source, which causes time correlated IF events in the fuel, result in additional coincident events from neutrons in the same fission chain. Even though the lower energy of AmLi neutrons have higher probability to get absorbed into the fuel assembly compared to the higher energy neutrons from ^{252}Cf, the results show higher coincidence count rates with ^{252}Cf source. This proves that the boost in coincidence counting with ^{252}Cf source is due to the TCIF effect.

It would be interesting to perform experimental calibration of AEFC with the fresh fuel containing higher percentage of ^{238}U- with the varying ^{235}U enrichment. The AEFC could be calibrated with the burned fuel containing various concentrations of fission products. Calibrations of AEFC with MTR fuel with various burnup, cooling time, and initial enrichment. Also, comparison of AEFC calibration with fresh fuel and spent fuel would be one of the works that could be done in the future.

REFERENCES

1. Einstein's letter to Roosevelt, August 2, 1939. (n.d.). Retrieved June 10, 2013, from http://www.dannen.com/ae-fdr.html
2. Kelly, C. C. "*The Manhattan project: the birth of the atomic bomb in the words of its creators, eyewitnesses, and historians*." New York: Black Dog & Leventhal Publishers: Distributed by Workman Pub, USA; 2007
3. Sagan, Scott D. "Why Do States Build Nuclear Weapons?: Three Models in Search of a Bomb." *International Security*, vol. 21, no. 3, 1996, pp. 54–86., www.jstor.org/stable/2539273.
4. "Hiroshima and Nagasaki Death Toll." *Hiroshima and Nagasaki Death Toll*. University of California, Los Angeles, 10 Oct. 2007. Web. 16 Feb. 2017. <http://www.aasc.ucla.edu/cab/200708230009.html>.
5. Farlow, Troy Jay. "*Gold Standard or Case-by-Case: Which Method Is Best for the Nonproliferation Regime*?" *Harvard University Library*. ProQuest Dissertations Publishing, Mar. 2014. Web. 16 Feb. 2017.
6. Menlove HO, et al.; *Field Tests of the AEFC for Verification of Research Reactor Spent Fuel at the WWR-SM Reactor at the Institute of Nuclear Physics Uzbekistan*; proc. INMM Annual Meeting; Orlando, Florida USA; 2012.
7. Root M.; *Technical Basis for the Use of a Correlated Neutron Source in the Uranium Neutron Coincidence Collar;* Los Alamos National Laboratory, Los Alamos, NM USA; Publication in Process 2016.
8. Crane, T.W., M.P. Baker.; *Neutron Detectors*; Passive Nondestructive Assay Manual-PANDA. N.p.: Los Alamos National Laboratory, 2007. pp. 379-406.
9. Knoll, Glenn F.; *Slow Neutron Detection*; Radiation *Detection and Measurement*. 3rd. ed. New York: Wiley, 1999. Print.
10. Trahan A C.; *Utilization of the Differential Die-Away Self-Interrogation Technique for Characterization and Verification of Spent Nuclear Fuel*; University of Michigan; Ann Arbor, Michigan USA; 2016.
11. Stewart, J.E.,; *Principles of Neutron Coincidence Counting*; Passive Nondestructive Assay Manual-PANDA. N.p.: Los Alamos National Laboratory, 2007. pp. 457-490.

12. Menlove HO, et al.; *The development of a new, neutron, time correlated, interrogation method for measurement of ^{235}U content in LWR fuel assemblies*; Nuclear Instruments and Methods in Physics; Volume 701, 2013.
13. A. Jehouani, J.C. Nimal, P. Reuss, "*Comparison of mutual shielding and self-shielding powers of ^{235}U, ^{238}U, ^{239}Pu and ^{240}Pu*," Annals of Nuclear Energy, Volume 19, Issue 4, 1992, Pages 195-202, ISSN 0306-4549,
14. Li Ke.; *Study of SF of 252Cf: Structure of Neutron-Rich Nuclei, Gamma-Ray Angular Correlation and G-factor Measurements*; Vanderbilt University; Nashville, Tennessee USA; 2008.
15. Beckurt, K.H. & Wirtz, K.,"Neutron Physics-Neutron Sources." Springer-Verlag, Berlin 1964.
16. Magill, Joseph. "*Nuclides.net: an Integrated Environment for Computations on Radionuclides and their Radiation*." Berlin, Heidelberg: Springer Berlin Heidelberg, 2003. Print.
17. Lamarsh, John R., and Anthony John Baratta. *Introduction to nuclear engineering*. Upper Saddle River, NJ: Prentice Hall, 2009. Print.
18. Menlove HO, et al., "*The Optimization and Calibration of the AWCC Using 252Cf Interrogation and the Comparison with an AmLi Neutron Source*." Los Alamos National Laboratory, USA, LA-UR-15-29620.
19. Ensslin, N., W. Harker, M. Krick, D. Langner, M. Pickrell, et al.; *Application Guide to Neutron Multiplicity Counting*; LA-UR-98-4090. 1998
20. "Summary." National Research Council. 2008. Radiation Source Use and Replacement; Abbreviated Version. Washington, DC
21. Patil A., "*Dead time and count loss determination for radiation detection systems in high count rate applications*." Doctoral Dissertations, Curtis Laws Wilson library, Missouri University of Science and Technology, Spring 2010
22. Ensslin, N.," *Principles of Neutron Coincidence Counting*;" *Passive Nondestructive Assay Manual-PANDA*. N.p.: Los Alamos National Laboratory, 2007. pp. 457-491.
23. Trellue, HR., Tobin, SJ., "*The State of Art of the Nondestructive Assay of Spent fuel Assemblies*." LA-UR- 16-20376, Los Alamos National Laboratory, USA, 02-25-2016.

24. Menlove, HO., "*The Advanced Experimental Fuel Counter – a Portable Detector for the Verification of Research Reactor Spent Fuel*." LA-UR- 11-01586, Los Alamos National Laboratory, USA, 04-05-2011.

7. APPENDICES

7.1. APPENDIX A: EXPERIMENTAL MEASUREMENT RESULTS

Table 7-1: MTR Assembly L-108 Scan with ^{252}Cf

Distance	singles	singles error	Doubles	Doubles error	Scaler 1	scaler 1 error	Scaler 2	Scaler 2 error
0	874.417	3.477	41.538	1.953	761.25	2.443	113.183	1.075
3	878.633	4.340	43.967	1.245	765.733	4.361	112.917	1.049
6	884.633	3.664	39.383	1.700	771.117	3.669	113.533	1.455
9	879.983	2.912	40.167	1.257	765.467	2.710	114.517	1.459
12	880.450	3.138	43.117	1.338	767.150	2.486	113.317	1.413
15	875.617	4.111	42.317	1.969	762.133	4.296	113.483	1.903
18	886.867	3.580	42.667	1.311	771.767	2.971	115.117	1.609
21	880.183	2.752	42.417	1.989	767.067	2.656	113.117	1.253
24	882.283	2.330	41.867	1.670	770.183	1.942	112.15	1.234
27	870.617	3.296	40.683	1.112	758.667	2.374	111.967	1.217
30	863.067	5.674	43.100	2.211	752.083	4.741	111.000	1.332
33	866.633	2.320	41.033	2.267	751.750	1.530	114.867	0.860
36	841.250	2.633	38.900	1.204	734.683	1.881	106.600	0.922
39	806.517	1.939	36.167	1.585	705.283	1.853	101.250	0.717
42	756.617	4.888	28.317	1.368	662.100	3.307	94.517	1.746
45	688.500	2.600	21.483	1.192	604.050	2.674	84.483	1.107
48	605.350	1.791	15.175	0.671	535.183	1.815	70.217	0.839
51	563.817	2.328	10.417	0.681	500.350	2.275	63.467	1.690
54	527.500	2.196	6.956	1.542	473.217	2.405	54.283	0.557
57	503.133	3.125	5.283	0.767	449.483	2.086	53.633	1.063
60	480.117	3.408	4.433	0.696	430.500	3.431	49.633	0.574
63	461.467	2.394	4.383	0.824	414.333	1.937	47.150	0.736
66	443.933	2.732	4.733	0.824	398.967	2.887	44.967	1.059

Table 7-2: MTR Assembly L-108 Scan with ^{252}Cf subtracted with ^{252}Cf background

Distance	singles	singles error	Doubles	Doubles error	Scaler 1	scaler 1 error	Scaler 2	Scaler 2 error
0	444.68	3.7226911	38.201	1.980186355	375.21	2.771593405	69.496	1.125395042
3	448.896	4.53921799	40.63	1.245	379.693	4.553218861	69.23	1.100586207
6	454.896	3.89792201	36.046	1.7	385.077	3.895515627	69.846	1.492619844
9	450.246	3.20135034	36.83	1.257	379.427	3.009581532	70.83	1.496519295
12	450.713	3.40821713	39.78	1.338	381.11	2.809568828	69.63	1.451708648
15	445.88	4.3207894	38.98	1.969	376.093	4.491001781	69.796	1.93191563
18	457.13	3.81907057	39.33	1.311	385.727	3.246586207	71.43	1.643097684
21	450.446	3.05653464	39.08	1.989	381.027	2.961049983	69.43	1.296494504
24	452.546	2.6828716	38.53	1.67	384.143	2.341974594	68.463	1.278141229
27	440.88	3.55422509	37.346	1.112	372.627	2.710969753	68.28	1.261736106
30	433.33	5.82779341	39.763	2.211	366.043	4.918390184	67.313	1.372994173
33	436.896	2.67419147	37.696	2.267	365.71	2.013549354	71.18	0.922219605
36	411.513	2.94984559	35.563	1.204	348.643	2.291646133	62.913	0.980292303
39	376.78	2.35130198	32.83	1.585	319.243	2.268719903	57.563	0.790555501
42	326.88	5.06571259	24.98	1.368	276.06	3.556645892	50.83	1.777471519
45	258.763	2.92042805	18.146	1.192	218.01	2.977206241	40.796	1.156000865
48	175.613	2.23082518	11.838	0.671	149.143	2.237790428	26.53	0.902668267
51	134.08	2.68113483	7.08	0.681	114.31	2.624710651	19.78	1.722494993
54	97.763	2.56735584	3.619	1.542	87.177	2.73815741	10.596	0.648951462
57	73.396	3.39625161	1.946	0.767	63.443	2.462697099	9.946	1.113938059
60	50.38	3.65832803	1.096	0.696	44.46	3.672225756	5.946	0.66360003
63	31.73	2.73863762	1.046	0.824	28.293	2.337830191	3.463	0.807827333
66	14.196	3.03853978	1.396	0.824	12.927	3.169897475	1.28	1.110121615

Table 7-3: ^{252}Cf Bkg and AmLi Bkg

	Singles	Singles Error	Doubles	Doubles Error	Scaler 1	Scaler 1 Error	Scaler 2	Scaler 2 Error
252Cf	429.737	1.330	3.337	0.327	836.040	1.309	43.687	0.333
AmLi	227.257	0.801	0.020	0.154	215.477	0.732	11.780	0.201
252Cf in fuel through hole	1817.085	1.808	70.363	1.021	1606.028	1.808	211.105	0.575

Table 7-4: MTR Assembly L-108 two-point scan with 252Cf and middle scan with AmLi

	Singles	Singles Error	Doubles	Doubles Error	Scaler 1	Scaler 1 Error	Scaler 2	Scaler 2 Error
Mid scan-252Cf	872.713	1.272	41.538	0.592	759.982	1.089	112.743	0.489
Mid scan-252Cf/ rotated 90 deg	857.085	1.420	41.720	0.613	744.987	1.264	112.107	0.501
Bottom-252Cf/21cm	806.042	1.420	36.798	0.443	701.392	1.283	104.675	0.350
Bottom-252Cf/18cm	808.373	1.272	39.743	0.558	699.392	1.289	108.992	0.437
Mid scan-AmLi	679.148	1.135	27.25	0.348	600.942	1.001	78.222	0.301
Mid scan- 252Cf inside fuel hole	2322.443	2.057	168.630	1.300	2009.89	1.892	312.665	0.697

Table 7-5: MTR assembly L-108 two-point scan with 252Cf and middle scan with AmLi minus Bkg

	Singles	Singles Error	Doubles	Doubles Error	Scaler 1	Scaler 1 Error	Scaler 2	Scaler 2 Error
Mid scan-252Cf	442.976	1.840	38.201	0.676	373.942	1.702	69.056	0.591
Mid scan-252Cf/ rotated 90 deg	427.348	1.945	38.383	0.694	358.947	1.819	68.420	0.601
Bottom-252Cf/21cm	376.305	1.945	33.461	0.551	315.352	1.833	60.988	0.483
Bottom-252Cf/18cm	378.636	1.840	36.406	0.647	313.352	1.837	65.305	0.549
Mid scan-AmLi	451.891	1.389	27.23	0.380	385.465	1.240	66.442	0.362
Mid scan- 252Cf inside fuel hole	505.358	2.738	98.267	1.653	403.862	2.617	101.560	0.904

Table 7-6: MTR assembly O-187R three-point scan and middle scan with AmLi

	Singles	Singles Error	Doubles	Doubles Error	Scaler 1	Scaler 1 Error	Scaler 2	Scaler 2 Error
Bottom scan-252Cf (21cm)	553.835	1.154	12.478	0.394	490.552	0.984	63.293	0.399
Bottom scan-252Cf (18cm)	583.245	1.019	14.282	0.368	516.092	0.970	67.155	0.259
Middle scan-252Cf	600.278	1.025	14.550	0.334	530.092	0.977	70.202	0.393
Top scan-252Cf (21cm)	58.080	1.058	14.488	0.334	528.453	1.006	69.635	0.295
Top scan-252Cf (18cm)	599.930	1.047	14.913	0.302	529.643	1.036	70.297	0.386
Mid scan-AmLi	391.912	0.094	8.241	0.026	355..635	0.089	36.280	0.028
Mid scan- 252Cf rotated 90 deg	583.808	0.928	14.325	0.424	514.195	0.875	69.622	0.422

Table 7-7: MTR assembly O-187R three-point scan and middle scan with AmLi minus Bkg

	Singles	Singles Error	Doubles	Doubles Error	Scaler 1	Scaler 1 Error	Scaler 2	Scaler 2 Error
Bottom scan-252Cf (21cm)	124.098	1.760	9.141	0.512	104.512	1.637	19.606	0.519
Bottom scan-252Cf (18cm)	153.508	1.675	10.945	0.492	130.052	1.629	23.468	0.422
Middle scan-252Cf	170.541	1.679	11.213	0.467	144.052	1.633	26.515	0.515
Top scan-252Cf (21cm)	168.343	1.699	11.151	0.467	142.413	1.651	25.948	0.445
Top scan-252Cf (18cm)	170.193	1.693	11.576	0.445	143.603	1.669	26.611	0.509
Mid scan-AmLi	164.665	0.806	8.221	0.156	140.158	0.737	24.5	0.203
Mid scan- 252Cf rotated 90 deg	154.071	1.621	10.988	0.535	128.155	1.574	25.935	0.537

7.2. APPENDIX B: MCNP SIMULATION RESULTS

Table 7-8: MCNP simulation raw results of MTR Assembly L-108 with ^{252}Cf source

Distance	singles	singles error	Doubles	Doubles error
0	878.33	0.13	49.20	0.61
3	880.17	0.13	49.32	0.61
6	881.46	0.13	49.45	0.61
9	881.93	0.13	49.49	0.61
12	882.33	0.13	49.57	0.61
15	882.34	0.13	49.47	0.61
18	881.85	0.13	49.45	0.61
21	881.44	0.13	49.63	0.61
24	879.32	0.13	49.16	0.61
27	874.16	0.13	48.68	0.62
30	863.84	0.13	47.57	0.63
33	841.03	0.13	44.54	0.64
36	798.51	0.13	39.51	0.67
39	730.73	0.14	31.79	0.74
42	642.38	0.14	22.64	0.87
45	560.24	0.15	14.37	1.05
48	499.96	0.16	8.56	1.32
51	463.84	0.16	5.61	1.55
54	445.28	0.17	4.15	1.76
57	437.47	0.17	3.67	1.85
60	433.86	0.17	3.52	1.89
63	432.05	0.17	3.48	1.9
66	432.18	0.17	3.48	1.9

Table 7-9: MCNP simulation raw results of MTR Assembly L-108 with ^{252}Cf source minus ^{252}Cf background

Distance	singles	singles error	Doubles	Doubles error
0	446.69	0.16	45.73	1.26
3	448.53	0.16	45.84	1.25
6	449.82	0.16	45.97	1.70
9	450.29	0.16	46.02	1.26
12	450.69	0.16	46.10	1.34
15	450.70	0.16	45.99	1.97
18	450.21	0.16	45.98	1.31
21	449.80	0.16	46.15	1.99
24	447.68	0.16	45.68	1.67
27	442.52	0.16	45.20	1.11
30	432.20	0.16	44.09	2.21
33	409.39	0.16	41.06	2.27
36	366.87	0.16	36.03	1.20
39	299.09	0.17	28.32	1.59
42	210.74	0.17	19.16	1.37
45	128.60	0.18	10.89	1.19
48	68.32	0.19	5.09	0.67
51	32.20	0.19	2.13	0.68
54	13.64	0.20	0.67	1.54
57	5.83	0.20	0.20	0.77
60	2.22	0.20	0.05	0.70
63	0.41	0.20	0.00	0.82
66	0.54	0.20	0.01	0.82

Table 7-10: ^{252}Cf and AmLi Background count rates from MCNP simulations

	Singles	Singles Error	Doubles	Doubles Error
^{252}Cf	431.64	0.10	3.48	1.10
AmLi	182.67	0.26	0.00	0.00
^{252}Cf in fuel through hole	1102.60	0.06	23.35	0.43

Table 7-11: MCNP results of MTR Assembly L-108; two-point scan with ^{252}Cf and middle point scan with AmLi

	Singles	Singles Error	Doubles	Doubles Error
Mid scan with ^{252}Cf	882.64	0.13	49.73	0.61
Mid scan-^{252}Cf/ rotated 90 deg	806.99	0.13	43.78	0.65
Bottom-^{252}Cf/18cm	852.48	0.13	46.08	0.63
Mid scan-AmLi	616.68	0.26	26.22	1.40
Mid scan- ^{252}Cf inside fuel hole	2517.40	0.08	270.22	0.29

Table 7-12: MCNP results of MTR Assembly L-108; two-point scan with ^{252}Cf and middle point scan with AmLi minus background

	Singles	Singles Error	Doubles	Doubles Error
Mid scan with ^{252}Cf	451.00	0.16	46.25	1.26
Mid scan-^{252}Cf/ rotated 90 deg	375.35	0.16	40.31	1.28

Bottom-^{252}Cf/18cm	420.84	0.16	42.60	1.27
Mid scan-AmLi	434.01	0.37	26.22	1.40
Mid scan- ^{252}Cf inside fuel hole	1414.80	0.10	246.87	0.52

Table 7-13: MCNP simulation results of the partial assembly; three-point scan with ^{252}Cf source

4-Plates Partial Assembly Scan with 252Cf source				
	singles	singles error	Doubles	Doubles error
top point	527.05	0.16	10.77	1.17
middle point	530.01	0.16	10.90	1.16
bottom point	523.34	0.16	10.55	1.18
6-Plates Partial Assembly Scan with 252Cf source				
Top scan (18cm)	560.48	0.16	14.77	1.03
Middle Scan	564.08	0.15	15.02	1.01
Bottom Scan (18cm)	554.10	0.15	14.38	1.03
8-Plates Partial Assembly Scan with 252Cf source				
top point	640.42	0.14	20.32	0.89
middle point	646.30	0.14	20.74	0.89
bottom point	631.79	0.15	19.67	0.91
10-Plates Partial Assembly Scan with 252Cf source				
top point	698.49	0.14	25.71	0.80
middle point	707.34	0.14	26.53	0.79
bottom point	689.06	0.14	25.24	0.81
12-Plates Partial Assembly Scan with 252Cf source				
top point	754.61	0.14	31.62	0.73
middle point	764.04	0.13	32.74	0.73

bottom point	741.60	0.14	30.65	0.75
14-Plates Partial Assembly Scan with 252Cf source				
top point	807.58	0.13	38.17	0.68
middle point	820.10	0.13	39.67	0.67
bottom point	792.77	0.13	36.78	0.70
16-Plates Partial Assembly Scan with 252Cf source				
top point	849.06	0.13	43.45	0.64
middle point	862.73	0.13	45.09	0.63
bottom point	832.24	0.13	41.75	0.66
18-Plates Partial Assembly Scan with 252Cf source				
top point	882.50	0.13	47.95	0.62
middle point	896.27	0.13	49.31	0.61
bottom point	863.47	0.13	45.20	0.63
19-Plates Partial Assembly Scan with 252Cf source				
top point	870.73	0.13	48.04	0.62
middle point	882.64	0.13	49.73	0.61
bottom point	852.48	0.13	46.08	0.63

Table 7-14: MCNP simulation results of the partial assembly; three-point scan with ^{252}Cf source minus background

4-Plates Partial Assembly Scan with 252Cf source				
	singles	singles error	Doubles	Doubles error
top point	95.41	0.19	7.30	1.61
middle point	98.37	0.19	7.43	1.60
bottom point	91.70	0.19	7.07	1.61
6-Plates Partial Assembly Scan with 252Cf source				

Top scan (18cm)	128.84	0.19	11.29	1.51
Middle Scan	132.44	0.18	11.54	1.49
Bottom Scan (18cm)	122.46	0.18	10.90	1.51
8-Plates Partial Assembly Scan with 252Cf source				
top point	208.78	0.17	16.84	1.41
middle point	214.66	0.17	17.26	1.41
bottom point	200.15	0.18	16.20	1.43
10-Plates Partial Assembly Scan with 252Cf source				
top point	266.85	0.17	22.23	1.36
middle point	275.70	0.17	23.05	1.35
bottom point	257.42	0.17	21.77	1.37
12-Plates Partial Assembly Scan with 252Cf source				
top point	322.97	0.17	28.14	1.32
middle point	332.40	0.16	29.26	1.32
bottom point	309.96	0.17	27.17	1.33
14-Plates Partial Assembly Scan with 252Cf source				
top point	375.94	0.16	34.70	1.29
middle point	388.46	0.16	36.19	1.29
bottom point	361.13	0.16	33.30	1.30
16-Plates Partial Assembly Scan with 252Cf source				
top point	417.42	0.16	39.97	1.27
middle point	431.09	0.16	41.61	1.27
bottom point	400.60	0.16	38.28	1.28
18-Plates Partial Assembly Scan with 252Cf source				
top point	450.86	0.16	44.47	1.26
middle point	464.63	0.16	45.84	1.26

bottom point	431.83	0.16	41.73	1.27
19-Plates Partial Assembly Scan with 252Cf source				
top point	439.09	0.16	44.57	1.26
middle point	451.00	0.16	46.25	1.26
bottom point	420.84	0.16	42.60	1.27

Table 7-15: MCNP simulation results of the partial assembly; three-point scan with AmLi source

4-Plates Partial Assembly Scan with AmLi source				
	singles	singles error	Doubles	Doubles error
top point	282.01	0.37	4.02	3.24
middle point	283.87	0.37	4.08	3.25
bottom point	260.81	0.39	3.73	3.42
6-Plates Partial Assembly Scan with AmLi source				
Top scan (18cm)	317.83	0.36	6.15	2.67
Middle Scan	319.73	0.35	6.20	2.67
Bottom Scan (18cm)	313.73	0.36	5.97	2.73
8-Plates Partial Assembly Scan with AmLi source				
top point	390.26	0.32	9.19	2.22
middle point	394.46	0.32	9.44	2.22
bottom point	384.72	0.32	8.89	2.27
10-Plates Partial Assembly Scan with AmLi source				
top point	448.47	0.30	12.88	1.91
middle point	454.10	0.30	13.35	1.87
bottom point	440.30	0.31	12.56	1.93
12-Plates Partial Assembly Scan with AmLi source				
top point	504.59	0.29	16.64	1.71

middle point	511.80	0.29	17.37	1.69
bottom point	493.38	0.29	16.08	1.75
14-Plates Partial Assembly Scan with AmLi source				
top point	551.30	0.28	19.68	1.56
middle point	560.68	0.27	20.55	1.54
bottom point	541.18	0.28	19.23	1.59
16-Plates Partial Assembly Scan with AmLi source				
top point	598.09	0.27	23.40	1.48
middle point	608.09	0.26	24.43	1.46
bottom point	585.39	0.27	22.90	1.51
18-Plates Partial Assembly Scan with AmLi source				
top point	627.440	0.26	25.279	1.41
middle point	638.010	0.26	26.550	1.4
bottom point	612.260	0.26	24.410	1.45
19-Plates Partial Assembly Scan with AmLi source				
top point	607.70	0.27	25.26	1.43
middle point	616.68	0.26	26.22	1.40
bottom point	593.53	0.27	24.71	1.45

Table 7-16: MCNP simulation results of the partial assembly; three-point scan with AmLi source minus background

4-Plates Partial Assembly Scan with AmLi source				
	singles	singles error	Doubles	Doubles error
top point	119.61	0.38	4.84	3.42
middle point	121.84	0.38	4.92	3.43
bottom point	94.08	0.40	4.49	3.59
6-Plates Partial Assembly Scan with AmLi source				

Top scan (18cm)	162.73	0.44	7.41	2.08
Middle Scan	165.02	0.44	7.46	2.05
Bottom Scan (18cm)	157.80	0.44	7.19	2.11
8-Plates Partial Assembly Scan with AmLi source				
top point	249.94	0.34	11.06	2.48
middle point	255.00	0.34	11.36	2.48
bottom point	243.27	0.34	10.71	2.52
10-Plates Partial Assembly Scan with AmLi source				
top point	320.02	0.32	15.51	2.20
middle point	326.80	0.32	16.07	2.17
bottom point	310.19	0.33	15.12	2.22
12-Plates Partial Assembly Scan with AmLi source				
top point	387.59	0.31	20.04	2.03
middle point	396.27	0.31	20.91	2.02
bottom point	374.09	0.31	19.36	2.07
14-Plates Partial Assembly Scan with AmLi source				
top point	443.83	0.30	23.70	1.91
middle point	455.12	0.29	24.74	1.89
bottom point	431.65	0.30	23.15	1.93
16-Plates Partial Assembly Scan with AmLi source				
top point	500.17	0.29	28.17	1.84
middle point	512.21	0.28	29.42	1.83
bottom point	484.87	0.29	27.57	1.87
18-Plates Partial Assembly Scan with AmLi source				
top point	535.50	0.28	30.44	1.79
middle point	548.23	0.28	31.97	1.78

bottom point	517.23	0.28	29.39	1.82
19-Plates Partial Assembly Scan with AmLi source				
top point	511.74	0.29	30.42	1.80
middle point	522.55	0.28	31.57	1.78
bottom point	494.68	0.29	29.75	1.82

Table 7-17: Comparison of top, middle, and bottom count rates with the average in case of ^{252}Cf

	Top		Middle		Bottom		Average	
235U Mass	S	D	S	D	S	D	S	D
48.78	95.41	7.30	98.37	7.43	91.70	7.07	95.16	7.26
73.16	128.84	11.29	132.44	11.54	122.46	10.90	127.91	11.25
97.55	208.78	16.84	214.66	17.26	200.15	16.20	207.86	16.77
121.94	266.85	22.23	275.70	23.05	257.42	21.77	266.66	22.35
146.33	322.97	28.14	332.40	29.26	309.96	27.17	321.78	28.19
170.72	375.94	34.70	388.46	36.19	361.13	33.30	375.18	34.73
195.10	417.42	39.97	431.09	41.61	400.60	38.28	416.37	39.95
219.49	450.86	44.47	464.63	45.84	431.83	41.73	449.11	44.01
231.69	439.09	44.57	451.00	46.25	420.84	42.60	436.98	44.47

Table 7-18: Comparison of top, middle, and bottom count rates with the average in case of AmLi

	Top		Middle		Bottom		Average	
235U Mass	S	D	S	D	S	D	S	D
48.78	119.61	4.84	121.84	4.92	94.08	4.49	111.84	4.75
73.16	162.73	7.41	165.02	7.46	157.80	7.19	161.85	7.35
97.55	249.94	11.06	255.00	11.36	243.27	10.71	249.40	11.04
121.94	320.02	15.51	326.80	16.07	310.19	15.12	319.00	15.57
146.33	387.59	20.04	396.27	20.91	374.09	19.36	385.99	20.11
170.72	443.83	23.70	455.12	24.74	431.65	23.15	443.53	23.86

195.10	500.17	28.17	512.21	29.42	484.87	27.57	499.08	28.39
219.49	535.50	30.44	548.23	31.97	517.23	29.39	533.65	30.60
231.69	511.74	30.42	522.55	31.57	494.68	29.75	509.65	30.58

7.3. APPENDIX C: MCNP 6.1.1 MODELS

7.3.1. MID-POINT SCAN WITH ^{252}CF

```
Advanced Experimental Fuel Counter (AEFC)
c
c Fresh MTR measurements at LANL
c Cf interrogating source, full MTR assembly
c
c AMLI Original CASE
c Modified:
c * March 2014 by Karen Miller - Cf neutron benchmark, new lead version
c * July 2015 by Karen Miller - Addition of IRT-4M & ion chamber
c * February 2016 by Alexis Trahan - Restructure of input deck, surfaces and cells
c * November 2016 by J. Joshi and B. Adigun
c
c ------------------------------------------------------------
c                        CELL CARDS
c ------------------------------------------------------------
c
100    1    -7.9     -101  102 -103  104                imp:n=1  $ SS shell main body
101    1    -7.9     -106  103 -108  110 400             imp:n=1  $ SS lid of main body
102    1    -7.9     -101 -104  105  111                imp:n=1  $ SS main body bottom
103    1    -7.9     -110  111  104 -108                imp:n=1  $ SS tube for fuel pass-thru
104    1    -7.9     -112  110 -103  113 400             imp:n=1  $ SS flange for fuel pass-thru tube
105    1    -7.9     -106  101 -103  107                imp:n=1  $ SS flange for main body
c
110    3   -11.34    -120 110 -121 104 #(-122 110 -123)
              #(-120 110 -124 123)                  imp:n=1  $ Pb shield
111    1    -7.9     -122 120 -121 104 110 #(-122 120 -123)    imp:n=1  $ outer SS tube for lead
shield
112    15 -9.58E-04  -122 110 -123                    imp:n=1  $ hole in lead shield
113    1    -7.9     -120 110 -124 123                imp:n=1  $ SS outer layer of hole in lead
shield
115    1    -7.9      115 -116                      imp:n=1  $ Funnel
c
c *** Detectors ***
c     mat    den     surfaces                      importance
201    3   -11.34    -231 221 -250 251                 imp:n=1  $ Pb shield for tube #1
```

```
202    3  -11.34    -232 222 -250 251 231          imp:n=1  $ Pb shield for tube #2
203    3  -11.34    -233 223 -250 251              imp:n=1  $ Pb shield for tube #3
204    3  -11.34    -234 224 -250 251 233          imp:n=1  $ Pb shield for tube #4
205    3  -11.34    -235 225 -250 251              imp:n=1  $ Pb shield for tube #5
206    3  -11.34    -236 226 -250 251 235          imp:n=1  $ Pb shield for tube #6
c
211    4   -2.7     -221 201 -252 251             imp:n=1  $ Al body for tube #1
212    4   -2.7     -222 202 -252 251             imp:n=1  $ Al body for tube #2
213    4   -2.7     -223 203 -252 251             imp:n=1  $ Al body for tube #3
214    4   -2.7     -224 204 -252 251             imp:n=1  $ Al body for tube #4
215    4   -2.7     -225 205 -252 251             imp:n=1  $ Al body for tube #5
216    4   -2.7     -226 206 -252 251             imp:n=1  $ Al body for tube #6
c
c 221    5   -2.3     -211 201 -252 251           imp:n=1  $ Boron liner for tube #1
c 222    5   -2.3     -212 202 -252 251           imp:n=1  $ Boron liner for tube #2
c 223    5   -2.3     -213 203 -252 251           imp:n=1  $ Boron liner for tube #3
c 224    5   -2.3     -214 204 -252 251           imp:n=1  $ Boron liner for tube #4
c 225    5   -2.3     -215 205 -252 251           imp:n=1  $ Boron liner tube #5
c 226    5   -2.3     -216 206 -252 251           imp:n=1  $ Boron liner tube #6
c
231    6  -4.991e-4  -201 -253 254                imp:n=1  $ active 4atm region of 3He tube #1
232    6  -4.991e-4  -202 -253 254                imp:n=1  $ active 4atm region of 3He tube #2
233    6  -4.991e-4  -203 -253 254                imp:n=1  $ active 4atm region of 3He tube #3
234    6  -4.991e-4  -204 -253 254                imp:n=1  $ active 4atm region of 3He tube #4
235    6  -4.991e-4  -205 -253 254                imp:n=1  $ 4 atm of 3He tube #5
236    6  -4.991e-4  -206 -253 254                imp:n=1  $ 4 atm of 3He tube #6
c
241    6  -4.991e-4  -201 -252 253                imp:n=1  $ top dead region of tube #1
242    6  -4.991e-4  -202 -252 253                imp:n=1  $ top dead region of tube #2
243    6  -4.991e-4  -203 -252 253                imp:n=1  $ top dead region of tube #3
244    6  -4.991e-4  -204 -252 253                imp:n=1  $ top dead region of tube #4
245    6  -4.991e-4  -205 -252 253                imp:n=1  $ top dead region of tube #5
246    6  -4.991e-4  -206 -252 253                imp:n=1  $ top dead region of tube #6
c
251    6  -4.991e-4  -201 -254 251                imp:n=1  $ bottom dead region of tube #1
252    6  -4.991e-4  -202 -254 251                imp:n=1  $ bottom dead region of tube #2
253    6  -4.991e-4  -203 -254 251                imp:n=1  $ bottom dead region of tube #3
254    6  -4.991e-4  -204 -254 251                imp:n=1  $ bottom dead region of tube #4
255    6  -4.991e-4  -205 -254 251                imp:n=1  $ bottom dead region of tube #5
256    6  -4.991e-4  -206 -254 251                imp:n=1  $ bottom dead region of tube #6
c
261    4   -1.83    -221 -255 252                imp:n=1  $ preamp for tube #1
262    4   -1.83    -222 -255 252                imp:n=1  $ preamp for tube #2
263    4   -1.83    -223 -255 252                imp:n=1  $ preamp for tube #3
264    4   -1.83    -224 -255 252                imp:n=1  $ preamp for tube #4
265    4   -1.83    -225 -255 252                imp:n=1  $ preamp for tube #5
```

```
266    4    -1.83    -226 -255 252                    imp:n=1  $ preamp for tube #6
c
271    2    -0.96    -241 #261                       imp:n=1  $ poly sleeve on top of tube #1
272    2    -0.96    -242 #262 #271                     imp:n=1  $ poly sleeve on top of tube #2
273    2    -0.96    -243 #263                       imp:n=1  $ poly sleeve on top of tube #3
274    2    -0.96    -244 #264 #273                     imp:n=1  $ poly sleeve on top of tube #4
275    2    -0.96    -245 #265                       imp:n=1  $ poly sleeve on top of tube #5
276    2    -0.96    -246 #266 #275                     imp:n=1  $ poly sleeve on top of tube #6
c
300    2    -0.96    -102 104 -260 #(-122 -260 104)          $ Outside SS for lead shield
              #(-231 -260 104) #(-232 -260 104)          $ 4 lead tubes (dets 1-4)
              #(-233 -260 104) #(-234 -260 104)
              #(-300 301 -302 -102 -260 104)          $ 4 air gaps
              #(-303 304 -302 -102 -260 104)
              #(-301 303 -302 305 -260 104)  110          $ Outside fuel pass thru tube
              #(104 -260  303 -301 -102 -305) #306          $ Outside new poly filler
              #(-400 -260 401) #310                imp:n=1  $ Guide tube for source, main poly
insert
301   15 -9.58E-04 -150 260 -103  #(-110 104 -103)          $ Outside pass thru tube
              #(-112 110 -103 113)                $ Outside pass thru tube flange
              #(-122 -121 260 110) #(-400 -103 260)          $ Outside lead shield, interrogation
tube
              #261 #262 #263 #264 #265 #266          $ Outside detectors
              #201 #202 #203 #204 #205 #206
              #271 #272 #273 #274 #275 #276 602       imp:n=1  $ air space above poly
302    2    -0.96    -102  150  260 -103             imp:n=1  $ poly sleeve
303    15 -9.58E-04  -300  301 -302 -102 -260 104       imp:n=1  $ air gap
304    15 -9.58E-04  -303  304 -302 -102 -260 104       imp:n=1  $ air gap
305    15 -9.58E-04  -301  303 -302  305 -260 104       imp:n=1  $ air gap
306    2    -0.96     104 -260  252 -153 -204 155 122 110    imp:n=1  $ new poly filler
307    2    -0.96     104 -260  303 -301 -102 -305 #(-236 -260 104)
              #(-235 -260  104) #309              imp:n=1  $ new poly in auxiliary moderator
308    15 -9.58E-04  -151  104 -105  122 110          imp:n=1  $ new air gap
309    3   -11.34     303 -301  270 -305 104 -271       imp:n=1  $ Pb shield under auxiliary
moderator
310    3   -11.34     272 -273 -274  302 104 -271 151
                275 276                    imp:n=1  $ Pb shield under main moderator
c
c  *** Interrogation Source Vessel ***
c
c     mat    den     surfaces                    importance
400    0           403 -405 -404 402                imp:n=1  $ source cavity, outside Cf source
401    2    -0.96    414 -412 -411 #(403 -405 -404)       imp:n=1  $ source vessel, poly
402    9    -0.01   -402                          imp:n=1  $ point source cell
403    0          -415 -413  414 #(414 -412 -411)       imp:n=1  $ void tube for AmLi guide
```

```
404    1    -7.9    -400 -413  401 #(-415 -413 414)          imp:n=1  $ SS guide tube for
interrogation source
c
c *** Ionization Chamber ***
c
c     mat    den      surfaces                        importance
600    14  -2.133E-2  -600                              imp:n=1  $ IC gas fill
601    1   -7.9       -601 600                         imp:n=1  $ IC wall
602    11  -19.25     -602 601                           imp:n=1  $ tungsten shield
c
c L-108 Fuel Assembly
c
700 12 -1.0 -997                    u=4  imp:n=1   $ PoolWater
705 10 -3.308 703 -707 705 -706 708 -704 u=12 imp:n=1   $ Fuel Meat
706 4 -2.7 #705                     u=12 imp:n=1   $ Fuel Clad
c
710 0 715 -718 716 -717 -711 719 -720 u=14 FILL=12 (601) imp:n=1   $ TestAssemSlot0a
711 0 715 -718 716 -717 -711 721 -722 u=14 FILL=12 (602) imp:n=1   $ TestAssemSlot00a
712 0 715 -718 716 -717 -711 723 -724 u=14 FILL=12 (603) imp:n=1   $ TestAssemSlot01a
c 713 0 715 -718 716 -717 -711 725 -726 u=14 FILL=12 (604) imp:n=1   $ TestAssemSlot02a
c 714 0 715 -718 716 -717 -711 727 -728 u=14 FILL=12 (605) imp:n=1   $ TestAssemSlot03a
c 715 0 715 -718 716 -717 -711 729 -730 u=14 FILL=12 (606) imp:n=1   $ TestAssemSlot04a
c 716 0 715 -718 716 -717 -711 731 -732 u=14 FILL=12 (607) imp:n=1   $ TestAssemSlot05a
c 717 0 715 -718 716 -717 -711 733 -734 u=14 FILL=12 (608) imp:n=1   $ TestAssemSlot06a
c 718 0 715 -718 716 -717 -711 735 -736 u=14 FILL=12 (609) imp:n=1   $ TestAssemSlot07a
c 719 0 715 -718 716 -717 -711 737 -738 u=14 FILL=12 (610) imp:n=1   $ TestAssemSlot08a
c 720 0 715 -718 716 -717 -711 739 -740 u=14 FILL=12 (611) imp:n=1   $ TestAssemSlot09a
c 721 0 715 -718 716 -717 -711 741 -742 u=14 FILL=12 (612) imp:n=1   $ TestAssemSlot10a
c 722 0 715 -718 716 -717 -711 743 -744 u=14 FILL=12 (613) imp:n=1   $ TestAssemSlot11a
c 723 0 715 -718 716 -717 -711 745 -746 u=14 FILL=12 (614) imp:n=1   $ TestAssemSlot12a
c 724 0 715 -718 716 -717 -711 747 -748 u=14 FILL=12 (615) imp:n=1   $ TestAssemSlot13a
c 725 0 715 -718 716 -717 -711 749 -750 u=14 FILL=12 (616) imp:n=1   $ TestAssemSlot14a
726 0 715 -718 716 -717 -711 751 -752 u=14 FILL=12 (617) imp:n=1   $ TestAssemSlot15a
727 0 715 -718 716 -717 -711 757 -758 u=14 FILL=12 (618) imp:n=1   $ TestAssemSlot18a
728 0 715 -718 716 -717 -711 759 -760 u=14 FILL=12 (619) imp:n=1   $ TestAssemSlot19a
c
730 0 716 -717  718                 u=14 FILL=4 imp:n=1   $ TestAssemAqua1a
731 0 716 -717 -715                 u=14 FILL=4 imp:n=1   $ TestAssemAqua2a
732 0 715 -718  716 -717 (711 : -759) u=14 FILL=4 imp:n=1   $ TestAssemAqua3a
c
739 0 715 -718 716 -717 -711 720      u=14 FILL=4 imp:n=1   $ TestAssemGap0a
740 0 715 -718 716 -717 -711 722 -719 u=14 FILL=4 imp:n=1   $ TestAssemGap00a
741 0 715 -718 716 -717 -711 724 -721 u=14 FILL=4 imp:n=1   $ TestAssemGap01a
c 742 0 715 -718 716 -717 -711 726 -723 u=14 FILL=4 imp:n=1   $ TestAssemGap02a
c 743 0 715 -718 716 -717 -711 728 -725 u=14 FILL=4 imp:n=1   $ TestAssemGap03a
c 744 0 715 -718 716 -717 -711 730 -727 u=14 FILL=4 imp:n=1   $ TestAssemGap04a
```

```
c 745 0 715 -718 716 -717 -711 732 -729 u=14 FILL=4 imp:n=1   $ TestAssemGap05a
c 746 0 715 -718 716 -717 -711 734 -731 u=14 FILL=4 imp:n=1   $ TestAssemGap06a
c 747 0 715 -718 716 -717 -711 736 -733 u=14 FILL=4 imp:n=1   $ TestAssemGap07a
c 748 0 715 -718 716 -717 -711 738 -735 u=14 FILL=4 imp:n=1   $ TestAssemGap08a
c 749 0 715 -718 716 -717 -711 740 -737 u=14 FILL=4 imp:n=1   $ TestAssemGap09a
c 750 0 715 -718 716 -717 -711 742 -739 u=14 FILL=4 imp:n=1   $ TestAssemGap10a
c 751 0 715 -718 716 -717 -711 744 -741 u=14 FILL=4 imp:n=1   $ TestAssemGap11a
c 752 0 715 -718 716 -717 -711 746 -743 u=14 FILL=4 imp:n=1   $ TestAssemGap12a
c 753 0 715 -718 716 -717 -711 748 -745 u=14 FILL=4 imp:n=1   $ TestAssemGap13a
c 754 0 715 -718 716 -717 -711 750 -747 u=14 FILL=4 imp:n=1   $ TestAssemGap14a
755 0 715 -718 716 -717 -711 752 -723 u=14 FILL=4 imp:n=1   $ TestAssemGap15a
756 0 715 -718 716 -717 -711 758 -751 u=14 FILL=4 imp:n=1   $ TestAssemGap18a
757 0 715 -718 716 -717 -711 760 -757 u=14 FILL=4 imp:n=1   $ TestAssemGap19a
c
760 2 -2.7 710 -712 713 -716 -720 -711 u=14       imp:n=1   $ TestAssemPanel1a
761 0 -716 #760                  u=14 FILL=4 imp:n=1   $ TestAssemPanel1Gapa
762 2 -2.7 710 -712 717 -714 -720 -711 u=14       imp:n=1   $ TestAssemPanel2a
763 0 717 #762                   u=14 FILL=4 imp:n=1   $ TestAssemPanel2Gapa
c
770 0 780 -781 -782 -783 784 -785   FILL=14 (620)       imp:n=1 $ Final L-108 fuel assembly
c
c *** Universe ***
c
c    mat    den     surfaces                          importance
996   12 -1.0       -998 111 #(-101 -108 105) #(-106 101 -103 107)
                 #(-106 101 103 -108) #(-400 108 -413)   imp:n=1  $ water
997   12 -1.0       -998 -111 #770 #115                  imp:n=1  $ water
998   2     -2.35   998 -999                          imp:n=1   $ pvc tank
999   0             999                               imp:n=0  $ the nothing

c ------------------------------------------------------------
c                      SURFACE CARDS
c ------------------------------------------------------------
c
c *** Detector Body ***
c
101      cz      17.098              $ outer radius of main body
102      cz      16.78               $ inner radius of main body
103      pz      46.72               $ top of main body
104      pz      0.0                 $ bottom of main body
105      pz     -0.3175              $ bottom of main body
106      cz      18.529              $ main body flange outer radius
107      pz      46.08               $ main body flange bottom
108      pz      47.5074             $ top of main body lid
c
110      c/z     0  4.29  6.17        $ outer radius of fuel pass-thru tube
```

```
111     c/z     0  4.29  5.85          $ inner radius of fuel pass-thru tube
112     c/z     0  4.29  7.42          $ fuel pass-thru flange outer radius
113     pz      45.45                $ fuel pass-thru flange bottom
c          Vx    Vy    Vz    Hx   Hy   Hz    R
115     rcc   0   4.29  46.73 0    0    10   5.74   $ inner radius of funnel
116     rcc   0   4.29  46.73 0    0    10   5.84   $ outer radius of funnel
c
120     c/z     0  2.54  7.239         $ outer radius of lead shield
121     pz      43.85               $ top of lead shield
122     c/z     0  2.54  7.477         $ outer radius of SS tube for lead shield
123     c/y     0  40.32  0.9525        $ hole in Pb shield
124     c/y     0  40.32  1.1049        $ SS layer for hole in lead shield
c
150    cz      16.61               $ poly liner
151   c/z      0  2.24  7.4777         $ inner radius of poly for air gap (mts)
152   px      -7.477
153   px       7.477
154   py       11.32
155   py       2.54
c
c DETECTORS
c             Vx    Vy      R
201    C/Z     -8.61  -3.22  1.188945     $ B inner radius for tube #1
202    C/Z     -5.98  -6.59  1.188945     $ B inner radius for tube #2
203    C/Z      8.61  -3.22  1.188945     $ B inner radius for tube #3
204    C/Z      5.98  -6.59  1.188945     $ B inner radius for tube #4
205    C/Z      2.19  -13.27 1.18882      $ B inner radius for tube #5
206    C/Z     -2.19  -13.27 1.18882      $ B inner radius for tube #6
c
211    C/Z     -8.61  -3.22  1.189        $ Al inner radius for tube #1
212    C/Z     -5.98  -6.59  1.189        $ Al inner radius for tube #2
213    C/Z      8.61  -3.22  1.189        $ Al inner radius for tube #3
214    C/Z      5.98  -6.59  1.189        $ Al inner radius for tube #4
215    C/Z      2.19  -13.27 1.189        $ Al inner radius for tube #5
216    C/Z     -2.19  -13.27 1.189        $ Al inner radius for tube #6
c
221    C/Z     -8.61  -3.22  1.27         $ Al outer radius for tube #1
222    C/Z     -5.98  -6.59  1.27         $ Al outer radius for tube #2
223    C/Z      8.61  -3.22  1.27         $ Al outer radius for tube #3
224    C/Z      5.98  -6.59  1.27         $ Al outer radius for tube #4
225    C/Z      2.19  -13.27 1.27         $ Al outer radius for tube #5
226    C/Z     -2.19  -13.27 1.27         $ Al outer radius for tube #6
c
231    C/Z     -8.61  -3.22  2.2225       $ Pb outer radius for tube #1
232    C/Z     -5.98  -6.59  2.2225       $ Pb outer radius for tube #2
233    C/Z      8.61  -3.22  2.2225       $ Pb outer radius for tube #3
```

```
234   C/Z     5.98  -6.59  2.2225      $ Pb outer radius for tube #4
235   C/Z     2.19  -13.27 2.2225      $ Pb outer radius for tube #5
236   C/Z    -2.19  -13.27 2.2225      $ Pb outer radius for tube #6
c          Vx   Vy      Vz    Hx   Hy   Hz    R
241   RCC  -8.61 -3.22    34.76  0.0  0.0  1.3  2.2225  $ poly sleeve on top of tube #1
242   RCC  -5.98 -6.59    34.76  0.0  0.0  1.3  2.2225  $ poly sleeve on top of tube #2
243   RCC   8.61 -3.22    34.76  0.0  0.0  1.3  2.2225  $ poly sleeve on top of tube #3
244   RCC   5.98 -6.59    34.76  0.0  0.0  1.3  2.2225  $ poly sleeve on top of tube #4
245   RCC   2.19 -13.27   34.76  0.0  0.0  1.3  2.2225  $ poly sleeve on top of tube #5
246   RCC  -2.19 -13.27   34.76  0.0  0.0  1.3  2.2225  $ poly sleeve on top of tube #6
c
250   PZ      34.76                $ Top of Pb tubes
251   PZ      1.280                $ Bottom of Pb tubes
252   PZ      32.40                $ Top of Al tube
253   PZ      29.54                $ Top of active region
254   PZ      4.140                $ Bottom of active region
255   PZ      41.29                $ Top of preamps
256   PZ      36.06                $ Top of tube poly sleeves
260   PZ      33.69                $ Bottom of poly sleeve
270    py     -15.59               $ side surface for Pb under auxiliary moderator
271    pz     1.28                 $ top surface for Pb under auxiliary moderator
272    px     -11.0                $ Pb shield under 4 tubes
273    px     11.0                 $ Pb shield under 4 tubes
274    py     -0.75                $ Pb shield under 4 tubes
275    p      1.0  1.0  0.0  -16.657   $ Pb shield under 4 tubes
276    p     -1.0  1.0  0.0  -16.657   $ Pb shield under 4 tubes
c
c
300    px     6.248                $ air gap around auxiliary moderator
301    px     6.197                $ air gap around auxiliary moderator
302    py    -10.46                $ air gap around auxiliary moderator
303    px    -6.197                $ air gap around auxiliary moderator
304    px    -6.248                $ air gap around auxiliary moderator
305    py    -10.51                $ air gap around auxiliary moderator
c
400    c/z    0.0  13.47  2.0        $ guide tube for interrogation source
401    pz     11.69                $ bottom of guide tube for interrogation source
402    s      0  13.47 13.7725 1e-6    $ SPHERE OF CF in interrogation tube
403    pz     13.2725               $ source cavity bottom
404    c/z    0  13.47  1.334        $ source cavity outer
405    pz     17.56                $ source cavity top
410    pz     12.480               $ source vessel bottom
411    c/z    0  13.47  1.5875       $ source vessel outer
412    pz     18.83                $ source vessel top
413    pz     50.32                $ top of void in source tube
414    pz     12.48                $ bottom of void in source tube
```

```
415     c/z      0.0  13.47  1.7          $ guide tube for interrogation source inner radius
c *** Ionization Chamber ***
c
c       Vx   Vy     Vz    Hx  Hy   Hz   R
600 rcc  0 -5.1524 40.32  0 -3.8252 0  0.9776  $ inner IC wall
601 rcc  0 -5      40.32  0 -4.13   0  1.13    $ outer IC wall
602 rcc  0 -5      40.32  0 -4.13   0  2.145   $ outer tungsten shield wall
c
c *** MTR Fuel ***
703  PZ -8.25                        $ TestAssemFuelStrip_Bottom
704  P   3.12377 -13.72501 0.0 42.72073   $ TestAssemFuelStrip_East
705  C/Z 13.676 0.0 14.0625             $ TestAssemFuelStrip_Inner
706  C/Z 13.676 0.0 14.08950             $ TestAssemFuelStrip_Outer
707  PZ  51.75                        $ TestAssemFuelStrip_Top
708  P -3.12377 -13.72501 0.0 -42.72073   $ TestAssemFuelStrip_West
c
709  PX -4.048                        $ TestAssemPanel_Back
710  PZ -9.5                         $ TestAssemPanel_Bottom
711  PX 4.048                         $ TestAssemPanel_Front
712  PZ 54                           $ TestAssemPanel_Top
c
713  PY -3.9519                       $ TestAssemPanel1_Left
714  PY 3.9519                        $ TestAssemPanel2_Right
c
715  PZ -8.75                        $ TestAssemSlot_Bottom
716  PY -3.556                        $ TestAssemSlot_Left
717  PY 3.556                         $ TestAssemSlot_Right
718  PZ  52.25                        $ TestAssemSlot_Top
c
719  C/Z 9.779 0.0 13.9998   $ TestAssemSlot0_Inner
720  C/Z 9.779 0.0 14.1522   $ TestAssemSlot0_Outer
721  C/Z 10.212 0.0 13.9998   $ TestAssemSlot00_Inner
722  C/Z 10.212 0.0 14.1522   $ TestAssemSlot00_Outer
723  C/Z 10.645 0.0 13.9998   $ TestAssemSlot01_Inner
724  C/Z 10.645 0.0 14.1522   $ TestAssemSlot01_Outer
725  C/Z 11.078 0.0 13.9998   $ TestAssemSlot02_Inner
726  C/Z 11.078 0.0 14.1522   $ TestAssemSlot02_Outer
727  C/Z 11.511 0.0 13.9998   $ TestAssemSlot03_Inner
728  C/Z 11.511 0.0 14.1522   $ TestAssemSlot03_Outer
729  C/Z 11.944 0.0 13.9998   $ TestAssemSlot04_Inner
730  C/Z 11.944 0.0 14.1522   $ TestAssemSlot04_Outer
731  C/Z 12.377 0.0 13.9998   $ TestAssemSlot05_Inner
732  C/Z 12.377 0.0 14.1522   $ TestAssemSlot05_Outer
733  C/Z 12.81 0.0 13.9998   $ TestAssemSlot06_Inner
734  C/Z 12.81 0.0 14.1522   $ TestAssemSlot06_Outer
735  C/Z 13.243 0.0 13.9998   $ TestAssemSlot07_Inner
```

```
736  C/Z 13.243 0.0 14.1522   $ TestAssemSlot07_Outer
737  C/Z 13.676 0.0 13.9998   $ TestAssemSlot08_Inner
738  C/Z 13.676 0.0 14.1522   $ TestAssemSlot08_Outer
739  C/Z 14.109 0.0 13.9998   $ TestAssemSlot09_Inner
740  C/Z 14.109 0.0 14.1522   $ TestAssemSlot09_Outer
741  C/Z 14.542 0.0 13.9998   $ TestAssemSlot10_Inner
742  C/Z 14.542 0.0 14.1522   $ TestAssemSlot10_Outer
743  C/Z 14.975 0.0 13.9998   $ TestAssemSlot11_Inner
744  C/Z 14.975 0.0 14.1522   $ TestAssemSlot11_Outer
745  C/Z 15.408 0.0 13.9998   $ TestAssemSlot12_Inner
746  C/Z 15.408 0.0 14.1522   $ TestAssemSlot12_Outer
747  C/Z 15.841 0.0 13.9998   $ TestAssemSlot13_Inner
748  C/Z 15.841 0.0 14.1522   $ TestAssemSlot13_Outer
749  C/Z 16.274 0.0 13.9998   $ TestAssemSlot14_Inner
750  C/Z 16.274 0.0 14.1522   $ TestAssemSlot14_Outer
751  C/Z 16.707 0.0 13.9998   $ TestAssemSlot15_Inner
752  C/Z 16.707 0.0 14.1522   $ TestAssemSlot15_Outer
753  C/Z 17.14 0.0 13.9998   $ TestAssemSlot16_Inner
754  C/Z 17.14 0.0 14.1522   $ TestAssemSlot16_Outer
755  C/Z 17.573 0.0 13.9998   $ TestAssemSlot17_Inner
756  C/Z 17.573 0.0 14.1522   $ TestAssemSlot17_Outer
757  C/Z 17.14 0.0 13.9998   $ TestAssemSlot18_Inner
758  C/Z 17.14 0.0 14.1522   $ TestAssemSlot18_Outer
759  C/Z 17.573 0.0 13.9998   $ TestAssemSlot19_Inner
760  C/Z 17.573 0.0 14.1522   $ TestAssemSlot19_Outer
c
780 999 pz -32.38
781 999 pz  75.88
782 999 C/Z 9.779 4.29 14.2   $ TestAssemSlot0_Outer px  -4.049
783 999 px   4.049
784 999 py   0.3
785 999 py   8.3
c
c *** Room ***
997  so  100
c          Vx   Vy   Vz  A1x  A1y  A1z  A2x  A2y   A2z  A3x  A3y  A3z
c 998  box   -100 -150 -50  200  0.0  0.0  0.0  300   0.0  0.0  0.0  500  $ room, inner surface
c 999  box   -115 -165 -65  230  0.0  0.0  0.0  330   0.0  0.0  0.0  515  $ room, outer surface
998 rcc 0 0 -51.1175   0 0 152.4   63.5
999 rcc 0 0 -52.3875  0 0 153.67   64.135

c
c ------------------------------------------------------------
c                      TRANSFORMATIONS
c ------------------------------------------------------------
C L108 Fuel into Throat
```

```
*TR601 -3.897 0.0  0.0
*TR602 -3.464 0.0  0.0
*TR603 -3.031 0.0  0.0
c *TR604 -2.598 0.0  0.0
c *TR605 -2.165 0.0  0.0
c *TR606 -1.732 0.0  0.0
c *TR607 -1.299 0.0  0.0
c *TR608 -0.866 0.0  0.0
c *TR609 -0.433 0.0  0.0
c *TR610  0.0   0.0  0.0
c *TR611  0.433 0.0  0.0
c *TR612  0.866 0.0  0.0
c *TR613  1.299 0.0  0.0
c *TR614  1.732 0.0  0.0
c *TR615  2.165 0.0  0.0
c *TR616  2.598 0.0  0.0
*TR617  3.031 0.0  0.0
*TR618  3.464 0.0  0.0
*TR619  3.897 0.0  0.0
*TR620  0.0   4.29  -4.91  -90 -180 -90  0 -90 90  90 90 0
*TR999  -4.29 4.29  -4.91  -90 -180 -90  0 -90 90  90 90 0
c ------------------------------------------------------------
c                      MATERIAL CARDS
c ------------------------------------------------------------
c
c *** Material 1: Stainless Steel 304 ***
c
m1    26057       0.6908
      28058       0.0892
      24052       0.1900
      25055       0.0200
      14028       0.0100
      nlib=.70c
c
c *** Material 2: High Density Polyethylene ***
c
m2    1001        0.6667
      6000        0.3333
      nlib=.70c
mt2   poly.10t                $ s(a,b) treatment for poly
c
c *** Material 3: High Purity Lead ***
c
m3    82206       0.241
      82207       0.221
      82208       0.524
```

```
      nlib=.70c
c
c *** Material 4: Aluminum ***
c
m4     13027        1.0
      nlib=.70c
c
c *** Material 5: Boron-10 ***
c
c m5      5010        1.0
c       nlib=.70c
c
c *** Material 6: Helium-3 ***
c
m6      2003        1.0
       nlib=.70c
c
c *** Material 7: Cadmium ***
c
c m7     48000        1.0
c        nlib=.70c
c
c
c *** Material 9: Californium-252 ***
c
c
m9     98252        1.0
      nlib=.70c
c
c *** Material-10, fresh fuel ***
c
m10    92235   -0.35715
      92238   -0.02464
      13027  -0.61821
      nlib=.70c
c
c *** Material 11: Tungsten ***
c
m11    74182       -0.3
      74184       -0.3
      74186       -0.3
      28060       -0.06
      29063       -0.04
      nlib=.70c
c
c *** Material 12: Water ***
```

```
c
m12     8016        0.33333
        1001        0.66667
        nlib=.70c
mt12 lwtr.10t                   $ s(a,b) treatment for water
c *** Material 14: Xenon gas fill in IC ***
m14   54129         0.264
      54130         0.0407
      54131         0.212
      54132         0.269
      nlib=.70c
c
m15   6000   -0.000124        $ Air (9.58e-4 g/cc in Los Alamos)
      7014   -0.755268        $ (from PNNL)
      8016   -0.231781
      18040  -0.012827
      nlib=.70c
c
c ---------------------------------------------------------------
c                         SOURCE CARDS
c ---------------------------------------------------------------
c
mode n
nps 1e7
sdef par=SF pos= 0  13.47 13.7725 WGT= 4.567E4
c sdef par=SF pos= 0  13.97 13.7725 WGT=1
prdmp j 1e8 1 2 5e6
c
c ---------------------------------------------------------------
c                         TALLY CARDS
c ---------------------------------------------------------------
c
c *f8:p  600
c
fc18   Doubles in Tubes 1-4
f18:n (231 232 233 234)
ft18 CAP 2003 GATE 450 12800
c
fc28   Doubles in Tubes 5-6
f28:n (235 236)
ft28 CAP 2003 GATE 450 12800
c
fc38   Doubles in Tubes 1-6
f38:n (231 232 233 234 235 236)
ft38 CAP 2003 GATE 450 12800
c
```

```
fc48   Singles in Tubes 1-4
f48:n (231 232 233 234)
ft48 CAP 2003
c
fc58   Singles in Tubes 5-6
f58:n (235 236)
ft58 CAP 2003
c
fc68   Singles in Tubes 1-6
f68:n (231 232 233 234 235 236)
ft68 CAP 2003
```

7.3.2. MID-POINT SCAN WITH AmLi

```
Advanced Experimental Fuel Counter (AEFC)
c
c Fresh MTR measurements at LANL
c Cf interrogating source, full MTR assembly
c
c AMLI Original CASE
c Modified:
c * March 2014 by Karen Miller - Cf neutron benchmark, new lead version
c * July 2015 by Karen Miller - Addition of IRT-4M & ion chamber
c * February 2016 by Alexis Trahan - Restructure of input deck, surfaces and cells
c * November 2016 by J. Joshi and B. Adigun
c
c ------------------------------------------------------------
c                      CELL CARDS
c ------------------------------------------------------------
c
100    1    -7.9     -101  102 -103  104                imp:n=1  $ SS shell main body
101    1    -7.9     -106  103 -108  110 400             imp:n=1  $ SS lid of main body
102    1    -7.9     -101 -104  105  111                imp:n=1  $ SS main body bottom
103    1    -7.9     -110  111  104 -108                imp:n=1  $ SS tube for fuel pass-thru
104    1    -7.9     -112  110 -103  113 400             imp:n=1  $ SS flange for fuel pass-thru tube
105    1    -7.9     -106  101 -103  107                imp:n=1  $ SS flange for main body
c
110    3   -11.34    -120 110 -121 104 #(-122 110 -123)
              #(-120 110 -124 123)                  imp:n=1  $ Pb shield
111    1    -7.9     -122 120 -121 104 110 #(-122 120 -123)    imp:n=1  $ outer SS tube for lead
shield
112    15 -9.58E-04  -122 110 -123                   imp:n=1  $ hole in lead shield
113    1    -7.9     -120 110 -124 123                imp:n=1  $ SS outer layer of hole in lead
shield
115    1    -7.9      115 -116                      imp:n=1  $ Funnel
c
c *** Detectors ***
```

```
c    mat    den     surfaces                    importance
201    3   -11.34    -231 221 -250 251              imp:n=1  $ Pb shield for tube #1
202    3   -11.34    -232 222 -250 251 231            imp:n=1  $ Pb shield for tube #2
203    3   -11.34    -233 223 -250 251              imp:n=1  $ Pb shield for tube #3
204    3   -11.34    -234 224 -250 251 233            imp:n=1  $ Pb shield for tube #4
205    3   -11.34    -235 225 -250 251              imp:n=1  $ Pb shield for tube #5
206    3   -11.34    -236 226 -250 251 235            imp:n=1  $ Pb shield for tube #6
c
211    4    -2.7     -221 201 -252 251             imp:n=1  $ Al body for tube #1
212    4    -2.7     -222 202 -252 251             imp:n=1  $ Al body for tube #2
213    4    -2.7     -223 203 -252 251             imp:n=1  $ Al body for tube #3
214    4    -2.7     -224 204 -252 251             imp:n=1  $ Al body for tube #4
215    4    -2.7     -225 205 -252 251             imp:n=1  $ Al body for tube #5
216    4    -2.7     -226 206 -252 251             imp:n=1  $ Al body for tube #6
c
c 221    5    -2.3     -211 201 -252 251             imp:n=1  $ Boron liner for tube #1
c 222    5    -2.3     -212 202 -252 251             imp:n=1  $ Boron liner for tube #2
c 223    5    -2.3     -213 203 -252 251             imp:n=1  $ Boron liner for tube #3
c 224    5    -2.3     -214 204 -252 251             imp:n=1  $ Boron liner for tube #4
c 225    5    -2.3     -215 205 -252 251             imp:n=1  $ Boron liner tube #5
c 226    5    -2.3     -216 206 -252 251             imp:n=1  $ Boron liner tube #6
c
231    6  -4.991e-4  -201 -253 254                imp:n=1  $ active 4atm region of 3He tube #1
232    6  -4.991e-4  -202 -253 254                imp:n=1  $ active 4atm region of 3He tube #2
233    6  -4.991e-4  -203 -253 254                imp:n=1  $ active 4atm region of 3He tube #3
234    6  -4.991e-4  -204 -253 254                imp:n=1  $ active 4atm region of 3He tube #4
235    6  -4.991e-4  -205 -253 254                imp:n=1  $ 4 atm of 3He tube #5
236    6  -4.991e-4  -206 -253 254                imp:n=1  $ 4 atm of 3He tube #6
c
241    6  -4.991e-4  -201 -252 253                imp:n=1  $ top dead region of tube #1
242    6  -4.991e-4  -202 -252 253                imp:n=1  $ top dead region of tube #2
243    6  -4.991e-4  -203 -252 253                imp:n=1  $ top dead region of tube #3
244    6  -4.991e-4  -204 -252 253                imp:n=1  $ top dead region of tube #4
245    6  -4.991e-4  -205 -252 253                imp:n=1  $ top dead region of tube #5
246    6  -4.991e-4  -206 -252 253                imp:n=1  $ top dead region of tube #6
c
251    6  -4.991e-4  -201 -254 251                imp:n=1  $ bottom dead region of tube #1
252    6  -4.991e-4  -202 -254 251                imp:n=1  $ bottom dead region of tube #2
253    6  -4.991e-4  -203 -254 251                imp:n=1  $ bottom dead region of tube #3
254    6  -4.991e-4  -204 -254 251                imp:n=1  $ bottom dead region of tube #4
255    6  -4.991e-4  -205 -254 251                imp:n=1  $ bottom dead region of tube #5
256    6  -4.991e-4  -206 -254 251                imp:n=1  $ bottom dead region of tube #6
c
261    4    -1.83    -221 -255 252              imp:n=1  $ preamp for tube #1
262    4    -1.83    -222 -255 252              imp:n=1  $ preamp for tube #2
263    4    -1.83    -223 -255 252              imp:n=1  $ preamp for tube #3
```

```
264    4    -1.83    -224 -255 252                    imp:n=1  $ preamp for tube #4
265    4    -1.83    -225 -255 252                    imp:n=1  $ preamp for tube #5
266    4    -1.83    -226 -255 252                    imp:n=1  $ preamp for tube #6
c
271    2    -0.96    -241 #261                      imp:n=1  $ poly sleeve on top of tube #1
272    2    -0.96    -242 #262 #271                   imp:n=1  $ poly sleeve on top of tube #2
273    2    -0.96    -243 #263                      imp:n=1  $ poly sleeve on top of tube #3
274    2    -0.96    -244 #264 #273                   imp:n=1  $ poly sleeve on top of tube #4
275    2    -0.96    -245 #265                      imp:n=1  $ poly sleeve on top of tube #5
276    2    -0.96    -246 #266 #275                   imp:n=1  $ poly sleeve on top of tube #6
c
300    2    -0.96    -102 104 -260 #(-122 -260 104)          $ Outside SS for lead shield
              #(-231 -260 104) #(-232 -260 104)          $ 4 lead tubes (dets 1-4)
              #(-233 -260 104) #(-234 -260 104)
              #(-300 301 -302 -102 -260 104)          $ 4 air gaps
              #(-303 304 -302 -102 -260 104)
              #(-301 303 -302 305 -260 104)  110          $ Outside fuel pass thru tube
              #(104 -260  303 -301 -102 -305) #306          $ Outside new poly filler
              #(-400 -260 401) #310          imp:n=1  $ Guide tube for source, main poly
insert
301   15 -9.58E-04 -150 260 -103  #(-110 104 -103)          $ Outside pass thru tube
              #(-112 110 -103 113)          $ Outside pass thru tube flange
              #(-122 -121 260 110) #(-400 -103 260)          $ Outside lead shield, interrogation
tube
              #261 #262 #263 #264 #265 #266          $ Outside detectors
              #201 #202 #203 #204 #205 #206
              #271 #272 #273 #274 #275 #276 602          imp:n=1  $ air space above poly
302    2    -0.96    -102  150  260 -103          imp:n=1  $ poly sleeve
303    15 -9.58E-04  -300  301 -302 -102 -260 104          imp:n=1  $ air gap
304    15 -9.58E-04  -303  304 -302 -102 -260 104          imp:n=1  $ air gap
305    15 -9.58E-04  -301  303 -302  305 -260 104          imp:n=1  $ air gap
306    2    -0.96     104 -260  252 -153 -204 155 122 110     imp:n=1  $ new poly filler
307    2    -0.96     104 -260  303 -301 -102 -305 #(-236 -260 104)
              #(-235 -260  104) #309          imp:n=1  $ new poly in auxiliary moderator
308    15 -9.58E-04  -151  104 -105  122 110          imp:n=1  $ new air gap
309    3   -11.34     303 -301  270 -305 104 -271          imp:n=1  $ Pb shield under auxiliary
moderator
310    3   -11.34     272 -273 -274  302 104 -271 151
                275 276                    imp:n=1  $ Pb shield under main moderator
c
c  *** Interrogation Source Vessel ***
c
c     mat    den     surfaces                    importance
400    0  403 -405 -404 402                imp:n=1  $ source cavity, outside Cf source
401    0  414 -412 -411 #(403 -405 -404)          imp:n=1  $ source vessel, poly
402    9  -0.01   -402                      imp:n=1  $ point source cell
```

```
403    0  -415 -413  414 #(414 -412 -411)          imp:n=1  $ void tube for AmLi/252Cf guide
404    0  -400 -413  401 #(-415 -413 414)          imp:n=1  $ SS guide tube for interrogation
source
c
c *** Ionization Chamber ***
c
c     mat    den      surfaces                    importance
600    14  -2.133E-2  -600                          imp:n=1  $ IC gas fill
601    1   -7.9       -601 600                     imp:n=1  $ IC wall
602    11  -19.25     -602 601                       imp:n=1  $ tungsten shield
c
c L-108 Fuel Assembly
c
700 12 -1.0 -997                    u=4  imp:n=1   $ PoolWater
705 10 -3.308 703 -707 705 -706 708 -704 u=12 imp:n=1   $ Fuel Meat
706 4 -2.7 #705                     u=12 imp:n=1   $ Fuel Clad
c
710 0 715 -718 716 -717 -711 719 -720 u=14 FILL=12 (601) imp:n=1   $ TestAssemSlot0a
711 0 715 -718 716 -717 -711 721 -722 u=14 FILL=12 (602) imp:n=1   $ TestAssemSlot00a
712 0 715 -718 716 -717 -711 723 -724 u=14 FILL=12 (603) imp:n=1   $ TestAssemSlot01a
713 0 715 -718 716 -717 -711 725 -726 u=14 FILL=12 (604) imp:n=1   $ TestAssemSlot02a
c 714 0 715 -718 716 -717 -711 727 -728 u=14 FILL=12 (605) imp:n=1   $ TestAssemSlot03a
c 715 0 715 -718 716 -717 -711 729 -730 u=14 FILL=12 (606) imp:n=1   $ TestAssemSlot04a
c 716 0 715 -718 716 -717 -711 731 -732 u=14 FILL=12 (607) imp:n=1   $ TestAssemSlot05a
c 717 0 715 -718 716 -717 -711 733 -734 u=14 FILL=12 (608) imp:n=1   $ TestAssemSlot06a
c 718 0 715 -718 716 -717 -711 735 -736 u=14 FILL=12 (609) imp:n=1   $ TestAssemSlot07a
c 719 0 715 -718 716 -717 -711 737 -738 u=14 FILL=12 (610) imp:n=1   $ TestAssemSlot08a
c 720 0 715 -718 716 -717 -711 739 -740 u=14 FILL=12 (611) imp:n=1   $ TestAssemSlot09a
c 721 0 715 -718 716 -717 -711 741 -742 u=14 FILL=12 (612) imp:n=1   $ TestAssemSlot10a
c 722 0 715 -718 716 -717 -711 743 -744 u=14 FILL=12 (613) imp:n=1   $ TestAssemSlot11a
c 723 0 715 -718 716 -717 -711 745 -746 u=14 FILL=12 (614) imp:n=1   $ TestAssemSlot12a
c 724 0 715 -718 716 -717 -711 747 -748 u=14 FILL=12 (615) imp:n=1   $ TestAssemSlot13a
725 0 715 -718 716 -717 -711 749 -750 u=14 FILL=12 (616) imp:n=1   $ TestAssemSlot14a
726 0 715 -718 716 -717 -711 751 -752 u=14 FILL=12 (617) imp:n=1   $ TestAssemSlot15a
727 0 715 -718 716 -717 -711 757 -758 u=14 FILL=12 (618) imp:n=1   $ TestAssemSlot18a
728 0 715 -718 716 -717 -711 759 -760 u=14 FILL=12 (619) imp:n=1   $ TestAssemSlot19a
c
730 0 716 -717  718                 u=14 FILL=4 imp:n=1   $ TestAssemAqua1a
731 0 716 -717 -715                 u=14 FILL=4 imp:n=1   $ TestAssemAqua2a
732 0 715 -718  716 -717 (711 : -759) u=14 FILL=4 imp:n=1   $ TestAssemAqua3a
c
739 0 715 -718 716 -717 -711 720      u=14 FILL=4 imp:n=1   $ TestAssemGap0a
740 0 715 -718 716 -717 -711 722 -719 u=14 FILL=4 imp:n=1   $ TestAssemGap00a
741 0 715 -718 716 -717 -711 724 -721 u=14 FILL=4 imp:n=1   $ TestAssemGap01a
742 0 715 -718 716 -717 -711 726 -723 u=14 FILL=4 imp:n=1   $ TestAssemGap02a
c 743 0 715 -718 716 -717 -711 728 -725 u=14 FILL=4 imp:n=1   $ TestAssemGap03a
```

```
c 744 0 715 -718 716 -717 -711 730 -727 u=14 FILL=4 imp:n=1   $ TestAssemGap04a
c 745 0 715 -718 716 -717 -711 732 -729 u=14 FILL=4 imp:n=1   $ TestAssemGap05a
c 746 0 715 -718 716 -717 -711 734 -731 u=14 FILL=4 imp:n=1   $ TestAssemGap06a
c 747 0 715 -718 716 -717 -711 736 -733 u=14 FILL=4 imp:n=1   $ TestAssemGap07a
c 748 0 715 -718 716 -717 -711 738 -735 u=14 FILL=4 imp:n=1   $ TestAssemGap08a
c 749 0 715 -718 716 -717 -711 740 -737 u=14 FILL=4 imp:n=1   $ TestAssemGap09a
c 750 0 715 -718 716 -717 -711 742 -739 u=14 FILL=4 imp:n=1   $ TestAssemGap10a
c 751 0 715 -718 716 -717 -711 744 -741 u=14 FILL=4 imp:n=1   $ TestAssemGap11a
c 752 0 715 -718 716 -717 -711 746 -743 u=14 FILL=4 imp:n=1   $ TestAssemGap12a
c 753 0 715 -718 716 -717 -711 748 -745 u=14 FILL=4 imp:n=1   $ TestAssemGap13a
754 0 715 -718 716 -717 -711 750 -725 u=14 FILL=4 imp:n=1   $ TestAssemGap14a
755 0 715 -718 716 -717 -711 752 -749 u=14 FILL=4 imp:n=1   $ TestAssemGap15a
756 0 715 -718 716 -717 -711 758 -751 u=14 FILL=4 imp:n=1   $ TestAssemGap18a
757 0 715 -718 716 -717 -711 760 -757 u=14 FILL=4 imp:n=1   $ TestAssemGap19a
c
760 2 -2.7 710 -712 713 -716 -720 -711 u=14       imp:n=1   $ TestAssemPanel1a
761 0 -716 #760                  u=14 FILL=4 imp:n=1   $ TestAssemPanel1Gapa
762 2 -2.7 710 -712 717 -714 -720 -711 u=14       imp:n=1   $ TestAssemPanel2a
763 0 717 #762                   u=14 FILL=4 imp:n=1   $ TestAssemPanel2Gapa
c
770 0 780 -781 -782 -783 784 -785   FILL=14 (620)       imp:n=1 $ Final L-108 fuel assembly
c
c *** Universe ***
c
c    mat    den     surfaces                          importance
996   12 -1.0       -998 111 #(-101 -108 105) #(-106 101 -103 107)
                  #(-106 101 103 -108) #(-400 108 -413)   imp:n=1  $ water
997   12 -1.0      -998 -111 #770 #115                   imp:n=1  $ water
998   2    -2.35   998 -999                           imp:n=1   $ pvc tank
999   0            999                               imp:n=0  $ the nothing

c ------------------------------------------------------------
c                      SURFACE CARDS
c ------------------------------------------------------------
c
c *** Detector Body ***
c
101      cz      17.098              $ outer radius of main body
102      cz      16.78               $ inner radius of main body
103      pz      46.72               $ top of main body
104      pz      0.0                 $ bottom of main body
105      pz     -0.3175              $ bottom of main body
106      cz      18.529              $ main body flange outer radius
107      pz      46.08               $ main body flange bottom
108      pz      47.5074             $ top of main body lid
c
```

```
110     c/z     0  4.29  6.17          $ outer radius of fuel pass-thru tube
111     c/z     0  4.29  5.85          $ inner radius of fuel pass-thru tube
112     c/z     0  4.29  7.42          $ fuel pass-thru flange outer radius
113     pz      45.45                $ fuel pass-thru flange bottom
c          Vx    Vy    Vz    Hx   Hy   Hz    R
115    rcc   0   4.29  46.73  0    0    10   5.74   $ inner radius of funnel
116    rcc   0   4.29  46.73  0    0    10   5.84   $ outer radius of funnel
c
120    c/z     0  2.54  7.239          $ outer radius of lead shield
121    pz      43.85                $ top of lead shield
122    c/z     0  2.54  7.477          $ outer radius of SS tube for lead shield
123    c/y     0  40.32  0.9525         $ hole in Pb shield
124    c/y     0  40.32  1.1049         $ SS layer for hole in lead shield
c
150    cz      16.61                $ poly liner
151   c/z      0  2.24  7.4777         $ inner radius of poly for air gap (mts)
152   px      -7.477
153   px       7.477
154   py       11.32
155   py       2.54
c
c DETECTORS
c             Vx    Vy      R
201    C/Z     -8.61  -3.22  1.188945     $ B inner radius for tube #1
202    C/Z     -5.98  -6.59  1.188945     $ B inner radius for tube #2
203    C/Z      8.61  -3.22  1.188945     $ B inner radius for tube #3
204    C/Z      5.98  -6.59  1.188945     $ B inner radius for tube #4
205    C/Z      2.19  -13.27 1.18882      $ B inner radius for tube #5
206    C/Z     -2.19  -13.27 1.18882      $ B inner radius for tube #6
c
211    C/Z     -8.61  -3.22  1.189        $ Al inner radius for tube #1
212    C/Z     -5.98  -6.59  1.189        $ Al inner radius for tube #2
213    C/Z      8.61  -3.22  1.189        $ Al inner radius for tube #3
214    C/Z      5.98  -6.59  1.189        $ Al inner radius for tube #4
215    C/Z      2.19  -13.27 1.189        $ Al inner radius for tube #5
216    C/Z     -2.19  -13.27 1.189        $ Al inner radius for tube #6
c
221    C/Z     -8.61  -3.22  1.27         $ Al outer radius for tube #1
222    C/Z     -5.98  -6.59  1.27         $ Al outer radius for tube #2
223    C/Z      8.61  -3.22  1.27         $ Al outer radius for tube #3
224    C/Z      5.98  -6.59  1.27         $ Al outer radius for tube #4
225    C/Z      2.19  -13.27 1.27         $ Al outer radius for tube #5
226    C/Z     -2.19  -13.27 1.27         $ Al outer radius for tube #6
c
231    C/Z     -8.61  -3.22  2.2225       $ Pb outer radius for tube #1
232    C/Z     -5.98  -6.59  2.2225       $ Pb outer radius for tube #2
```

```
233   C/Z     8.61  -3.22  2.2225      $ Pb outer radius for tube #3
234   C/Z     5.98  -6.59  2.2225      $ Pb outer radius for tube #4
235   C/Z     2.19  -13.27 2.2225      $ Pb outer radius for tube #5
236   C/Z    -2.19  -13.27 2.2225      $ Pb outer radius for tube #6
c          Vx    Vy      Vz    Hx   Hy   Hz    R
241   RCC  -8.61 -3.22    34.76  0.0  0.0  1.3  2.2225  $ poly sleeve on top of tube #1
242   RCC  -5.98 -6.59    34.76  0.0  0.0  1.3  2.2225  $ poly sleeve on top of tube #2
243   RCC   8.61 -3.22    34.76  0.0  0.0  1.3  2.2225  $ poly sleeve on top of tube #3
244   RCC   5.98 -6.59    34.76  0.0  0.0  1.3  2.2225  $ poly sleeve on top of tube #4
245   RCC   2.19 -13.27   34.76  0.0  0.0  1.3  2.2225  $ poly sleeve on top of tube #5
246   RCC  -2.19 -13.27   34.76  0.0  0.0  1.3  2.2225  $ poly sleeve on top of tube #6
c
250   PZ      34.76               $ Top of Pb tubes
251   PZ      1.280               $ Bottom of Pb tubes
252   PZ      32.40               $ Top of Al tube
253   PZ      29.54               $ Top of active region
254   PZ      4.140               $ Bottom of active region
255   PZ      41.29               $ Top of preamps
256   PZ      36.06               $ Top of tube poly sleeves
260   PZ      33.69               $ Bottom of poly sleeve
270    py     -15.59              $ side surface for Pb under auxiliary moderator
271    pz     1.28                $ top surface for Pb under auxiliary moderator
272    px     -11.0               $ Pb shield under 4 tubes
273    px     11.0                $ Pb shield under 4 tubes
274    py     -0.75               $ Pb shield under 4 tubes
275    p      1.0  1.0  0.0  -16.657   $ Pb shield under 4 tubes
276    p     -1.0  1.0  0.0  -16.657   $ Pb shield under 4 tubes
c
c
300    px     6.248               $ air gap around auxiliary moderator
301    px     6.197               $ air gap around auxiliary moderator
302    py    -10.46               $ air gap around auxiliary moderator
303    px    -6.197               $ air gap around auxiliary moderator
304    px    -6.248               $ air gap around auxiliary moderator
305    py    -10.51               $ air gap around auxiliary moderator
c
400    c/z    0.0  13.47  2.0        $ guide tube for interrogation source
401    pz     11.69               $ bottom of guide tube for interrogation source
402    s      0  13.47 13.7725 1e-6    $ SPHERE OF CF in interrogation tube
403    pz     13.2725              $ source cavity bottom
404    c/z    0  13.47  1.334        $ source cavity outer
405    pz     17.56               $ source cavity top
410    pz     12.480              $ source vessel bottom
411    c/z    0  13.47  1.5875       $ source vessel outer
412    pz     18.83               $ source vessel top
413    pz     50.32               $ top of void in source tube
```

```
414     pz       12.48                  $ bottom of void in source tube
415     c/z      0.0  13.47  1.7          $ guide tube for interrogation source inner radius
c *** Ionization Chamber ***
c
c       Vx   Vy     Vz    Hx  Hy   Hz   R
600 rcc  0 -5.1524 40.32  0 -3.8252 0  0.9776  $ inner IC wall
601 rcc  0 -5      40.32  0 -4.13   0  1.13    $ outer IC wall
602 rcc  0 -5      40.32  0 -4.13   0  2.145   $ outer tungsten shield wall
c
c *** MTR Fuel ***
703  PZ -8.25                        $ TestAssemFuelStrip_Bottom
704  P   3.12377 -13.72501 0.0 42.72073   $ TestAssemFuelStrip_East
705  C/Z 13.676 0.0 14.0625              $ TestAssemFuelStrip_Inner
706  C/Z 13.676 0.0 14.0895              $ TestAssemFuelStrip_Outer
707  PZ  51.75                        $ TestAssemFuelStrip_Top
708  P -3.12377 -13.72501 0.0 -42.72073   $ TestAssemFuelStrip_West
c
709  PX -4.048                        $ TestAssemPanel_Back
710  PZ -9.5                         $ TestAssemPanel_Bottom
711  PX 4.048                         $ TestAssemPanel_Front
712  PZ 54                           $ TestAssemPanel_Top
c
713  PY -3.9519                       $ TestAssemPanel1_Left
714  PY 3.9519                        $ TestAssemPanel2_Right
c
715  PZ -8.75                        $ TestAssemSlot_Bottom
716  PY -3.556                        $ TestAssemSlot_Left
717  PY 3.556                         $ TestAssemSlot_Right
718  PZ  52.25                        $ TestAssemSlot_Top
c
719  C/Z 9.779 0.0 13.9998   $ TestAssemSlot0_Inner
720  C/Z 9.779 0.0 14.1522   $ TestAssemSlot0_Outer
721  C/Z 10.212 0.0 13.9998   $ TestAssemSlot00_Inner
722  C/Z 10.212 0.0 14.1522   $ TestAssemSlot00_Outer
723  C/Z 10.645 0.0 13.9998   $ TestAssemSlot01_Inner
724  C/Z 10.645 0.0 14.1522   $ TestAssemSlot01_Outer
725  C/Z 11.078 0.0 13.9998   $ TestAssemSlot02_Inner
726  C/Z 11.078 0.0 14.1522   $ TestAssemSlot02_Outer
727  C/Z 11.511 0.0 13.9998   $ TestAssemSlot03_Inner
728  C/Z 11.511 0.0 14.1522   $ TestAssemSlot03_Outer
729  C/Z 11.944 0.0 13.9998   $ TestAssemSlot04_Inner
730  C/Z 11.944 0.0 14.1522   $ TestAssemSlot04_Outer
731  C/Z 12.377 0.0 13.9998   $ TestAssemSlot05_Inner
732  C/Z 12.377 0.0 14.1522   $ TestAssemSlot05_Outer
733  C/Z 12.81 0.0 13.9998   $ TestAssemSlot06_Inner
734  C/Z 12.81 0.0 14.1522   $ TestAssemSlot06_Outer
```

```
735  C/Z 13.243 0.0 13.9998   $ TestAssemSlot07_Inner
736  C/Z 13.243 0.0 14.1522   $ TestAssemSlot07_Outer
737  C/Z 13.676 0.0 13.9998   $ TestAssemSlot08_Inner
738  C/Z 13.676 0.0 14.1522   $ TestAssemSlot08_Outer
739  C/Z 14.109 0.0 13.9998   $ TestAssemSlot09_Inner
740  C/Z 14.109 0.0 14.1522   $ TestAssemSlot09_Outer
741  C/Z 14.542 0.0 13.9998   $ TestAssemSlot10_Inner
742  C/Z 14.542 0.0 14.1522   $ TestAssemSlot10_Outer
743  C/Z 14.975 0.0 13.9998   $ TestAssemSlot11_Inner
744  C/Z 14.975 0.0 14.1522   $ TestAssemSlot11_Outer
745  C/Z 15.408 0.0 13.9998   $ TestAssemSlot12_Inner
746  C/Z 15.408 0.0 14.1522   $ TestAssemSlot12_Outer
747  C/Z 15.841 0.0 13.9998   $ TestAssemSlot13_Inner
748  C/Z 15.841 0.0 14.1522   $ TestAssemSlot13_Outer
749  C/Z 16.274 0.0 13.9998   $ TestAssemSlot14_Inner
750  C/Z 16.274 0.0 14.1522   $ TestAssemSlot14_Outer
751  C/Z 16.707 0.0 13.9998   $ TestAssemSlot15_Inner
752  C/Z 16.707 0.0 14.1522   $ TestAssemSlot15_Outer
753  C/Z 17.14 0.0 13.9998   $ TestAssemSlot16_Inner
754  C/Z 17.14 0.0 14.1522   $ TestAssemSlot16_Outer
755  C/Z 17.573 0.0 13.9998   $ TestAssemSlot17_Inner
756  C/Z 17.573 0.0 14.1522   $ TestAssemSlot17_Outer
757  C/Z 17.14 0.0 13.9998   $ TestAssemSlot18_Inner
758  C/Z 17.14 0.0 14.1522   $ TestAssemSlot18_Outer
759  C/Z 17.573 0.0 13.9998   $ TestAssemSlot19_Inner
760  C/Z 17.573 0.0 14.1522   $ TestAssemSlot19_Outer
c
780 999 pz -27.38
781 999 pz  70.88
782 999 C/Z 9.779 4.29 14.2   $ TestAssemSlot0_Outer px  -4.049
783 999 px   4.049
784 999 py   0.3
785 999 py   8.3
c
c *** Room ***
997  so  100
c          Vx   Vy   Vz  A1x  A1y  A1z  A2x  A2y   A2z  A3x  A3y  A3z
c 998  box   -100 -150 -50  200  0.0  0.0  0.0  300   0.0  0.0  0.0  500  $ room, inner surface
c 999  box   -115 -165 -65  230  0.0  0.0  0.0  330   0.0  0.0  0.0  515  $ room, outer surface
998 rcc 0 0 -51.1175   0 0 152.4   63.5
999 rcc 0 0 -52.3875  0 0 153.67   64.135

c
c ------------------------------------------------------------
c                      TRANSFORMATIONS
c ------------------------------------------------------------
```

```
C L108 Fuel into Throat
*TR601 -3.897 0.0  0.0
*TR602 -3.464 0.0  0.0
*TR603 -3.031 0.0  0.0
*TR604 -2.598 0.0  0.0
c *TR605 -2.165 0.0  0.0
c *TR606 -1.732 0.0  0.0
c *TR607 -1.299 0.0  0.0
c *TR608 -0.866 0.0  0.0
c *TR609 -0.433 0.0  0.0
c *TR610  0.0   0.0  0.0
c *TR611  0.433 0.0  0.0
c *TR612  0.866 0.0  0.0
c *TR613  1.299 0.0  0.0
c *TR614  1.732 0.0  0.0
c *TR615  2.165 0.0  0.0
*TR616  2.598 0.0  0.0
*TR617  3.031 0.0  0.0
*TR618  3.464 0.0  0.0
*TR619  3.897 0.0  0.0
*TR620  0.0   4.29 -4.91  -90 -180 -90  0 -90 90  90 90 0
*TR999  -4.29 4.29 -4.91  -90 -180 -90  0 -90 90  90 90 0
c ------------------------------------------------------------
c                      MATERIAL CARDS
c ------------------------------------------------------------
c
c *** Material 1: Stainless Steel 304 ***
c
m1    26057       0.6908
      28058       0.0892
      24052       0.1900
      25055       0.0200
      14028       0.0100
      nlib=.70c
c
c *** Material 2: High Density Polyethylene ***
c
m2    1001        0.6667
      6000        0.3333
      nlib=.70c
mt2   poly.10t                $ s(a,b) treatment for poly
c
c *** Material 3: High Purity Lead ***
c
m3    82206       0.241
      82207       0.221
```

```
      82208        0.524
      nlib=.70c
c
c *** Material 4: Aluminum ***
c
m4     13027        1.0
      nlib=.70c
c
c *** Material 5: Boron-10 ***
c
c m5      5010        1.0
c       nlib=.70c
c
c *** Material 6: Helium-3 ***
c
m6      2003        1.0
       nlib=.70c
c
c *** Material 7: Cadmium ***
c
c m7     48000        1.0
c        nlib=.70c
c
c
c *** Material 9: AmLi ***
c
m9     95241        1.0
      3007         1.0
      nlib=.70c
c
c *** Material-10, fresh fuel ***
c
m10    92235   -0.35715
      92238   -0.02464
      13027  -0.61821
      nlib=.70c
c
c *** Material 11: Tungsten ***
c
m11    74182       -0.3
      74184       -0.3
      74186       -0.3
      28060       -0.06
      29063       -0.04
      nlib=.70c
c
```

```
c *** Material 12: Water ***
c
m12     8016       0.33333
        1001       0.66667
        nlib=.70c
mt12 lwtr.10t                  $ s(a,b) treatment for water
c *** Material 14: Xenon gas fill in IC ***
m14   54129        0.264
      54130        0.0407
      54131        0.212
      54132        0.269
      nlib=.70c
c
m15   6000   -0.000124       $ Air (9.58e-4 g/cc in Los Alamos)
      7014   -0.755268       $ (from PNNL)
      8016   -0.231781
      18040  -0.012827
      nlib=.70c
c
c ------------------------------------------------------------
c                        SOURCE CARDS
c ------------------------------------------------------------
c
mode n
nps 1e7
sdef par=n pos= 0  13.47 13.7725 ERG=D1 WGT= 3.794E4
c sdef par=SF pos= 0  13.97 13.7725 WGT=1
prdmp j 1e8 1 2 5e6
si1 h 0.00 0.25 0.50 0.75 1.00 1.25 1.50 1.75 2.00 2.25
      2.50 2.75 3.00 3.25 3.50 3.75 4.00 4.25 4.50 4.75
      5.00 5.25 5.50 5.75 6.00
sp1 d 0.00E+00 2.05E-01 2.52E-01 2.24E-01 1.79E-01 1.09E-01
      3.16e-02 4.06E-05 4.55E-05 5.71E-05 6.55E-05 6.69E-05
      6.25e-05 5.12E-05 3.93E-05 2.81E-05 1.75E-05 8.19E-06
      2.74e-06 6.64E-07 5.41E-07 4.14E-07 2.85E-07 1.18E-07
      4.49e-09
c
c ------------------------------------------------------------
c                        TALLY CARDS
c ------------------------------------------------------------
c
c *f8:p  600
c
fc18   Doubles in Tubes 1-4
f18:n (231 232 233 234)
ft18 CAP 2003 GATE 450 12800
```

```
c
fc28   Doubles in Tubes 5-6
f28:n (235 236)
ft28 CAP 2003 GATE 450 12800
c
fc38   Doubles in Tubes 1-6
f38:n (231 232 233 234 235 236)
ft38 CAP 2003 GATE 450 12800
c
fc48   Singles in Tubes 1-4
f48:n (231 232 233 234)
ft48 CAP 2003
c
fc58   Singles in Tubes 5-6
f58:n (235 236)
ft58 CAP 2003
c
fc68   Singles in Tubes 1-6
f68:n (231 232 233 234 235 236)
ft68 CAP 2003
```

VITA

Jay P Joshi was born and raised in Nepal where he completed his education up to the High School. He was inclined towards math and science from the young age. After he moved to the US he joined Austin Community College to acquire some college credits before he was admitted to the University of Texas at Austin. He graduated with a BS in Radiation Physics from the University of Texas at Austin in Dec 2013. He started his MS degree in Nuclear Engineering in Jan 2015. In May, 2016 he started working at the Los Alamos National Laboratory, where is performed his MS research. He received his MS degree in Nuclear Engineering from the Missouri University of Science and Technology in May 2017.